Finite volume method for modelling of linear elastic deformation:

Extension to three dimensions and comparison with finite element method

Romanos Tselempis
Student ID: 4812387

Faculty of Civil Engineering & Geosciences, TU Delft
17 December 2020

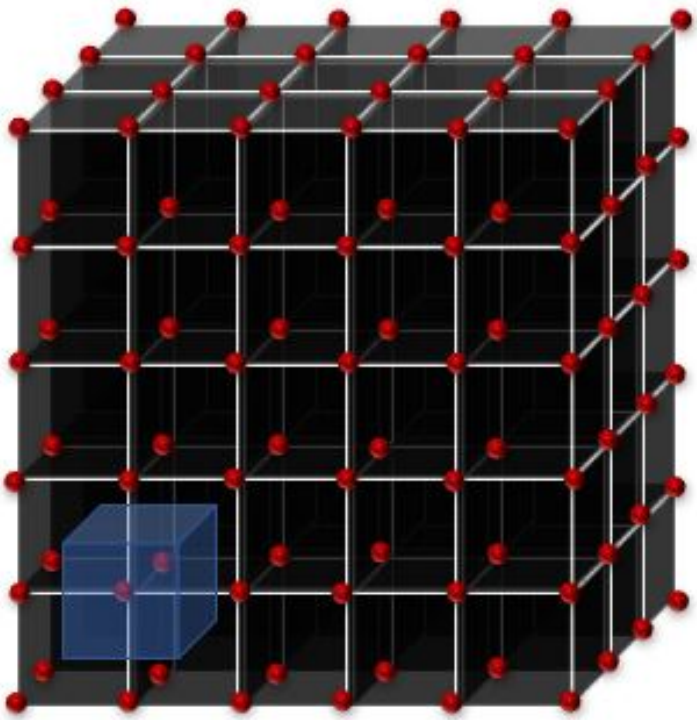

TU Delft

Finite volume method for modelling of linear elastic deformation: Extension to three dimensions and comparison with finite element method

by

Romanos Tselempis

Student ID: 4812387

to obtain the degree of Master of Science
at the Delft University of Technology,
to be defended publicly on December 17, 2020 at 11:30 AM.

Student number:	4812387	
Project duration:	October 1, 2019 – December 17, 2020	
Advisor:	Associate Prof. Dr. Hadi Hajibeygi,	CITG, TU Delft
co-supervisor:	Ir. Kishan Ramesh Kumar,	CITG, TU Delft
co-supervisor:	Ir. Sara Shokrollahzadeh Behbahani,	CITG, TU Delft
Other committee members:	Associate Prof. Dr. Marc Gerritsma,	AWEP, TU Delft
	Associate Prof. Annemarie Muntendam-Bos,	CITG, TU Delft

This thesis is confidential and cannot be made public until December 17, 2020.

TU Delft

Preface

A MSc program period comes to an end, something that would have never been accomplished, without the scholarship from the company Hellenic Petroleum, to which I owe everything. This MSc thesis is a result of the Delft Advanced Reservoir Simulation (DARSim) research group of which I had the honour to be part of. I would like to thank my supervisor Dr. Hadi Hajibeygi for his faith in me, his patience to teach me and his efforts to help me not only as a student, but also in personal level. I will keep his lessons always on my mind for any of my next career and life stages.

I would like to thank PhD candidates Kishan Ramesh Kumar and Sara Shokrollahzadeh Behbahani, who provided me with great support and they transfered me a lot of their knowledge throughout this period and also to Mousa Hosseinimehr, who is PhD candidate and teaching assistant in the course of Reservoir Simulation and he introduced us the meaning of discretization and simulation in an appealing way.

Special thanks to my very good friend and soon colleague Antonio Barion, for whom I hope he will as good scientist as he was as a friend. Furthermore wishes for their career to my colleagues and friends, who helped me adapt to a new wolrd for me: Janio Piguave Tomala, Artur Makhmutov, and Nordin Tippersma.

I feel responsible to thank my parents, who gave me strength and motivation to bring this MSc to an end.

Romanos Tselempis
Student ID: 4812387
Delft, December 17 2020

Abstract

The demand for accurate and efficient simulations in order to test the geomechanical effects is a reality for the entire geoscience community. The motivation that arises from that need is the development and the evolution of modelling methods to study these effects. Deep understanding of any problem in fine scale is crucial, especially when it extends to much coarser scales. In this work the finite volume method (FVM) is used for mechanical modelling of deformation in elastic media. The momentum balance equation is solved as the governing equation for mechanics, assuming linear elasticity for the stress tensor. Here, displacement is mapped onto a vertex-centred grid in three dimensions (3D). A set of eight trilinear basis functions are used to locally interpolate the value of displacement within each grid cube. In the finite volume method, the discretized form of the equations are obtained by integrating the governing equation over control volume surfaces, since in 3D the control volume is a cube. Hence, discretized forms are obtained by considering 24 surfaces, which form between a displacement node and its neighbouring displacement cells. This required extensive derivation. The implementation of the numerical model was carried out by writing a code in MATLAB.

Several numerical test cases are presented to demonstrate the capability of this model. In the first place, the consistency of the model is checked through comparison with synthetic analytical solutions, which are compared to the numerical solutions. Furthermore, the simple test case of uniaxial compression, has been carried out with this model, but also compared to the results with a 2D FVM model and a 3D finite element (3D FEM) one. In another test case, ground plain strain subsidence is studied in a real hydrocarbon field with a heterogeneous map for elasticity parameters. It is shown that 3D FVM is in close agreement with 3D FEM in predicting the subsidence due to field depletion. Last but not least, displacement and stresses, in a faulted reservoir in which fluids are injected, are modelled and the results are shown to coincide with a robust analytical solutions for the system.

Finally, the aim of this work is to shed some more light on the finite volume method for mechanics and bring it closer to the audience of science.

Contents

Nomenclature

Γ^B	Bottom border in 3d domain Ω
Γ^E	East border in 2d,3d domain Ω
Γ^N	North border in 2d,3d domain Ω
Γ^S	South border in 2d,3d domain Ω
Γ^T	Top border in 3d domain Ω
Γ^W	West border in 2d,3d domain Ω
λ	First Lamé parameter, [Pa]
μ	Second Lamé parameter or shear modulus, [Pa]
σ_{xx}	Principal stress in x direction, [Pa]
σ_{xy}	Shear stress in x direction caused by force in y direction, [Pa]
σ_{xz}	Shear stress in x direction caused by force in z direction, [Pa]
σ_x	Total stress in x direction, [Pa]
σ_{yx}	Shear stress in y direction caused by force in x direction, [Pa]
σ_{yy}	Principal stress in y direction, [Pa]
σ_{yz}	Shear stress in y direction caused by force in z direction, [Pa]
σ_y	Total stress in y direction, [Pa]
σ_{zx}	Shear stress in z direction caused by force in x direction, [Pa]
σ_{zy}	Shear stress in z direction caused by force in y direction, [Pa]
σ_{zz}	Principal stress in z direction, [Pa]
σ_z	Total stress in z direction, [Pa]
b	Biot's constant, [-]
f_x	Source term in force balance equation in x direction, [Pa]
f_y	Source term in force balance equation in y direction, [Pa]
f_z	Source term in force balance equation in z direction, [Pa]
G_x	Scaled displacement in x direction, [m]
g_x	Green function in x direction, [m]
G_y	Scaled displacement in y direction, [m]
g_y	Green function in y direction, [m]
G_z	Scaled displacement in z direction, [m]
g_z	Green function in z direction, [m]

$u_{analytical}$ Analytical displacement, [m]

$u_{numerical}$ Numerical displacement, [m]

u_x Displacement in x direction, [m]

u_y Displacement in y direction, [m]

u_z Displacement in z direction, [m]

v Poisson's ratio, [-]

1 Introduction

Geomechanical effects play crucial role in geoscience applications, especially when we want to qualify key parameters that may have impact on the geological section of interest. Subsurface geological formations are often highly heterogeneous and heavily or partially fractured at multiple scales. Heterogeneity of the deformation properties (e.g.elasticity coefficients) can be of several orders of magnitude, which occurs at fine scale (cm) resolution, but has sometimes significant impact on the reservoirs, which span in kms. For that reason numerical simulation of mechanical deformation for such complex systems is necessary to optimise the geo-engineering operations [1, 22], and assess their safety and manage the associated risks (e.g. subsidence) [32].

Also many reservoirs that contain water or hydrocarbons around the world have multiple faults, which affect the flow of the fluids inside the reservoir [2]. Injection of waste water or CO_2 in the deep subsurface or production of natural gas can cause significant subsidence, especially when there are faults that have been subjected to earlier movements [16]. The modelling of geomechanical properties requires accurate simulations, especially when pore pressure is involved or the heterogeneity of the elastic properties.

Finite element method (FEM) and FVM are two very famous discretization schemes with the former one being dominant in the field of computational continuum mechanics (CCM), and the latter one in the field of computational fluid dynamics (CFD) over the past years [17, 31]. Both methods can be easily formulated to allow implementation on unstructured meshes [5, 23]. The major advantage of FEM, especially in the field of mechanics, is its capability of increasing the order of elements by approximating the physics fields with higher order polynomials [23]. Moreover, it provides the option to refine the mesh locally, a technique known as ”adaptive mesh refinement”. These features of FEM are very important for the modelling of stress in an accurate way [25]. However, the application of FEM is complex and it requires mathematical expertise and that is one of the reasons why many scientists do not embrace it sometimes. Another drawback is that there is no local conservation, since only the net flux over the domain boundaries is guaranteed to be in balance [13].

On the other hand, in FVM there is local conservation of the numerical fluxes, which means that numerical flux is conserved from one discretization cell to its neighbour. That feature makes FVM dominant in the field of CFD in combination with the easier and appealing mathematical application gains more audience in the field of CCM [7, 12, 28]. This also holds for nonlinear problems, which makes it extra powerful for robust handling of (nonlinear) conservation laws [25]. ”Finite volume” refers to the small volume surrounding each node point on a mesh [10, 20]. The discretized cell is often referred as control volume in which the local conservation of the fluxes holds.

Theory of linear elasticity is a simplified version of the non linear elasticity theory [26] and describes how solid media become deformed, due to prescribed loading conditions, which are called boundary conditions, when solving partial differential equations. Boundary conditions are a set of additional constraints imposed in the boundaries of the domain to ensure that there is unique solution in the system.

FEM has been introduced in many literature books [5, 15, 24] and articles [3, 4, 11, 32] for the linear elasticity method. FVM on the other hand, is more recent method in the CCM field and so far it has not been implemented to model linear elasticity problem in three dimensions, using trilinear local shape

functions in order to interpolate the displacement in every node of the computational domain. A novel model has been developed, extending the 2D FVM one developed by Irina Sokolova et al. [27] to 3D FVM.

This thesis work is a research on the linear elasticity problem in three dimensions with finite volume method (3D FVM) in which the elastic deformation is modelled in an accurate way. The displacement is mapped onto a vertex-centred grid. The consistency of 3D FVM model has been tested with the application of synthetic solutions (analytical solutions), which are provided as exact solutions in the boundaries of the domain and they are compared to the numerical solutions for the entire domain, through error analysis for elastic deformation [27]. The finite element method in three dimensions (3D FEM) has been also studied for the linear elasticity problem. The model of 3D FEM [19] is used in this research in order to benchmark the numerical results of 3D FVM with 2D FVM and 3D FEM in several test cases that have been carried out, starting with uniaxial compression test case. Furthermore, the incorporation of the pore pressure to study mechanical deformation is achieved by adding it to right hand side (RHS) of the momentum balance equation as part of the force vector (source term) [27]. In plain strain subsidence test case the effect of heterogeneity in a deformable domain in combination with the pore pressure effect due to the depletion in a porous media (reservoir) is investigated [3, 27]. In the last test case heterogeneity does not exist, but the geometry is more complex and concerns about a reservoir with infinite boundaries and a displaced fault in its center [16]. These two test cases concern the application in real field and have been carried out using 2D FVM, 3D FVM and 3D FEM.

This thesis is structured as follows: Chapter two includes the governing equations, the general constitutive relationships and the assumptions that have been taken into account. Chapter three introduces the FVM and the numerical strategy that has been followed. In chapter four the FEM numerical strategy is described. Chapter five includes all the numerical results of the test cases that have been carried out. Finally, after the conclusions in chapter six, in the Appendix there is a simple flow chart of the 3D FVM model that has been developed in Matlab, examples about the code implementation and all the double integrals of the derivatives of the shape functions in 3D FVM, which have been calculated.

2

Governing equations

2.1. Problem formulation

A deformable and porous medium is considered, which is modelled under linear elastic behaviour [26]. According to the second law of Newton the momentum balance equation is stated as:

$$\nabla \cdot (\vec{\sigma} - bpI) = \vec{f}, \tag{2.1}$$

where $\vec{\sigma}$, b, p, I and $\vec{f}$ are the effective stress vector, the Biot's constant, the pore pressure, the identity matrix and the body forces vector respectively . The term $(\vec{\sigma} - bpI)$ is called total stress [14]. If the deformable medium has no pore pressure, the momentum balance equation takes the form:

$$\nabla \cdot (\vec{\sigma}) = \vec{f}, \tag{2.2}$$

The generic formulation that relates effective stress to strain is stated as:

$$\vec{\sigma} = \boldsymbol{C_{dr}} : \nabla^s \vec{u}, \tag{2.3}$$

where $\boldsymbol{C_{dr}}$ is the drained elasticity tensor, $\vec{u}$ is the displacement vector and ∇^s is the symmetric gradient operator. In linear elastic theory σ is related linearly to $\nabla^s \cdot \vec{u}$. The drained elasticity tensor in three dimensions is given as

$$\boldsymbol{C_{dr}} = \begin{bmatrix} \lambda + 2\mu & \lambda & \lambda & 0 & 0 & 0 \\ \lambda & \lambda + 2\mu & \lambda & 0 & 0 & 0 \\ \lambda & \lambda & \lambda + 2\mu & 0 & 0 & 0 \\ 0 & 0 & 0 & \mu & 0 & 0 \\ 0 & 0 & 0 & 0 & \mu & 0 \\ 0 & 0 & 0 & 0 & 0 & \mu \end{bmatrix}, \tag{2.4}$$

where λ and μ are the first and second Lamé parameters respectively. Let us derive the equations that relate the displacement derivatives to the forces in three directions. Linear elasticity suggests that $\vec{\sigma_{xy}} = \vec{\sigma_{yx}}$, $\vec{\sigma_{xz}} = \vec{\sigma_{zx}}$ and $\vec{\sigma_{zy}} = \vec{\sigma_{yz}}$. With the use of the Voigt notation [15, 29], the stress tensor is expressed as:

$$\vec{\sigma} = \begin{bmatrix} \vec{\sigma_{xx}} \\ \vec{\sigma_{yy}} \\ \vec{\sigma_{zz}} \\ \vec{\sigma_{xy}} \\ \vec{\sigma_{yz}} \\ \vec{\sigma_{xz}} \end{bmatrix} = \begin{bmatrix} \lambda+2\mu & \lambda & \lambda & 0 & 0 & 0 \\ \lambda & \lambda+2\mu & \lambda & 0 & 0 & 0 \\ \lambda & \lambda & \lambda+2\mu & 0 & 0 & 0 \\ 0 & 0 & 0 & \mu & 0 & 0 \\ 0 & 0 & 0 & 0 & \mu & 0 \\ 0 & 0 & 0 & 0 & 0 & \mu \end{bmatrix} \begin{bmatrix} \frac{\partial \vec{u_x}}{\partial x} \\ \frac{\partial \vec{u_y}}{\partial y} \\ \frac{\partial \vec{u_z}}{\partial z} \\ \frac{\partial \vec{u_x}}{\partial y} + \frac{\partial \vec{u_y}}{\partial x} \\ \frac{\partial \vec{u_y}}{\partial z} + \frac{\partial \vec{u_z}}{\partial y} \\ \frac{\partial \vec{u_x}}{\partial z} + \frac{\partial \vec{u_z}}{\partial x} \end{bmatrix}, \tag{2.5}$$

According to relationship 2.5 the formulas for the stresses are expressed as follows:

$$\vec{\sigma_{xx}} = (\lambda+2\mu)\frac{\partial \vec{u_x}}{\partial x} + \lambda\frac{\partial \vec{u_y}}{\partial y} + \lambda\frac{\partial \vec{u_z}}{\partial z} \tag{2.6}$$

$$\vec{\sigma_{yy}} = \lambda\frac{\partial \vec{u_x}}{\partial x} + (\lambda+2\mu)\frac{\partial \vec{u_y}}{\partial y} + \lambda\frac{\partial \vec{u_z}}{\partial z} \tag{2.7}$$

$$\vec{\sigma_{zz}} = \lambda\frac{\partial \vec{u_x}}{\partial x} + \lambda\frac{\partial \vec{u_y}}{\partial y} + (\lambda+2\mu)\frac{\partial \vec{u_z}}{\partial z} \tag{2.8}$$

$$\vec{\sigma_{xy}} = \mu\left(\frac{\partial \vec{u_x}}{\partial y} + \frac{\partial \vec{u_y}}{\partial x}\right) \tag{2.9}$$

$$\vec{\sigma_{yz}} = \mu\left(\frac{\partial \vec{u_y}}{\partial z} + \frac{\partial \vec{u_z}}{\partial y}\right) \tag{2.10}$$

$$\vec{\sigma_{xz}} = \mu\left(\frac{\partial \vec{u_x}}{\partial z} + \frac{\partial \vec{u_z}}{\partial x}\right) \tag{2.11}$$

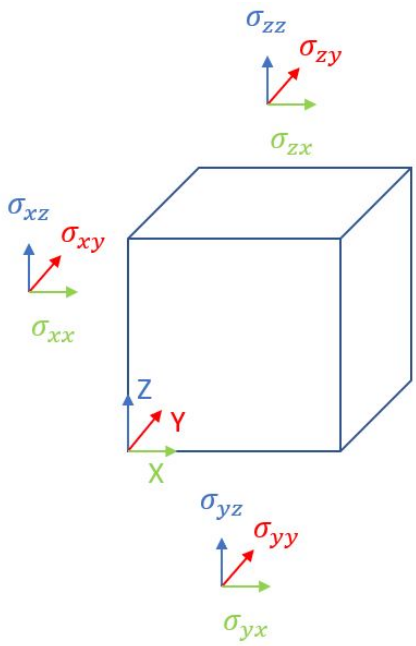

Figure 2.1: Stresses directions in 3D.

Stresses directions are presented in fig. 2.1. After the matrix multiplication in the right hand side (RHS) of relationship 2.5 the final matrix that relates stress to displacement is stated as:

$$\vec{\sigma} = \begin{bmatrix} (\lambda+2\mu)\frac{\partial \vec{u_x}}{\partial x} + \lambda\frac{\partial \vec{u_y}}{\partial y} + \lambda\frac{\partial \vec{u_z}}{\partial z} \\ \lambda\frac{\partial \vec{u_x}}{\partial x} + (\lambda+2\mu)\frac{\partial \vec{u_y}}{\partial y} + \lambda\frac{\partial \vec{u_z}}{\partial z} \\ \lambda\frac{\partial \vec{u_x}}{\partial x} + \lambda\frac{\partial \vec{u_y}}{\partial y} + (\lambda+2\mu)\frac{\partial \vec{u_z}}{\partial z} \\ \mu(\frac{\partial \vec{u_x}}{\partial y} + \frac{\partial \vec{u_y}}{\partial x}) \\ \mu(\frac{\partial \vec{u_y}}{\partial z} + \frac{\partial \vec{u_z}}{\partial y}) \\ \mu(\frac{\partial \vec{u_x}}{\partial z} + \frac{\partial \vec{u_z}}{\partial x}) \end{bmatrix} \tag{2.12}$$

Finally in order to honour the problem formulation as stated in eq. 2.2 :

$$\nabla \cdot \vec{\sigma} = \begin{bmatrix} \frac{d}{dx} & 0 & 0 & \frac{d}{dy} & 0 & \frac{d}{dz} \\ 0 & \frac{d}{dy} & 0 & \frac{d}{dx} & \frac{d}{dz} & 0 \\ 0 & 0 & \frac{d}{dz} & 0 & \frac{d}{dy} & \frac{d}{dx} \end{bmatrix} \begin{bmatrix} (\lambda+2\mu)\frac{\partial \vec{u_x}}{\partial x} + \lambda\frac{\partial \vec{u_y}}{\partial y} + \lambda\frac{\partial \vec{u_z}}{\partial z} \\ \lambda\frac{\partial \vec{u_x}}{\partial x} + (\lambda+2\mu)\frac{\partial \vec{u_y}}{\partial y} + \lambda\frac{\partial \vec{u_z}}{\partial z} \\ \lambda\frac{\partial \vec{u_x}}{\partial x} + \lambda\frac{\partial \vec{u_y}}{\partial y} + (\lambda+2\mu)\frac{\partial \vec{u_z}}{\partial z} \\ \mu(\frac{\partial \vec{u_x}}{\partial y} + \frac{\partial \vec{u_y}}{\partial x}) \\ \mu(\frac{\partial \vec{u_y}}{\partial z} + \frac{\partial \vec{u_z}}{\partial y}) \\ \mu(\frac{\partial \vec{u_x}}{\partial z} + \frac{\partial \vec{u_z}}{\partial x}) \end{bmatrix} = \vec{f} \tag{2.13}$$

After the matrix multiplication in relationship 2.13 the three force balance equations, which relate displacement to force in 3D are formed as follows:

$$\frac{\partial\left((\lambda+2\mu)\frac{\partial \vec{u_x}}{\partial x} + \lambda(\frac{\partial \vec{u_y}}{\partial y} + \frac{\partial \vec{u_z}}{\partial z})\right)}{\partial x} + \frac{\partial\left(\mu(\frac{\partial \vec{u_x}}{\partial y} + \frac{\partial \vec{u_y}}{\partial x})\right)}{\partial y} + \frac{\partial\left(\mu(\frac{\partial \vec{u_x}}{\partial z} + \frac{\partial \vec{u_z}}{\partial x})\right)}{\partial z} = \vec{f_x} \tag{2.14}$$

$$\frac{\partial\left(\mu(\frac{\partial \vec{u_x}}{\partial y} + \frac{\partial \vec{u_y}}{\partial x})\right)}{\partial x} + \frac{\partial\left((\lambda+2\mu)\frac{\partial \vec{u_y}}{\partial y} + \lambda(\frac{\partial \vec{u_x}}{\partial x} + \frac{\partial \vec{u_z}}{\partial z})\right)}{\partial y} + \frac{\partial\left(\mu(\frac{\partial \vec{u_y}}{\partial z} + \frac{\partial \vec{u_z}}{\partial y})\right)}{\partial z} = \vec{f_y} \tag{2.15}$$

$$\frac{\partial\left(\mu(\frac{\partial \vec{u_x}}{\partial z} + \frac{\partial \vec{u_z}}{\partial x})\right)}{\partial x} + \frac{\partial\left(\mu(\frac{\partial \vec{u_y}}{\partial z} + \frac{\partial \vec{u_z}}{\partial y})\right)}{\partial y} + \frac{\partial\left((\lambda+2\mu)\frac{\partial \vec{u_z}}{\partial z} + \lambda(\frac{\partial \vec{u_x}}{\partial x} + \frac{\partial \vec{u_y}}{\partial y})\right)}{\partial z} = \vec{f_z} \tag{2.16}$$

3

Numerical modelling 2D FVM - 3D FVM

3.1. Computational domain

In this chapter the discretization strategy for finite volume method in two and three dimensions in a vertex centered gird is presented. The displacement is placed in the cell vertices. This type of grid allows the easy application of boundary conditions. According to FVM theory stress/displacement control volumes exist around each displacement node. The discretization takes place in the borders of the stress control volume, which interacts with the volume of the interaction volume (IV), with four displacement nodes in 2D and 8 displacement nodes in 3D (IV).

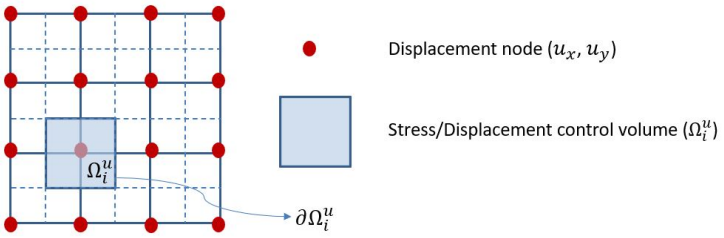

Figure 3.1: Displacement grid for 2D FVM mechanical deformation.

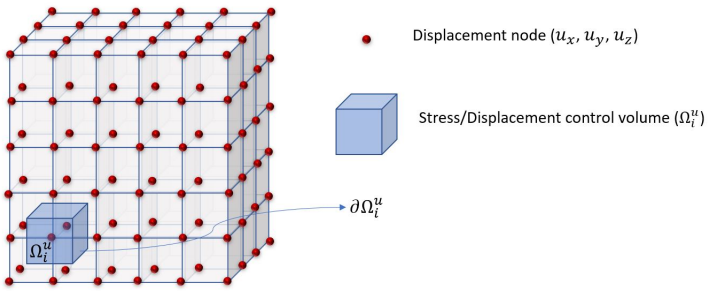

Figure 3.2: Displacement grid for 3D FVM mechanical deformation.

In fig. 3.1 and 3.2 are presented the grids for 2D and 3D modelling of finite volume method and it is shown that each stress/displacement control volume $\Omega_i^{\boldsymbol{u}}$ has in its point of symmetry a displacement node.

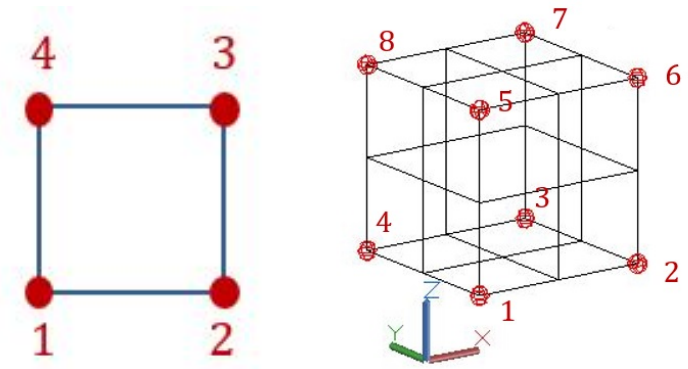

(a) IV in 2D (b) IV in 3D

Figure 3.3: Enumeration of displacement nodes of IV in 2D and 3D.

In fig. 3.3a, 3.3b are presented, two full IV of the general grids of fig. 3.1 and 3.2 for 2D and 3D grids respectively.

After applying finite volume theory on equation 2.1 is derived that:

$$\int_{\Omega_i^{\boldsymbol{u}}} \nabla \cdot (\vec{\sigma} - bpI) dV = \int_{\Omega_i^{\boldsymbol{u}}} \vec{f} dV, \tag{3.1}$$

where $\Omega_i^{\boldsymbol{u}}$ stands for the stress/displacement control volumes in which the linear momentum balance (eq.3.3) is integrated (fig. 3.1, 3.2). With the use of the divergence theorem eq. 3.1 is stated as:

$$\int_{\partial\Omega_i^{\boldsymbol{u}}} (\vec{\sigma}) \cdot \vec{n} dS = \int_{\Omega_i^{\boldsymbol{u}}} \vec{f} dV + (b \int_{\partial\Omega_i^{\boldsymbol{u}}} pI) \cdot \vec{n} dS \tag{3.2}$$

The porous part $(b \int_{\partial\Omega_i^{\boldsymbol{u}}} pI) \cdot \vec{n} dS$ is added to the RHS as part of the forces distributed in the boundaries of the porous medium (reservoir). If there is no pore pressure in the medium then eq. 3.1 is written as follows:

$$\int_{\Omega_i^{\boldsymbol{u}}} \nabla \cdot (\vec{\sigma}) dV = \int_{\Omega_i^{\boldsymbol{u}}} \vec{f} dV, \tag{3.3}$$

With the use of the divergence theorem eq. 3.3 is stated as:

$$\int_{\partial\Omega_i^{\boldsymbol{u}}} (\vec{\sigma}) \cdot \vec{n} dS = \int_{\Omega_i^{\boldsymbol{u}}} \vec{f} dV \tag{3.4}$$

3.2. Discretization 2D FVM

In 2D domain eq. 3.4 is discretized over the north, south, east, west borders of the $\partial\Omega_i^{\boldsymbol{u}}$.

Border	Value
Γ^N	$(0, 1)$
Γ^S	$(0, -1)$
Γ^E	$(1, 0)$
Γ^W	$(-1, 0)$

Table 3.1: Coordinate values of directional operator in 2D.

In a 2D domain according to the values of the directional operator in table 3.1, the left hand side (LHS) of eq. 3.4 is stated in x direction as follows:

$$\int_{\partial\Omega_i^{\boldsymbol{u}}} (\vec{\sigma}_x) \cdot \vec{n} d\Gamma = \int_{\Gamma^N} (\vec{\sigma}_{xy}) dx + \int_{\Gamma^E} (\vec{\sigma}_{xx}) dy - \int_{\Gamma^W} (\vec{\sigma}_{xx}) dy - \int_{\Gamma^S} (\vec{\sigma}_{xy}) dx \tag{3.5}$$

Similarly for the y direction holds:

$$\int_{\partial\Omega_i^{\boldsymbol{u}}} (\vec{\sigma}_y) \cdot \vec{n} d\Gamma = \int_{\Gamma^E} (\vec{\sigma}_{yx}) dy + \int_{\Gamma^N} (\vec{\sigma}_{yy}) dx - \int_{\Gamma^W} (\vec{\sigma}_{yx}) dy - \int_{\Gamma^S} (\vec{\sigma}_{yy}) dx \tag{3.6}$$

In eq. 3.5 and 3.6 the borders of the surface integrals are the Γ^N, Γ^S, Γ^E and Γ^W standing for north, south, east, west boundary of any stress control volume. Eq. 3.5, 3.6 are discretized for all the stress/displacement control volumes and then the stress is related to the displacement as eq. 2.3 suggests.

3.2.1. Bilinear shape functions

In FVM the continuum displacement based on the nodal discrete values needs to be described [27]. The displacement is interpolated using the following formula:

$$\vec{u} \approx \sum_{i=1}^{4} \vec{u_i} N_i(x, y) \text{ in } \bar{\Omega}_i^{\boldsymbol{u}}, \tag{3.7}$$

where $\vec{u_i}$ is the nodal displacement and N_i are the shape functions corresponding to each node of the element $\bar{\Omega}_i^{\boldsymbol{u}}$, which consists an IV. The four shape functions are given as follows:

$$N_1 = (1 - \frac{x}{dx})(1 - \frac{y}{dy}) \tag{3.8}$$

$$N_2 = (\frac{x}{dx})(1 - \frac{y}{dy}) \tag{3.9}$$

$$N_3 = (\frac{x}{dx})(\frac{y}{dy}) \tag{3.10}$$

$$N_4 = (1 - \frac{x}{dx})(\frac{y}{dy}) \tag{3.11}$$

Here dx and dy are the length and the width of one control volume.

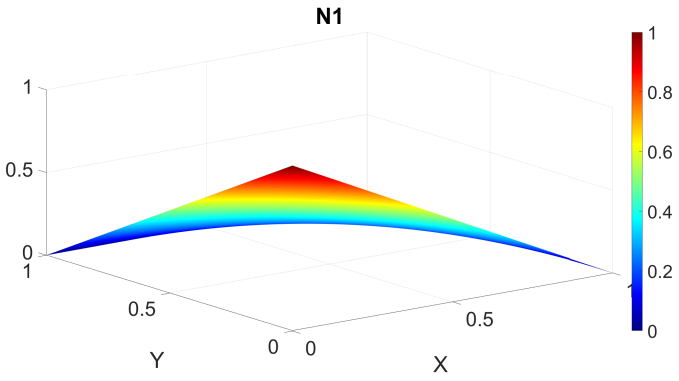

(a) N1 shape function in 2D

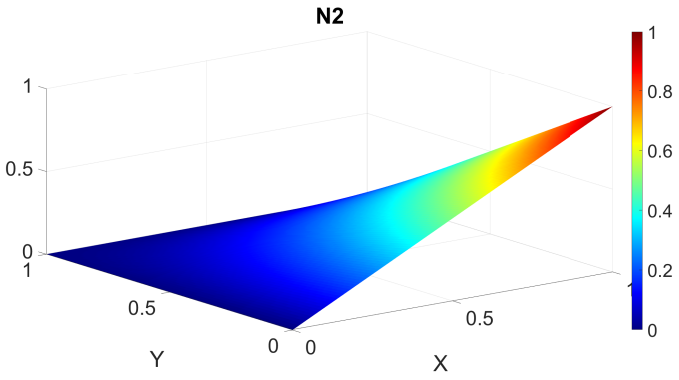

(b) N2 shape function in 2D

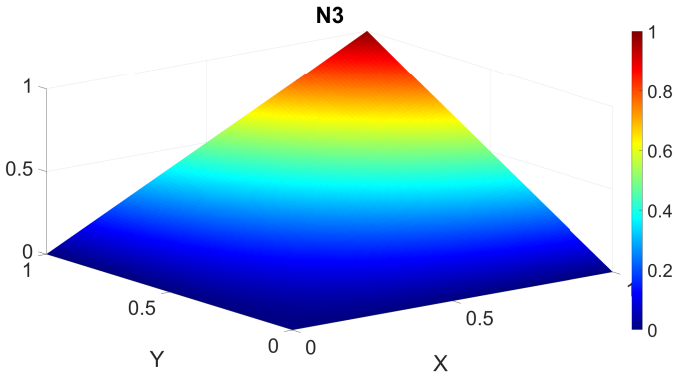

(c) N3 shape function in 2D

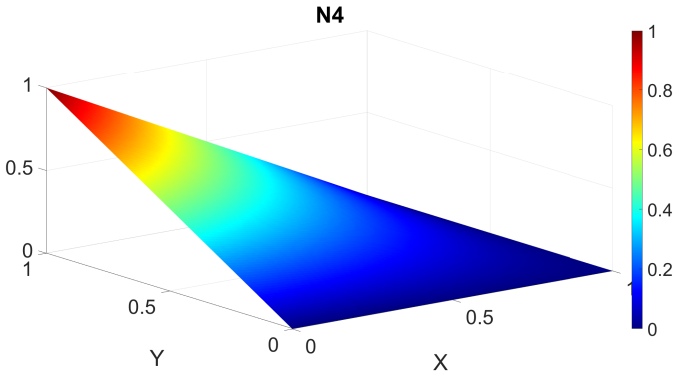

(d) N4 shape function in 2D

Figure 3.4: Shape functions in 2D.

Eq.3.8 - 3.11 are represented in fig. 3.4a - 3.4d and it is observed that each shape function is equal

to 1 in the node that is used to interpolate the displacement and equal to 0 in all the other nodes.

3.2.2. Integration over derivative displacements in 2D

Shape functions as stated in eq. 3.8 - 3.11 are used to approximate the derivatives of the displacements in relationship 2.3, so as to substitute stresses finally in eq. 3.5, 3.6. For instance for the derivative of the displacement over x direction holds:

$$\frac{\partial \vec{u}}{\partial x} \approx \sum_{i=1}^{4} \vec{u_i} \frac{\partial N_i}{\partial x} \tag{3.12}$$

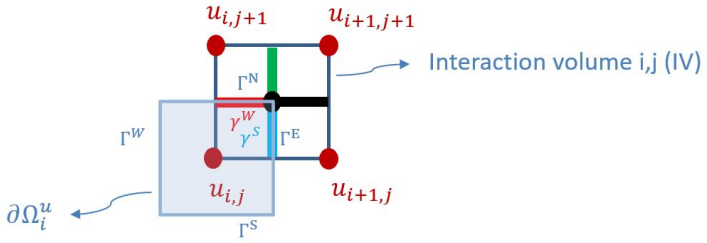

Figure 3.5: Integrals calculation in the stress/displacement control volume of $u_{i,j}$.

In fig. 3.5 is depicted an IV of the general mesh presented in fig. 3.1. The contribution of $u_{i,j}$ in the x direction is calculated as:

$$\int_{\Gamma^E} \vec{\sigma_{xx}} dy = \int_{\gamma S} \vec{\sigma_{xx}} dy = (\lambda + 2\mu) \int_{\gamma S} \frac{\partial \vec{u_x}}{dx} dy + \lambda \int_{\gamma S} \frac{\partial \vec{u_y}}{dy} dy, \tag{3.13}$$

where the $\int_{\gamma S}$ shows the surface (here is line) inside the IV, in which the term $\frac{\partial \vec{u_x}}{dx}$ is integrated. In that case $\int_{\gamma S} = \int_0^{\frac{dy}{2}}$ as shown in fig. 3.5, where dy is the full width of this IV if the 0 is placed in the bottom left node $u_{i,j}$.

$$\int_{\Gamma^N} \vec{\sigma_{xy}} dx = \int_{\gamma W} \vec{\sigma_{xy}} dx = \mu \int_{\gamma W} \frac{\partial \vec{u_x}}{dy} dx + \mu \int_{\gamma W} \frac{\partial \vec{u_y}}{dx} dx \tag{3.14}$$

The contribution of $u_{i,j}$ in the y direction is calculated as:

$$\int_{\gamma W} \vec{\sigma_{yy}} dx = \lambda \int_{\gamma W} \frac{\partial \vec{u_x}}{dx} dx + (\lambda + 2\mu) \int_{\gamma W} \frac{\partial \vec{u_y}}{dy} dx \tag{3.15}$$

$$\int_{\gamma S} \vec{\sigma_{yx}} dy = \mu \int_{\gamma S} \frac{\partial \vec{u_x}}{dy} dy + \mu \int_{\gamma S} \frac{\partial \vec{u_y}}{dx} dy \tag{3.16}$$

In eq. 3.13, 3.14, 3.15 and 3.16 the integrals γ^S, and γ^W are inside the IV as shown in fig. 3.5.

Inside each IV along x direction, the area where $x \in [0, \frac{dx}{2}]$ is called West and the integral is the γ^W. When $x \in [\frac{dx}{2}, dx]$ the region is called East and the integral is the γ^E. Then in the y direction the are where $y \in [0, \frac{dy}{2}]$ is called South with integral γ^S and the area where $y \in [\frac{dy}{2}, dy]$ is called North with integral γ^N.

3.3. Discretization 3D FVM

For the x direction in three dimensions eq. 3.4 is expressed for the north, south, east, west, top, bottom borders of the $\partial\Omega_i^{\boldsymbol{u}}$ as follows:

$$\int_{\partial\Omega_i^{\boldsymbol{u}}}(\vec{\sigma_x})\cdot\vec{n}d\Gamma=\int_{\Gamma^T}(\vec{\sigma_x})\cdot\vec{n}d\Gamma+\int_{\Gamma^N}(\vec{\sigma_x})\cdot\vec{n}d\Gamma+\int_{\Gamma^E}(\vec{\sigma_x})\cdot\vec{n}d\Gamma+\int_{\Gamma^B}(\vec{\sigma_x})\cdot\vec{n}d\Gamma+\int_{\Gamma^S}(\vec{\sigma_x})\cdot\vec{n}d\Gamma+\int_{\Gamma^W}(\vec{\sigma_x})\cdot\vec{n}d\Gamma \tag{3.17}$$

Border	Value
Γ^T	$(0,0,1)$
Γ^B	$(0,0,-1)$
Γ^N	$(0,1,0)$
Γ^S	$(0,-1,0)$
Γ^E	$(1,0,0)$
Γ^W	$(-1,0,0)$

Table 3.2: Coordinate values of directional operator in 3D.

In eq. 3.17 Γ^T, Γ^N, Γ^E, Γ^B, Γ^S and Γ^W are the boundaries of top, north, east, bottom, south and west surface integrals in each stress/displacement control volume respectively.

For $\vec{\sigma_x}$ holds: $\vec{\sigma_x}=(\vec{\sigma_{xx}},\vec{\sigma_{xy}},\vec{\sigma_{xz}})$. Then for eq. 3.17 according to the value of the directional operator $\vec{n}$ in table 3.2, holds:

$$\begin{aligned}\int_{\partial\Omega_i^{\boldsymbol{u}}}(\vec{\sigma_x})\cdot\vec{n}d\Gamma=&\int_{\Gamma^T}(\vec{\sigma_{xz}})dxdy+\int_{\Gamma^N}(\vec{\sigma_{xy}})dxdz+\int_{\Gamma^E}(\vec{\sigma_{xx}})dydz\\&-\int_{\Gamma^B}(\vec{\sigma_{xz}})dxdy-\int_{\Gamma^S}(\vec{\sigma_{xy}})dxdz-\int_{\Gamma^W}(\vec{\sigma_{xx}})dydz\end{aligned} \tag{3.18}$$

Similarly for the y direction:

$$\begin{aligned}\int_{\partial\Omega_i^{\boldsymbol{u}}}(\vec{\sigma_y})\cdot\vec{n}d\Gamma=&\int_{\Gamma^T}(\vec{\sigma_{yz}})dxdy+\int_{\Gamma^N}(\vec{\sigma_{yy}})dxdz+\int_{\Gamma^E}(\vec{\sigma_{yx}})dydz\\&-\int_{\Gamma^B}(\vec{\sigma_{yx}})dxdy-\int_{\Gamma^S}(\vec{\sigma_{yy}})dxdz-\int_{\Gamma^W}(\vec{\sigma_{yx}})dydz\end{aligned} \tag{3.19}$$

Finally for the z direction holds:

$$\begin{aligned}\int_{\partial\Omega_i^{\boldsymbol{u}}}(\vec{\sigma_z})\cdot\vec{n}d\Gamma=&\int_{\Gamma^T}(\vec{\sigma_{zz}})dxdy+\int_{\Gamma^N}(\vec{\sigma_{zy}})dxdz+\int_{\Gamma^E}(\vec{\sigma_{zx}})dydz\\&-\int_{\Gamma^B}(\vec{\sigma_{zz}})dxdy-\int_{\Gamma^S}(\vec{\sigma_{zy}})dxdz-\int_{\Gamma^W}(\vec{\sigma_{zx}})dydz\end{aligned} \tag{3.20}$$

The eq. 3.18, 3.19 and 3.20 can be expressed in terms of displacement.
In the x direction for $\vec{\sigma}_{xx}$ holds:

$$\begin{aligned}&\int_{\Gamma^E}(\vec{\sigma_{xx}})dydz-\int_{\Gamma^W}(\vec{\sigma_{xx}})dydz=\int_{\Gamma^E}(\lambda+2\mu)\frac{\partial\vec{u}_x}{\partial x}dydz+\int_{\Gamma^E}\lambda\frac{\partial\vec{u}_y}{\partial y}dydz\\&+\int_{\Gamma^E}\lambda\frac{\partial\vec{u}_z}{\partial z}dydz-\int_{\Gamma^W}(\lambda+2\mu)\frac{\partial\vec{u}_x}{\partial x}dydz-\int_{\Gamma^W}\lambda\frac{\partial\vec{u}_y}{\partial y}dydz-\int_{\Gamma^W}\lambda\frac{\partial\vec{u}_z}{\partial z}dydz\end{aligned} \tag{3.21}$$

For $\vec{\sigma}_{xy}$ holds:

$$\int_{\Gamma^N}(\vec{\sigma}_{xy})dxdz - \int_{\Gamma^S}(\vec{\sigma}_{xy})dxdz = \int_{\Gamma^N}\mu\frac{\partial\vec{u}_x}{\partial y}dxdz + \int_{\Gamma^N}\mu\frac{\partial\vec{u}_y}{\partial x}dxdz - \int_{\Gamma^S}\mu\frac{\partial\vec{u}_x}{\partial y}dxdz - \int_{\Gamma^S}\mu\frac{\partial\vec{u}_y}{\partial x}dxdz \tag{3.22}$$

For $\vec{\sigma}_{xz}$ holds:

$$\int_{\Gamma^T}(\vec{\sigma}_{xz})dxdy - \int_{\Gamma^B}(\vec{\sigma}_{xz})dxdy = \int_{\Gamma^T}\mu\frac{\partial\vec{u}_x}{\partial z}dxdy + \int_{\Gamma^T}\mu\frac{\partial\vec{u}_z}{\partial x}dxdy - \int_{\Gamma^B}\mu\frac{\partial\vec{u}_x}{\partial z}dxdy - \int_{\Gamma^B}\mu\frac{\partial\vec{u}_z}{\partial x}dxdy \tag{3.23}$$

In the y direction holds for $\vec{\sigma}_{yx}$:

$$\int_{\Gamma^E}(\vec{\sigma}_{yx})dydz - \int_{\Gamma^W}(\vec{\sigma}_{yx})dydz = \int_{\Gamma^E}\mu\frac{\partial\vec{u}_x}{\partial y}dydz + \int_{\Gamma^E}\mu\frac{\partial\vec{u}_y}{\partial x}dydz - \int_{\Gamma^W}\mu\frac{\partial\vec{u}_x}{\partial y}dydz - \int_{\Gamma^W}\mu\frac{\partial\vec{u}_y}{\partial x}dydz \tag{3.24}$$

For $\vec{\sigma}_{yy}$ holds:

$$\int_{\Gamma^N}(\vec{\sigma}_{yy})dxdz - \int_{\Gamma^S}(\vec{\sigma}_{yy})dxdz = \int_{\Gamma^N}\lambda\frac{\partial\vec{u}_x}{\partial x}dxdz + \int_{\Gamma^N}(\lambda+2\mu)\frac{\partial\vec{u}_y}{\partial y}dxdz + \int_{\Gamma^N}\lambda\frac{\partial\vec{u}_z}{\partial z}dxdz - \int_{\Gamma^S}\lambda\frac{\partial\vec{u}_x}{\partial x}dxdz - \int_{\Gamma^S}(\lambda+2\mu)\frac{\partial\vec{u}_y}{\partial y}dxdz - \int_{\Gamma^S}\lambda\frac{\partial\vec{u}_z}{\partial z}dxdz \tag{3.25}$$

Finally for $\vec{\sigma}_{yz}$ holds:

$$\int_{\Gamma^T}(\vec{\sigma}_{yz})dxdy - \int_{\Gamma^B}(\vec{\sigma}_{yz})dxdy = \int_{\Gamma^T}\mu\frac{\partial\vec{u}_y}{\partial z}dxdy + \int_{\Gamma^T}\mu\frac{\partial\vec{u}_z}{\partial y}dxdy - \int_{\Gamma^B}\mu\frac{\partial\vec{u}_y}{\partial z}dxdy - \int_{\Gamma^B}\mu\frac{\partial\vec{u}_z}{\partial y}dxdy \tag{3.26}$$

In the z direction $\vec{\sigma}_{zx}$ equals to:

$$\int_{\Gamma^E}(\vec{\sigma}_{zx})dydz - \int_{\Gamma^W}(\vec{\sigma}_{zx})dydz = \int_{\Gamma^E}\mu\frac{\partial\vec{u}_x}{\partial z}dydz + \int_{\Gamma^E}\mu\frac{\partial\vec{u}_z}{\partial x}dydz - \int_{\Gamma^W}\mu\frac{\partial\vec{u}_x}{\partial z}dydz - \int_{\Gamma^W}\mu\frac{\partial\vec{u}_z}{\partial x}dydz \tag{3.27}$$

For $\vec{\sigma}_{zy}$ holds:

$$\int_{\Gamma^N}(\vec{\sigma}_{zy})dxdz - \int_{\Gamma^S}(\vec{\sigma}_{zy})dxdz = \int_{\Gamma^N}\mu\frac{\partial\vec{u}_y}{\partial z}dxdz + \int_{\Gamma^N}\mu\frac{\partial\vec{u}_z}{\partial y}dxdz - \int_{\Gamma^S}\mu\frac{\partial\vec{u}_y}{\partial z}dxdz - \int_{\Gamma^S}\mu\frac{\partial\vec{u}_z}{\partial y}dxdz \tag{3.28}$$

Finally for $\vec{\sigma}_{zz}$ holds:

$$\int_{\Gamma^T}(\vec{\sigma}_{zz})dxdy - \int_{\Gamma^B}(\vec{\sigma}_{zz})dxdy = \int_{\Gamma^T}\lambda\frac{\partial\vec{u}_x}{\partial x}dxdy + \int_{\Gamma^T}\lambda\frac{\partial\vec{u}_y}{\partial y}dxdy + \int_{\Gamma^T}(\lambda+2\mu)\frac{\partial\vec{u}_z}{\partial z}dxdy - \int_{\Gamma^B}\lambda\frac{\partial\vec{u}_x}{\partial x}dxdy - \int_{\Gamma^B}\lambda\frac{\partial\vec{u}_y}{\partial y}dxdy - \int_{\Gamma^B}(\lambda+2\mu)\frac{\partial\vec{u}_z}{\partial z}dxdy \tag{3.29}$$

3.3.1. Trilinear shape functions

In three dimensions there are 8 interpolation functions for displacement, compared to two dimension where 4 are used. They are trilinear and they allow for convenient integration of the displacement and its derivatives over any interface, especially over finite volume control volumes.

$$\vec{u} \approx \sum_{i=1}^{8} \vec{u_i} N_i(x,y,z) \text{ in } \bar{\Omega}_i^{\boldsymbol{u}} \tag{3.30}$$

More analytically these 8 interpolators are expressed as follows:

$$N_1 = (1 - \frac{x}{dx})(1 - \frac{y}{dy})(1 - \frac{z}{dz}) \tag{3.31}$$

$$N_2 = (\frac{x}{dx})(1 - \frac{y}{dy})(1 - \frac{z}{dz}) \tag{3.32}$$

$$N_3 = (\frac{x}{dx})(\frac{y}{dy})(1 - \frac{z}{dz}) \tag{3.33}$$

$$N_4 = (1 - \frac{x}{dx})(\frac{y}{dy})(1 - \frac{z}{dz}) \tag{3.34}$$

$$N_5 = (1 - \frac{x}{dx})(1 - \frac{y}{dy})(\frac{z}{dz}) \tag{3.35}$$

$$N_6 = (\frac{x}{dx})(1 - \frac{y}{dy})(\frac{z}{dz}) \tag{3.36}$$

$$N_7 = (\frac{x}{dx})(\frac{y}{dy})(\frac{z}{dz}) \tag{3.37}$$

$$N_8 = (1 - \frac{x}{dx})(\frac{y}{dy})(\frac{z}{dz}) \tag{3.38}$$

Here dx, dy and dz are the length, the width and the height of the IV respectively and they are finite.

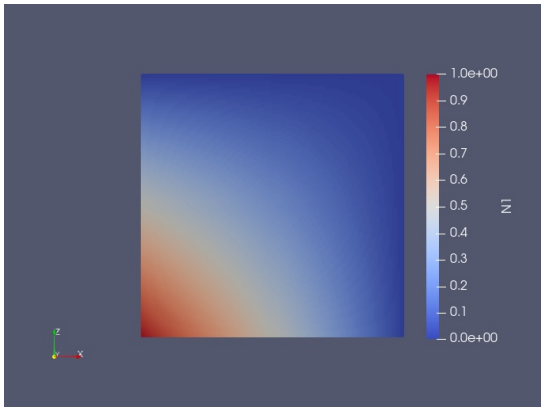

(a) N1 shape function in 3D

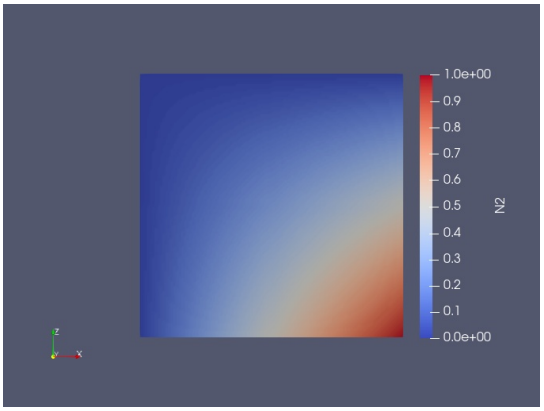

(b) N2 shape function in 3D

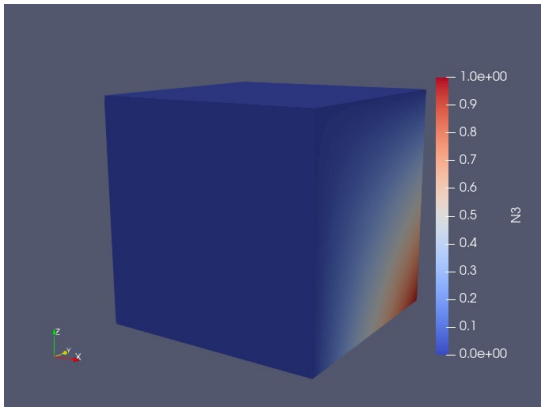

(c) N3 shape function in 3D

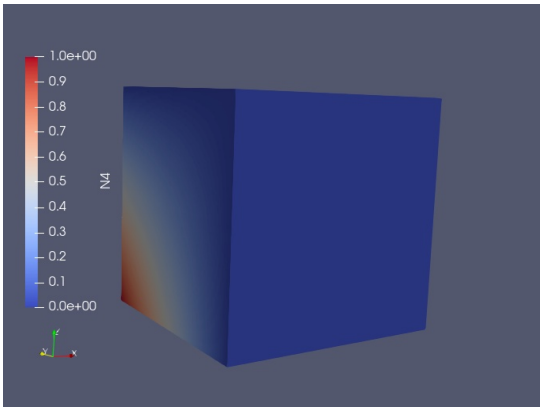

(d) N4 shape function in 3D

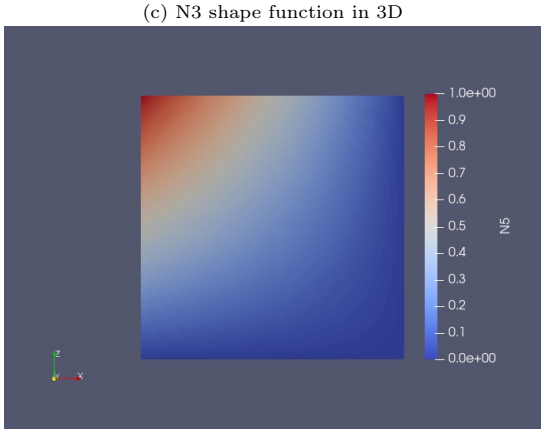

(e) N5 shape function in 3D

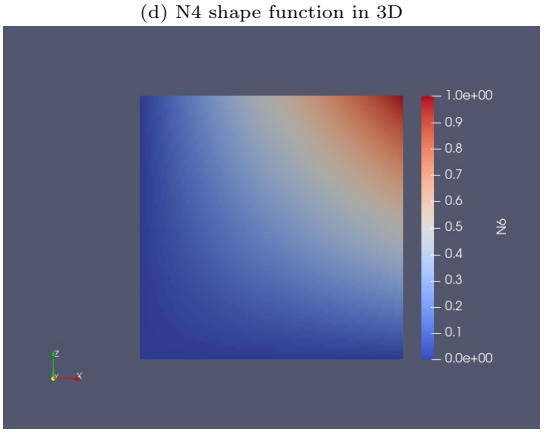

(f) N6 shape function in 3D

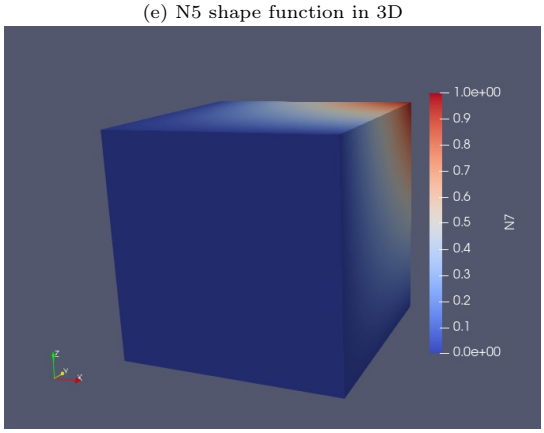

(g) N7 shape function in 3D

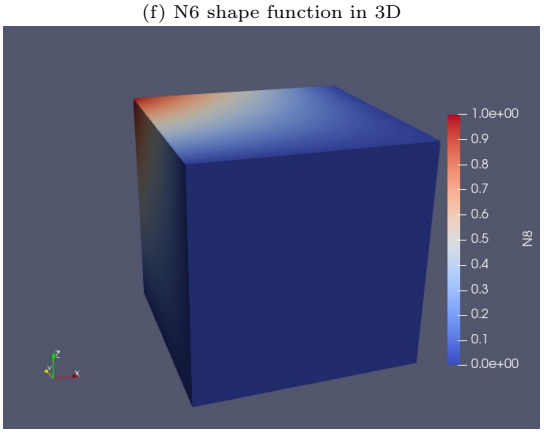

(h) N8 shape function in 3D

Figure 3.6: Shape functions in 3D.

Eq. 3.31 - 3.38 are represented in fig. 3.6a - 3.6h. It is observed that each shape function is equal to 1 in the node that is used to interpolate the displacement and equal to 0 in all the other nodes.

3.3.2. Integration over derivative displacements in 3D

Inside each IV e there are regions, which have to be defined.

In the x direction within an IV the area where $x \in [0, \frac{dx}{2}]$ is called West (W) and the area where $x \in [\frac{dx}{2}, dx]$ is called East (E). Then in the y direction the area where $y \in [0, \frac{dy}{2}]$ is called South (S) and the area where $y \in [\frac{dy}{2}, dy]$ is called North (N). Finally in the z direction the area where $z \in [0, \frac{dz}{2}]$ is called Bottom and the area where $z \in [\frac{dz}{2}, dz]$ is called Top (T).

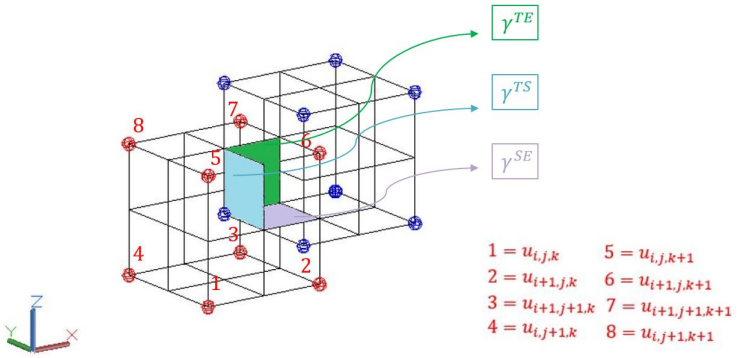

Figure 3.7: Stress control volume of $u_{i+1,j,k+1}$(cube with blue nodes) in the element control volume of $u_{i,j,k}$(cube with red nodes).

Fig. 3.7 shows an IV cube in which the red nodes in the corners stand for displacement nodes and it interacts with a stress control volume, presented as cube with blue nodes. Around each IV there are 8 stress control volumes. The area TS (Top - South) refers to the plane area, where $z \in [\frac{dz}{2}, dz]$ and $y \in [0, \frac{dy}{2}]$, perpendicular to the x direction. There are in total 12 areas, each one of which represents a surface, which is perpendicular to the third direction [8]. These areas play significant role in the integration in each IV, since in these areas are calculated the integrals of the displacements and their derivatives.

In fig. 3.7 are depicted three surfaces (one blue, one green and one purple), which represent three calculated double integrals, which show the contribution of $u_{i+1,j,k+1}$ to the f_x, f_y and to the f_z. The blue surface is calculated from the integration of the stresses that act on the yz plane (σ_{xx}, σ_{yx}, σ_{zx}), the green from the ones that act on the xz plane (σ_{xy}, σ_{yy}, σ_{zy}) and the purple one comes from the ones that act on the xy plane (σ_{xz}, σ_{yz}, σ_{zz}). The TE surface double integral refers to the surface integral inside the IV (green surface in fig. 3.7). The cube with the red corner nodes is the IV i, j, k, which is named after the lower left node. Eight displacement nodes are presented and each one of them contributes in f_x, f_y and in f_z.

Shape functions, as stated in eq. 3.31 - 3.38, are used to approximate the derivatives of the displacements in relationship 2.3 and to substitute stresses in eq. 3.21 - 3.29. For instance for the derivative of the displacement over x direction holds:

$$\frac{\partial \vec{u}}{\partial x} \approx \sum_{i=1}^{8} \vec{u_i} \frac{\partial N_i}{\partial x} \tag{3.39}$$

The analysis for the stress/displacement control volume of $u_{i+1,j,k+1}$ in the x direction is stated as:

$$\int_{\Gamma^W} \vec{\sigma_{xx}}\, dy\, dz = \int_{\gamma^T}\int_{\gamma^S} \vec{\sigma_{xx}}\, dy\, dz = \int_{\frac{dz}{2}}^{dz}\int_{0}^{\frac{dy}{2}} \vec{\sigma_{xx}}\, dy\, dz = -(\lambda+2\mu)\int_{\frac{dz}{2}}^{dz}\int_{0}^{\frac{dy}{2}} \frac{\partial \vec{u_x}}{\partial x}\, dy\, dz \tag{3.40}$$

$$-\lambda\int_{\frac{dz}{2}}^{dz}\int_{0}^{\frac{dy}{2}} \frac{\partial \vec{u_y}}{\partial y}\, dy\, dz - \lambda\int_{\frac{dz}{2}}^{dz}\int_{0}^{\frac{dy}{2}} \frac{\partial \vec{u_z}}{\partial z}\, dy\, dz$$

$$\int_{\Gamma^N} \vec{\sigma_{xy}}\, dx\, dz = \int_{\gamma^T}\int_{\gamma^E} \vec{\sigma_{xy}}\, dx\, dz = \int_{\frac{dz}{2}}^{dz}\int_{\frac{dx}{2}}^{dx} \vec{\sigma_{xy}}\, dx\, dz = \mu\left(\int_{\frac{dz}{2}}^{dz}\int_{\frac{dx}{2}}^{dx} \frac{\partial \vec{u_x}}{\partial y}\, dx\, dz + \int_{\frac{dz}{2}}^{dz}\int_{\frac{dx}{2}}^{dx} \frac{\partial \vec{u_y}}{\partial x}\, dx\, dz\right) \tag{3.41}$$

$$\int_{\Gamma^B} \vec{\sigma_{xz}}\, dx\, dy = \int_{\gamma^S}\int_{\gamma^E} \vec{\sigma_{xz}}\, dx\, dy = \int_{0}^{\frac{dy}{2}}\int_{\frac{dx}{2}}^{dx} \vec{\sigma_{xz}}\, dx\, dy = -\mu\left(\int_{0}^{\frac{dy}{2}}\int_{\frac{dx}{2}}^{dx} \frac{\partial \vec{u_x}}{\partial z}\, dx\, dy + \int_{0}^{\frac{dy}{2}}\int_{\frac{dx}{2}}^{dx} \frac{\partial \vec{u_z}}{\partial x}\, dx\, dy\right) \tag{3.42}$$

The analysis for the stress/displacement control volume of $u_{i+1,j,k+1}$ in the y direction is stated as:

$$\int_{\Gamma^W} \vec{\sigma_{yx}}\, dy\, dz = \int_{\gamma^T}\int_{\gamma^S} \vec{\sigma_{yx}}\, dy\, dz = \int_{\frac{dz}{2}}^{dz}\int_{0}^{\frac{dy}{2}} \vec{\sigma_{yx}}\, dy\, dz = -\mu\left(\int_{\frac{dz}{2}}^{dz}\int_{0}^{\frac{dy}{2}} \frac{\partial \vec{u_x}}{\partial y}\, dy\, dz + \int_{\frac{dz}{2}}^{dz}\int_{0}^{\frac{dy}{2}} \frac{\partial \vec{u_y}}{\partial x}\, dy\, dz\right) \tag{3.43}$$

$$\int_{\Gamma^N} \vec{\sigma_{yy}}\, dx\, dz = \int_{\gamma^T}\int_{\gamma^E} \vec{\sigma_{yy}}\, dx\, dz = \int_{\frac{dz}{2}}^{dz}\int_{\frac{dx}{2}}^{dx} \vec{\sigma_{yy}}\, dx\, dz = \lambda\int_{\frac{dz}{2}}^{dz}\int_{\frac{dx}{2}}^{dx} \frac{\partial \vec{u_x}}{\partial x}\, dx\, dz \tag{3.44}$$

$$+(\lambda+2\mu)\int_{\frac{dz}{2}}^{dz}\int_{\frac{dx}{2}}^{dx} \frac{\partial \vec{u_y}}{\partial y}\, dx\, dz + \lambda\int_{\frac{dz}{2}}^{dz}\int_{\frac{dx}{2}}^{dx} \frac{\partial \vec{u_z}}{\partial z}\, dx\, dz$$

$$\int_{\Gamma^B} \vec{\sigma_{yz}}\, dx\, dy = \int_{\gamma^S}\int_{\gamma^E} \vec{\sigma_{yz}}\, dx\, dy = \int_{0}^{\frac{dy}{2}}\int_{\frac{dx}{2}}^{dx} \vec{\sigma_{yz}}\, dx\, dy = -\mu\left(\int_{0}^{\frac{dy}{2}}\int_{\frac{dx}{2}}^{dx} \frac{\partial \vec{u_y}}{\partial z}\, dx\, dy + \int_{0}^{\frac{dy}{2}}\int_{\frac{dx}{2}}^{dx} \frac{\partial \vec{u_z}}{\partial y}\, dx\, dy\right) \tag{3.45}$$

The analysis for the stress/displacement control volume of $u_{i+1,j,k+1}$ in the z direction is stated as:

$$\int_{\Gamma^W} \vec{\sigma_{zx}}\, dy\, dz = \int_{\gamma^T}\int_{\gamma^S} \vec{\sigma_{zx}}\, dy\, dz = \int_{\frac{dz}{2}}^{dz}\int_{0}^{\frac{dy}{2}} \vec{\sigma_{zx}}\, dy\, dz = -\mu\Big(\int_{\frac{dz}{2}}^{dz}\int_{0}^{\frac{dy}{2}} \frac{\partial \vec{u_x}}{\partial z}\, dy\, dz + \int_{\frac{dz}{2}}^{dz}\int_{0}^{\frac{dy}{2}} \frac{\partial \vec{u_z}}{\partial x}\, dy\, dz\Big) \tag{3.46}$$

$$\int_{\Gamma^N} \vec{\sigma_{zy}}\, dx\, dz = \int_{\gamma^T}\int_{\gamma^E} \vec{\sigma_{zy}}\, dx\, dz = \int_{\frac{dz}{2}}^{dz}\int_{\frac{dx}{2}}^{dx} \vec{\sigma_{zy}}\, dx\, dz = \mu\Big(\int_{\frac{dz}{2}}^{dz}\int_{\frac{dx}{2}}^{dx} \frac{\partial \vec{u_y}}{\partial z}\, dx\, dz + \int_{\frac{dz}{2}}^{dz}\int_{\frac{dx}{2}}^{dx} \frac{\partial \vec{u_z}}{\partial y}\, dx\, dz\Big) \tag{3.47}$$

$$\int_{\Gamma^B} \vec{\sigma_{zz}}\, dx\, dy = \int_{\gamma^S}\int_{\gamma^E} \vec{\sigma_{zz}}\, dx\, dy = \int_{0}^{\frac{dy}{2}}\int_{\frac{dx}{2}}^{dx} \vec{\sigma_{zz}}\, dx\, dy = -\lambda \int_{0}^{\frac{dy}{2}}\int_{\frac{dx}{2}}^{dx} \frac{\partial \vec{u_x}}{\partial x}\, dx\, dy - \lambda \int_{0}^{\frac{dy}{2}}\int_{\frac{dx}{2}}^{dx} \frac{\partial \vec{u_y}}{\partial y}\, dx\, dy \tag{3.48}$$

$$-(\lambda + 2\mu) \int_{0}^{\frac{dy}{2}}\int_{\frac{dx}{2}}^{dx} \frac{\partial \vec{u_z}}{\partial z}\, dx\, dy$$

The displacements are expressed with the linear interpolation (eq. 3.30) of the shape functions (eq. 3.31 - 3.38). For instance in eq. 3.40 the first term is calculated as follows:

$$\int_{\Gamma^W} \frac{\partial \vec{u_x}}{\partial x}\, dy\, dz = \int_{\gamma^T}\int_{\gamma^S} \frac{\partial \vec{u_x}}{\partial x}\, dy\, dz = \int_{\frac{dz}{2}}^{dz}\int_{0}^{\frac{dy}{2}} \frac{\partial \vec{u_x}}{\partial x}\, dy\, dz = \int_{\frac{dz}{2}}^{dz}\int_{0}^{\frac{dy}{2}} \frac{\partial \vec{u_x}}{\partial x}\, dy\, dz \tag{3.49}$$

$$= \frac{dy\, dz}{dx}\left[-\frac{3}{64}, \frac{3}{64}, \frac{1}{64}, -\frac{1}{64}, -\frac{9}{64}, \frac{9}{64}, \frac{3}{64}, -\frac{3}{64}\right][u_1, u_2, u_3, u_4, u_5, u_6, u_7, u_8]^{\mathsf{T}}$$

The rest of the coefficients, which are calculated and fill eq. 3.21 - 3.29 are presented in sections A.3.1, A.3.2 and A.3.3. There are in total 36 double integrals to be calculated, since there are 3 planes, each one of which has 4 possible integrals and the derivatives of the shape functions and their displacement are over x, y and z direction.

3.3.3. Linear system of equations in 3D FVM

The 3D mechanical deformation system is described as follows:

$$\underbrace{\begin{bmatrix} \boldsymbol{A_{xx}} & \boldsymbol{A_{xy}} & \boldsymbol{A_{xy}} \\ \boldsymbol{A_{yx}} & \boldsymbol{A_{yy}} & \boldsymbol{A_{yz}} \\ \boldsymbol{A_{zx}} & \boldsymbol{A_{zy}} & \boldsymbol{A_{zz}} \end{bmatrix}}_{\boldsymbol{A}} \underbrace{\begin{bmatrix} \vec{u_x} \\ \vec{u_y} \\ \vec{u_z} \end{bmatrix}}_{\vec{u}} = \underbrace{\begin{bmatrix} \vec{f_x} \\ \vec{f_y} \\ \vec{f_z} \end{bmatrix}}_{\vec{f}} \tag{3.50}$$

In the system the unknown is the displacement, the A matrix consists of the weight of the displacements, which are the calculated coefficients from the double integrals of the shape functions for each corner of an IV. The right hand side is the source vector. After elastic deformation computation, stress can be calculated from eq. 2.3.

4

Numerical modelling for 3D FEM

4.1. Discretization

The problem formulation starts with the same assumptions of linear elasticity theory in eq. 2.2.

After applying Gauss divergence theorem in eq. 2.2 and expressing effective stress in terms of displacement according to eq. 2.3, the final discrete form for each element control volume [19] is:

$$\int_{\Omega_e} (\boldsymbol{B}^T \boldsymbol{C_{dr}} \boldsymbol{B} \vec{u}_e) dV = \int_{\Omega_e} \boldsymbol{N}^T \vec{f} dV, \tag{4.1}$$

where $\vec{u}$ is the nodal in each element control volume dV, Ω_e is the control volume of each element, $\vec{f}$ are the volumetric forces and $\boldsymbol{B}$ is the matrix that contains the derivatives of the shape functions.

Shape functions are expressed in terms of local coordinates as follows:

$$\boldsymbol{N} \approx \frac{1}{8}(1 \pm \xi)(1 \pm \eta)(1 \pm \zeta) \qquad -1 \leq \xi, \eta, \zeta \leq 1 \tag{4.2}$$

and the $\boldsymbol{B}$ is given by

$$\boldsymbol{B} = \begin{bmatrix} \frac{\partial}{\partial x} & 0 & 0 \\ 0 & \frac{\partial}{\partial y} & 0 \\ 0 & 0 & \frac{\partial}{\partial z} \\ 0 & \frac{\partial}{\partial z} & \frac{\partial}{\partial y} \\ \frac{\partial}{\partial z} & 0 & \frac{\partial}{\partial x} \\ \frac{\partial}{\partial y} & \frac{\partial}{\partial x} & 0 \end{bmatrix} \boldsymbol{N}, \tag{4.3}$$

where

From eq. 4.1 the element stiffness matrix is stated as:

$$\boldsymbol{A}_e = \int_{\Omega_e} \boldsymbol{B}^T \boldsymbol{C_{dr}} \boldsymbol{B} dV \tag{4.4}$$

and the element load vector is stated as:

$$\vec{f}_e = \int_{\Omega_e} \vec{f} dV \tag{4.5}$$

4.1.1. Element integration

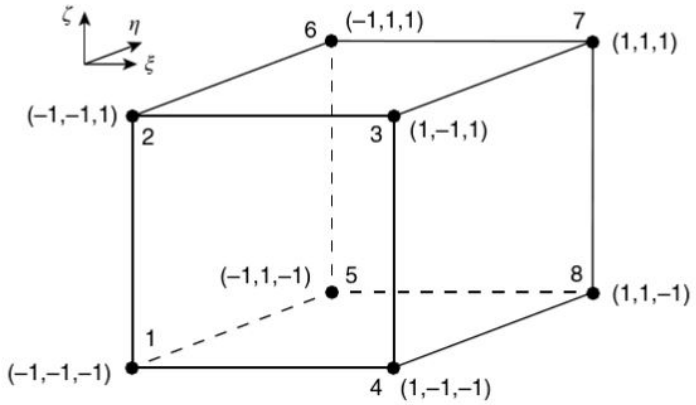

Figure 4.1: Hexaedron element with eight corner nodes in the local coordinate system(ξ, η, ζ [24]).

The element matrices $\boldsymbol{A}_e$ and the element load vector $\vec{f}_e$ the shape functions or their derivatives, which are integrated over the volume represented by finite hexahedra. The integrals are computed numerically with the use of Gauss-Legendre quadrature [24]. The rule in 3D is stated as:

$$\int_{\Omega_e} f(\xi,\eta,\zeta)dV = \int_{-1}^{1}\int_{-1}^{1}\int_{-1}^{1} f(\xi,\eta,\zeta)d\xi d\eta d\zeta \simeq \sum_{i=1}^{nipx}\sum_{j=1}^{nipy}\sum_{m=1}^{nipz} f(\xi_i,\eta_j,\zeta_m)w_i w_j w_m \tag{4.6}$$

$$= \sum_{k=1}^{nip} f(\xi_k,\eta_k,\zeta_k)w_k, \tag{4.7}$$

where ξ, η and ζ are local coordinates on the normalized volume $[-1,1]^3$. The $nipx$, $nipy$ and $nipz$ are the integration points in x, y and z direction respectively and nip is the total number of integration points. Also w_i, w_j and w_m are the weights in the positions ξ_i, η_j and ζ_m in each direction in local coordinates and w_k are the weights in the ξ_k, η_k and ζ_k of all the integrated points in local coordinates. The shape functions (fig. 4.1) and their derivatives in local coordinate system have to be rescaled to present element integrals in physical coordinates.

The derivatives of the shape functions with respect to local coordinates are given below:

$$\frac{\partial N_1}{\partial \xi} = -\frac{1}{8}(1-\eta)(1-\zeta) \qquad \frac{\partial N_1}{\partial \eta} = -\frac{1}{8}(1-\xi)(1-\zeta) \qquad \frac{\partial N_1}{\partial \zeta} = -\frac{1}{8}(1-\xi)(1-\eta) \tag{4.8}$$

$$\frac{\partial N_2}{\partial \xi} = -\frac{1}{8}(1-\eta)(1+\zeta) \qquad \frac{\partial N_2}{\partial \eta} = -\frac{1}{8}(1-\xi)(1+\zeta) \qquad \frac{\partial N_2}{\partial \zeta} = \frac{1}{8}(1-\xi)(1-\eta) \tag{4.9}$$

$$\frac{\partial N_3}{\partial \xi} = \frac{1}{8}(1-\eta)(1+\zeta) \qquad \frac{\partial N_3}{\partial \eta} = -\frac{1}{8}(1+\xi)(1+\zeta) \qquad \frac{\partial N_3}{\partial \zeta} = \frac{1}{8}(1+\xi)(1-\eta) \tag{4.10}$$

$$\frac{\partial N_4}{\partial \xi} = \frac{1}{8}(1-\eta)(1-\zeta) \qquad \frac{\partial N_4}{\partial \eta} = -\frac{1}{8}(1+\xi)(1-\zeta) \qquad \frac{\partial N_4}{\partial \zeta} = -\frac{1}{8}(1+\xi)(1-\eta) \tag{4.11}$$

$$\frac{\partial N_5}{\partial \xi} = -\frac{1}{8}(1+\eta)(1-\zeta) \qquad \frac{\partial N_5}{\partial \eta} = \frac{1}{8}(1-\xi)(1-\zeta) \qquad \frac{\partial N_5}{\partial \zeta} = -\frac{1}{8}(1-\xi)(1+\eta) \tag{4.12}$$

$$\frac{\partial N_6}{\partial \xi} = -\frac{1}{8}(1+\eta)(1+\zeta) \qquad \frac{\partial N_6}{\partial \eta} = \frac{1}{8}(1-\xi)(1+\zeta) \qquad \frac{\partial N_6}{\partial \zeta} = \frac{1}{8}(1-\xi)(1+\eta) \tag{4.13}$$

$$\frac{\partial N_7}{\partial \xi} = \frac{1}{8}(1+\eta)(1+\zeta) \qquad \frac{\partial N_7}{\partial \eta} = \frac{1}{8}(1+\xi)(1+\zeta) \qquad \frac{\partial N_7}{\partial \zeta} = \frac{1}{8}(1+\xi)(1+\eta) \tag{4.14}$$

$$\frac{\partial N_8}{\partial \xi} = \frac{1}{8}(1+\eta)(1-\zeta) \qquad \frac{\partial N_8}{\partial \eta} = \frac{1}{8}(1+\xi)(1-\zeta) \qquad \frac{\partial N_8}{\partial \zeta} = -\frac{1}{8}(1+\xi)(1+\eta) \tag{4.15}$$

The transformation from the local (ξ, η, ζ) to the physical coordinate system (x, y, z) is done with the use of chain rule:

$$\begin{bmatrix} \frac{\partial}{\partial \xi} \\ \frac{\partial}{\partial \eta} \\ \frac{\partial}{\partial \zeta} \end{bmatrix} \boldsymbol{N} = \begin{bmatrix} \frac{\partial x}{\partial \xi} & \frac{\partial y}{\partial \xi} & \frac{\partial z}{\partial \xi} \\ \frac{\partial x}{\partial \eta} & \frac{\partial y}{\partial \eta} & \frac{\partial z}{\partial \eta} \\ \frac{\partial x}{\partial \zeta} & \frac{y}{\partial \zeta} & \frac{\partial z}{\partial \zeta} \end{bmatrix} \begin{bmatrix} \frac{\partial}{\partial x} \\ \frac{\partial}{\partial y} \\ \frac{\partial}{\partial z} \end{bmatrix} \boldsymbol{N} = \boldsymbol{J} \begin{bmatrix} \frac{\partial}{\partial x} \\ \frac{\partial}{\partial y} \\ \frac{\partial}{\partial z} \end{bmatrix} \boldsymbol{N} \tag{4.16}$$

The Jacobian matrix $\boldsymbol{J}$ in eq. 4.16 can be found by differentiating the global coordinates with respect to the local coordinates.

$$\boldsymbol{J} = \begin{bmatrix} \frac{\partial N_1}{\partial \xi} & \frac{\partial N_2}{\partial \xi} & \cdots & \frac{\partial N_8}{\partial \xi} \\ \frac{\partial N_1}{\partial \eta} & \frac{\partial N_2}{\partial \eta} & \cdots & \frac{\partial N_8}{\partial \eta} \\ \frac{\partial N_1}{\partial \zeta} & \frac{\partial N_2}{\partial \zeta} & \cdots & \frac{\partial N_8}{\partial \zeta} \end{bmatrix} \begin{bmatrix} x_1 & y_1 & z_1 \\ x_2 & y_2 & z_2 \\ \vdots & \vdots & \vdots \\ x_8 & y_8 & z_8 \end{bmatrix}, \tag{4.17}$$

where in the above equation x_1, y_1, z_1 are the coordinates of node 1 and so on. The derivatives of the shape functions in terms of physical coordinates are expressed as:

$$\begin{bmatrix} \frac{\partial}{\partial x} \\ \frac{\partial}{\partial y} \\ \frac{\partial}{\partial z} \end{bmatrix} \boldsymbol{N} = \boldsymbol{J}^{-1} \begin{bmatrix} \frac{\partial}{\partial \xi} \\ \frac{\partial}{\partial \eta} \\ \frac{\partial}{\partial \zeta} \end{bmatrix} \boldsymbol{N} \tag{4.18}$$

Transformation of the limits of integration is carried out using the determinant of the Jacobian $|\boldsymbol{J}|$, according to the following relationship:

$$\int_{\Omega} \vec{f}(x,y,z)dxdydz = \int_{-1}^{1}\int_{-1}^{1}\int_{-1}^{1} f(\xi,\eta,\zeta)|\boldsymbol{J}|d\xi d\eta d\zeta, \tag{4.19}$$

which is written in terms of integration points as:

$$\int_{\Omega} \vec{f}(x,y,z)dxdydz = \sum_{k=1}^{nip} \boldsymbol{f}(\xi_k,\eta_k,\zeta_k)|\boldsymbol{J}|w_k \tag{4.20}$$

, where nip is the number of the integration points ,ξ_k, η_k, ζ_k are the local coordinates in terms of integration points and w_k is the weight in a specific integration point [24].

4.1.2. Linear system of equations in 3D FEM

After assembling the formulation for each element and integrating in the global coordinate system the global stiffness matrix is given as:

$$\boldsymbol{A} = \int_{\Omega} \boldsymbol{B}^T \boldsymbol{C_{dr}} \nabla \boldsymbol{B} dxdydz = \int_{\Omega_e} \boldsymbol{B}^T \boldsymbol{C_{dr}} \nabla \boldsymbol{B} |\boldsymbol{J}| d\xi d\eta d\zeta \tag{4.21}$$

$$\underbrace{\begin{bmatrix} \boldsymbol{A_{xx}} & \boldsymbol{A_{xy}} & \boldsymbol{A_{xy}} \\ \boldsymbol{A_{yx}} & \boldsymbol{A_{yy}} & \boldsymbol{A_{yz}} \\ \boldsymbol{A_{zx}} & \boldsymbol{A_{zy}} & \boldsymbol{A_{zz}} \end{bmatrix}}_{\boldsymbol{A}} \underbrace{\begin{bmatrix} \vec{u_x} \\ \vec{u_y} \\ \vec{u_z} \end{bmatrix}}_{\vec{u}} = \underbrace{\begin{bmatrix} \vec{f_x} \\ \vec{f_y} \\ \vec{f_z} \end{bmatrix}}_{\vec{f}_{\text{global}}}, \tag{4.22}$$

where $\vec{f_x}$, $\vec{f_y}$ and $\vec{f_z}$ are transformed to the global load vectors as suggested in eq. 4.20. After the computation of the elastic deformation in 4.22, the stress can be evaluated as eq. 2.3 suggests.

5

Numerical results for 3D FVM

In this chapter are presented the numerical results that concern about the 3D FVM model and the comparison with the results from 2D FVM and 3D FEM models. Firstly, results for mechanical equilibrium test case are presented, so as to show the consistency of the 3D FVM model. Furthermore, uniaxial compression test case is carried out for 2D FVM, 3D FVM, 3D FEM models in order to compare them.

The last two test cases that are presented in this chapter (Plain strain subsidence test case and vertical fault in an infinite reservoir test case), are simulated with 2D FVM, 3D FVM and with 3D FEM. The 3D models are used as 2D and this is achieved by reducing significantly the length of the domain in the y direction. In the 3D models the matrices of displacements and of the stresses are 3D, but the same along the y direction and we can plot them as 2D. For these two test cases, whenever a plot is derived from a three dimensional simulator and is plotted as surface is because the property stays the same along y direction. So the resolution of all the graphs is reported in 2D. This allows the immediate comparison between the 2D and the 3D simulators.

5.1. Synthetic solution for mechanical equilibrium

The consistency of the 3D FVM method is checked with synthetic analytical solutions. The analytical solutions are applied as exact solutions in the boundaries of the domain and the functionality of the solver is tested by calculating the error between the analytical and the numerical solution. The analytical solutions are given as follows:

$$\vec{u_x} = 10^{-5} \sin(\pi \frac{x}{L}) \sin(\pi \frac{y}{W}) \sin(\pi \frac{z}{H}) \tag{5.1}$$

$$\vec{u_y} = 10^{-5} \cos(\pi \frac{L-x}{L}) \sin(\pi \frac{y}{W}) \sin(\pi \frac{z}{H}) \tag{5.2}$$

$$\vec{u_z} = 10^{-5} \sin(\pi \frac{x}{L}) \sin(\pi \frac{y}{W}) \cos(\pi \frac{H-z}{H}), \tag{5.3}$$

where x, y and z are Cartesian coordinates and L, W and Z are domain's length, width and height respectively. A homogeneous medium is considered with $L = W = H = 1$ m and with elastic parameters $\lambda = 3 \times 10^8$ Pa and $\mu = 1.5 \times 10^8$ Pa.

5.1.1. Boundary conditions for mechanical equilibrium

The governing equation that describes the boundary conditions is stated as:

$$\text{Prescribed boundary displacement:} \quad \vec{u_\Gamma} = \vec{u} \quad \text{on} \quad \Gamma^B \cup \Gamma^T \cup \Gamma^W \cup \Gamma^E \cup \Gamma^S \cup \Gamma^N \tag{5.4}$$

5.1.2. Error analysis for mechanical equilibrium

The momentum balance equation expressed in terms of displacement is 2^{nd} order partial differential equation with respect to space, so it is expected that the error analysis to give second order accuracy [18, 21]. For the error analysis the second norm is used as follows:

$$\epsilon = \sqrt{\int_{\Omega} (u_{analytical} - u_{numerical})^2 dV}, \tag{5.5}$$

where dV is the volume of each element in which the difference between the analytical and the numerical solution is calculated [19]. The error as shown in eq. 5.5 is calculated for grid resolutions $10 \times 10 \times 10$, $20 \times 20 \times 20$ and $40 \times 40 \times 40$ number of elements in x y and z direction respectively.

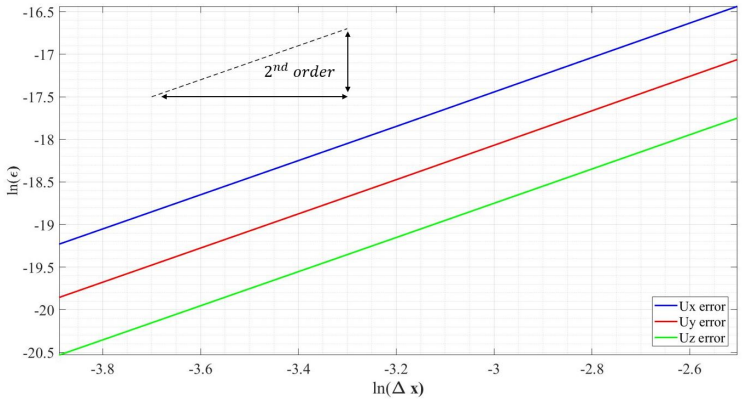

Figure 5.1: Error refinement analysis for mechanical equilibrium for $10, 20, 40$ elements in each direction. The displacement solutions in x y and z directions are 2^{nd} order accurate in space.

The error analysis that is presented in fig. 5.1 shows that the displacement solutions in x, y and z direction are 2^{nd} order accurate in space in the calculation of elastic deformation [18, 21].

Here is presented also another way of estimating the difference between numerical and analytical solution with the use of scaled - L^{∞} [27] as follows:

$$\epsilon = \frac{\|x_{ref} - x\|_{\infty}}{\|x_{ref}\|_{\infty}}, \tag{5.6}$$

where x_{ref} is the analytical solution, x is the numerical solution .

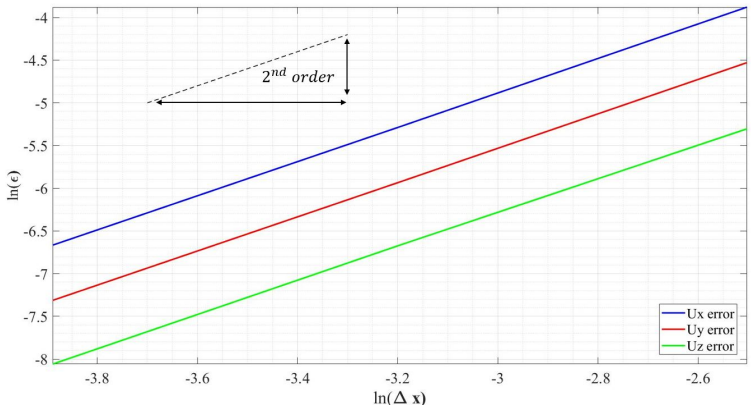

Figure 5.2: Error refinement analysis for mechanical equilibrium for $10, 20, 40$ elements in each direction. The displacement solutions in x y and z directions are 2^{nd} order accurate in space.

The error analysis with eq. 5.6 confirms that displacement solutions in x, y and z direction are 2^{nd} order accurate in space.

5.2. Uniaxial compression

In this section the simple uxiaxial compression is applied for testing the functionality of the 3D model. The domain is subjected to rollers constrains at north, east, south, west boundaries, whereas in the top boundary, which is traction-free, is applied compressive force equal to $5 \times 10^5 \frac{N}{m^2}$. The bottom boundary is set to have 0 displacement ("glued").

For comparison the same boundary conditions are applied in a 3D FEM and in a 2D FVM model. In the 2D FVM model east, west boundaries are subjected to roller boundary conditions, the north boundary is traction-free and south boundary is set to have displacement 0 ("glued"). The compressive force in the vertical direction is equal to $5 \times 10^5 \frac{N}{m^2}$. In the 3D as well as in the 2D models the lengths in each direction are 1 [m]. The compressive force is applied as Neumann boundary condition in the north boundary in 2D and in top boundary in 3D, is called traction ($\vec{t}$).

5.2.1. Boundary conditions for uniaxial compression

The set of govening equations, which describe the boundary conditions for this test case In two dimensions they are given as follows:

Roller constraints	$\vec{u} \cdot \vec{n} = 0$	on	$\Gamma^W \cup \Gamma^E$	(5.7)
Prescribed boundary displacement:	$\vec{u_\Gamma} = 0$	on	Γ^S	(5.8)
Prescribed boundary traction:	$\vec{\sigma} \cdot \vec{n} = \vec{t}$	on	Γ^N	(5.9)

and in three dimensions as:

Roller constraints	$\vec{u} \cdot \vec{n} = 0$	on	$\Gamma^W \cup \Gamma^E \cup \Gamma^S \cup \Gamma^N$	(5.10)
Prescribed boundary displacement:	$\vec{u_\Gamma} = 0$	on	Γ^B	(5.11)
Prescribed boundary traction:	$\vec{\sigma} \cdot \vec{n} = \vec{t}$	on	Γ^T	(5.12)

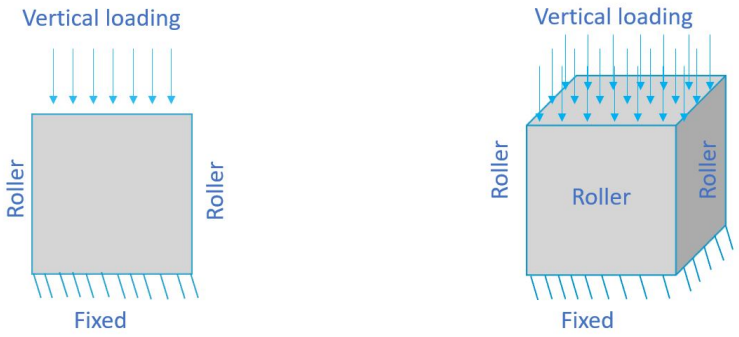

Figure 5.3: Schematic in 2D and 3D uniaxial compression.

The boundary conditions presented in eq. 5.7 - 5.9 for 2D and in eq. 5.10 - 5.12 for 3D are shown schematically in fig. 5.3.

5.2.2. Numerical results for uniaxial compression

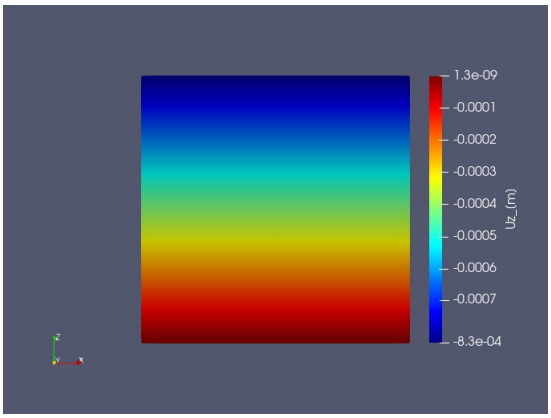

(a) FVM 3D, Displacement in z direction [m]

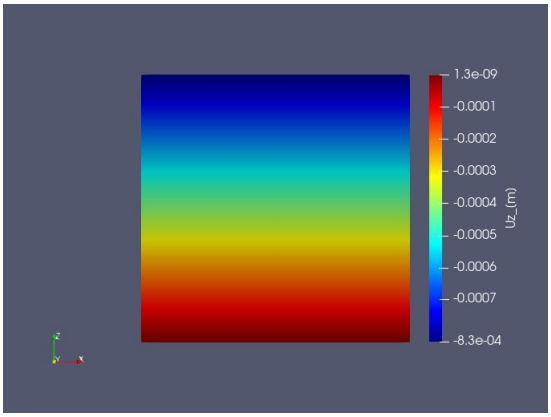

(b) FEM 3D, Displacement in z direction [m]

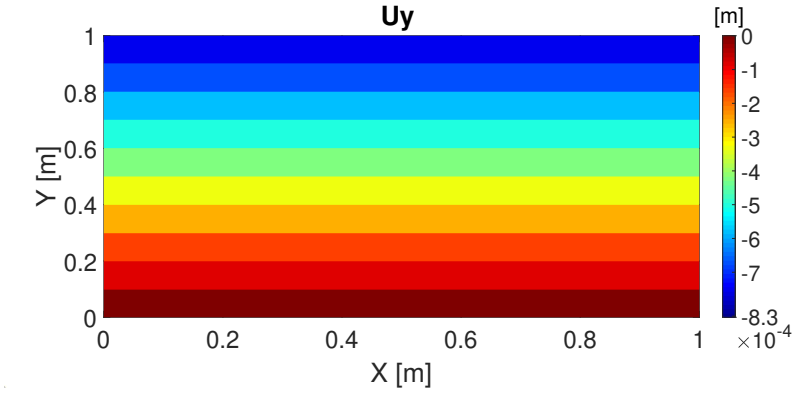

(c) FVM 2D, Displacement in y direction [m]

Figure 5.4: Displacement in vertical direction in uniaxial compression. Resolution of 3D FEM: $\mathbf{10 \times 10 \times 10}$, 3D FVM: $\mathbf{10 \times 10 \times 10}$, 2D FVM: $\mathbf{10 \times 10}$.

As it is observed from fig. 5.4a, 5.4b and 5.4c the three different methods give the same solution, which is negative in the vertical direction (y for 2D, z for 3D). The domain is subjected to compression and the maximum negative value is exactly 8.33×10^{-4} m.

5.2.3. Error analysis for uniaxial compression

In order to quantify the difference between the three methods in the compression test case, we calculate the difference of the displacement solutions in vertical direction between the 3D FVM and the 3D FEM and also between the 3D FVM and the 2D FVM. Since compression is actually one dimensional test

case the matrices of the vertical displacements are the same along x and y direction in 3D and along x direction in 2D.

$$\epsilon = \sqrt{(uz_{\text{(3D FVM)}} - uz_{\text{(3D FEM)}})^2} = 1.12 \times 10^{-16} \tag{5.13}$$

$$\epsilon = \sqrt{(uz_{\text{(3D FVM)}} - uy_{\text{(2D FVM)}})^2} = 5.79 \times 10^{-18} \tag{5.14}$$

5.3. Plain strain subsidence test case

The injection or production from a porous medium can cause subsidence. In the following test case the subsurface is considered as heterogeneous porous medium in which the elastic properties vary in the z direction[27]. For that reason a 3D problem can be reduced to 2D under plain strain conditions. The producing reservoir is 120 m thick and 1200 m wide. The modelled domain has dimensions 10 km is x direction and 3 km in y direction. The reservoir top is located at 1000 m depth. The distribution of Young's modulus in the subsurface is obtained based on a constitutive model for one-dimensional vertical compressibility, developed in [6] for the northern Adriatic sedimentary basin. The model that this study concerns is the Adriatic sedimentary basin in which the vertical uniaxial compressibility is related to the vertical effective stress σ_y as follows:

$$c_M = 0.01241|\sigma_y|^{-1.1342}, \tag{5.15}$$

where y is the vertical offset in [m] c_M and σ_y are expressed in [bar^{-1}] and bar respectively and the vertical effective stress is obtained as superposition of total vertical stress $\sigma_y^{'}$ and hydrostatic pressure p [3, 14] as follows:

$$\sigma_y = \sigma_y^{'} + p = \underbrace{-0.12218|y|^{1.0766}}_{\sigma_y^{'}} + \underbrace{0.1|y|}_{p} \tag{5.16}$$

It needs to be mentioned here that for 2D FVM model, vertical direction is considered the y and according to that the literature eq. 5.15, 5.16 are expressed as in Nicola Castelletto et al. paper [3]. In the 3D FVM and 3D FEM models the z is considered the vertical direction. The equations are not duplicated here for the z direction, so as to avoid confusion.

The Poisson's ratio is $\nu = 0.3$ for the whole geological section. Thus the Young's modulus E, is expressed as a function of depth as:

$$\frac{(1-2\nu)(1+\nu)}{(1-\nu)c_M} \tag{5.17}$$

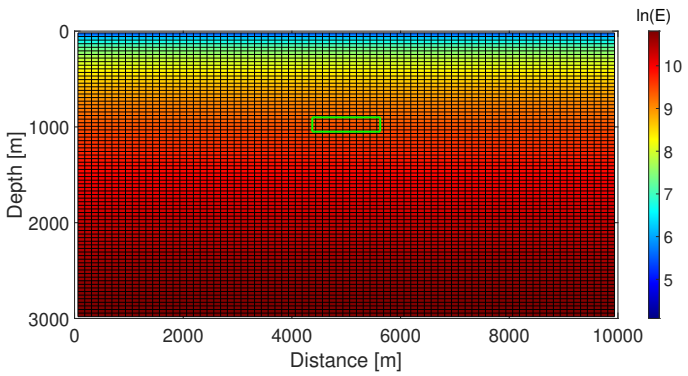

Figure 5.5: Plain strain subsidence test case: Young's modulus (E) distribution. Resolution: 80×80.

As shown in fig. 5.5 the reservoir (green box) is located exactly in the middle of the domain. The white spaces denote that E is assigned in the cell centers as all of the elastic parameters. Since uniaxial compressibility is calculated in [bar^{-1}], Young's modulus is calculated in [bar]. The total pressure drop is 100 bars in the reservoir, which is fully depleted.

5.3.1. Boundary conditions for plain strain subsidence test case

The domain is subjected to roller constrains at all boundaries, except from the north boundary in 2D and top boundary in 3D, where constant loading is applied [3, 27].

For two dimensions the set of governing equations that describe the boundary conditions [3] are stated as:

$$\text{Roller constraints} \quad \vec{u} \cdot \vec{n} = 0 \quad \text{on} \quad \Gamma^S \cup \Gamma^W \cup \Gamma^E \tag{5.18}$$

$$\text{Traction free} \quad \vec{\sigma} \cdot \vec{n} = 0 \quad \text{on} \quad \Gamma^N \tag{5.19}$$

For three dimensions the set of governing equations that describe the above boundary conditions are stated as:

$$\text{Roller constraints} \quad \vec{u} \cdot \vec{n} = 0 \quad \text{on} \quad \Gamma^B \cup \Gamma^W \cup \Gamma^E \cup \Gamma^S \cup \Gamma^N \tag{5.20}$$

$$\text{Traction free} \quad \vec{\sigma} \cdot \vec{n} = 0 \quad \text{on} \quad \Gamma^T \tag{5.21}$$

Figure 5.6: Schematic in 2D and 3D plain strain subsidence.

The boundary conditions presented in eq, 5.18, 5.19 for 2D and in eq. 5.20, 5.21 for 3D are shown schematically in fig. 5.6.

5.3.2. Numerical results for plain strain subsidence

From equations 5.15,5.16 and 5.17 it is clear that Young's modulus depends on the vertical offset y, which changes with depth.

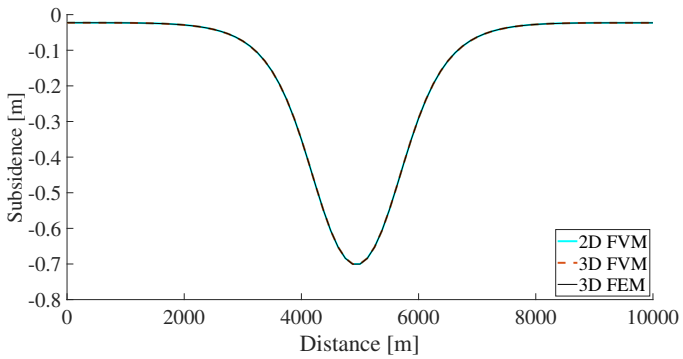

Figure 5.7: Plain strain subsidence test case: Comparison FEM-FVM in fine scale. Resolution of 3D FEM: Resolution: 80×80, 3D FVM: 80×80, 2D FVM: 80×80.

In fig. 5.7 is shown the subsidence, which corresponds to the case when Young's modulus distribution is as depicted in fig. 5.5. The finite element and the finite volume method predict the same subsidence.

Proceeding, we change the location of the reservoir, which is shifted in such a way to stop in the middle of the domain in x direction and still be in the same depth. This is the first of the three new cases that we study in which the Young's modulus distribution depends again on eq. 5.15, 5.16 and 5.17. Moreover we study two other test cases in which the vertical effective stress σ_y depends on the following relationships:

$$\sigma_y = \sigma_y^{'} + p = \underbrace{-0.12218|100 - y|^{1.0766}}_{\sigma_y^{'}} + \underbrace{0.1|100 - y|}_{p} \tag{5.22}$$

$$\sigma_y = \sigma_y^{'} + p = \underbrace{-0.12218|100 + y|^{1.0766}}_{\sigma_y^{'}} + \underbrace{0.1|100 + y|}_{p} \tag{5.23}$$

In eq. 5.22 the vertical offset is 100 - initial vertical offset y and in eq. 5.23 the vertical offset is 100 + initial vertical offset y. This of course will have impact on the E distribution with depth as shown in the following figures. The change in the vertical offset, which results in different Young's modulus distribution is a result of the presence of a vertical fault in the geological section.

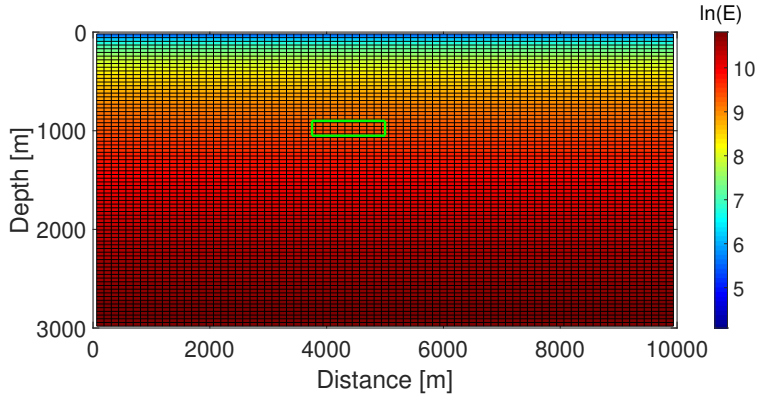

(a) Base case

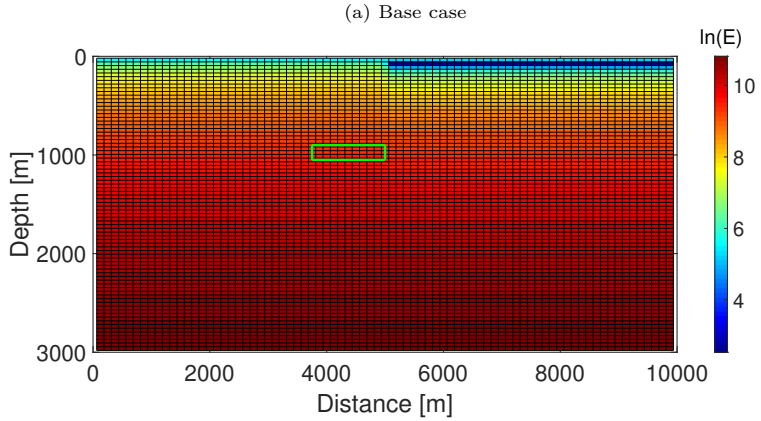

(b) $100 - |y|$

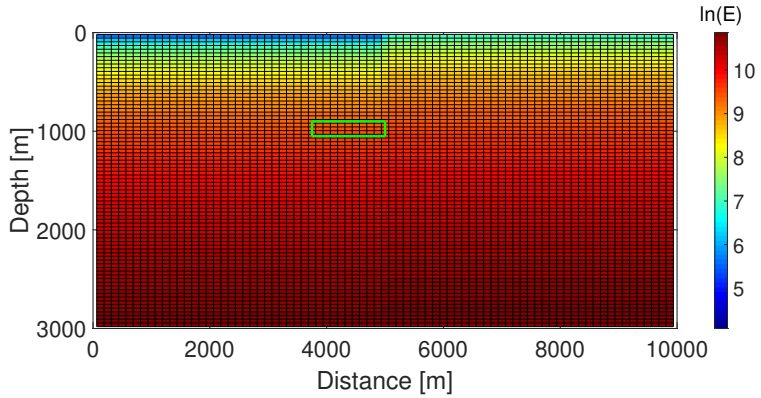

(c) $100 + |y|$

Figure 5.8: Plain strain subsidence test case: Young's modulus (E) distribution in the geological section. Resolution: 80×80.

In fig. 5.8a, 5.8b, 5.8c is observed the variation of Young's modulus E with depth in a logarithmic scale. In fig. 5.8a Young's Modulus changes as eq. 5.15,5.16 and 5.17 suggest. In fig. 5.8b we have 100 - vertical offset in [m] [3]. Finally in fig. 5.8c we have 100 + vertical offset in meters [3]. These changes in the Young's modulus distribution result in greater heterogeneity.

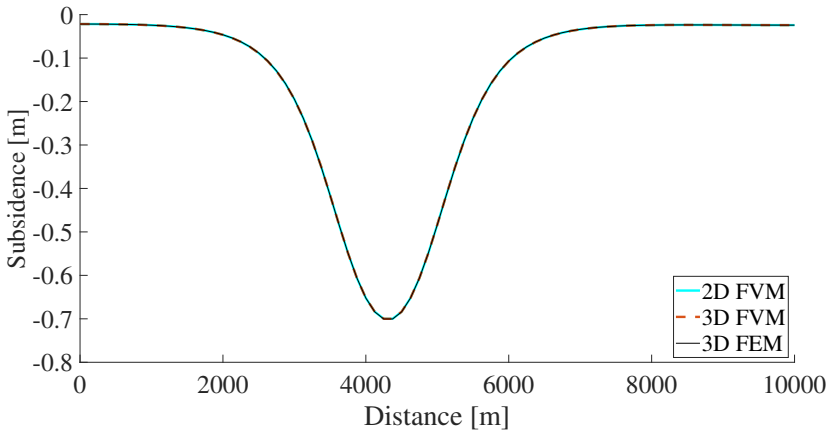

(a) Base case

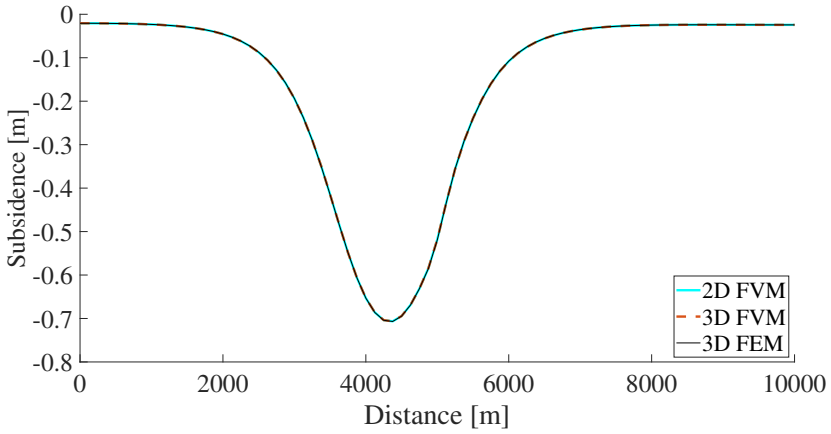

(b) $100 - |y|$

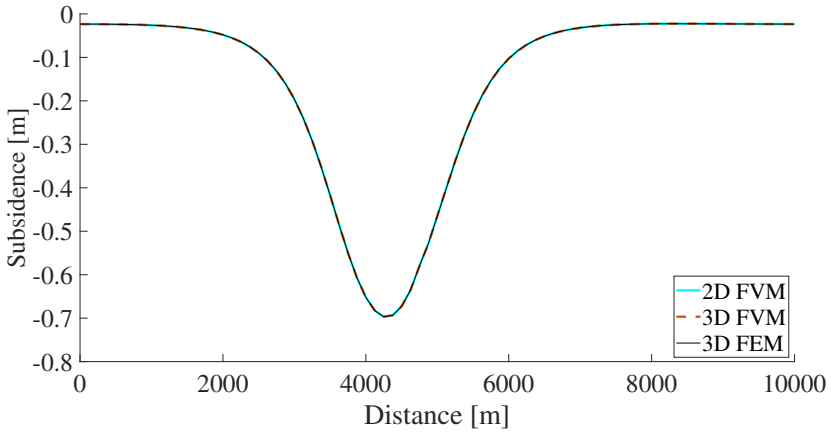

(c) $100 + |y|$

Figure 5.9: Plain strain subsidence test case: Comparison FEM-FVM in fine scale. Resolution of 3D FEM: 80×80, 3D FVM: 80×80, 2D FVM: 80×80.

From fig. 5.7, 5.9a, 5.9b and 5.8c it is deduced that finite element and finite volume method predict the subsidence.

Method	Subsidence maximum value [m]
FVM 2D	−0.7000
FVM 3D	−0.7000
FEM 3D	−0.7003

Table 5.1: Maximum subsidence value for each method

For the cases presented in fig. 5.7 and in fig. 5.9a the maximum value of the subsidence for each method is provided in table 5.1. In both cases the methods predict the same subsidence since only the location of the reservoir changes.

Method	Subsidence maximum value [m]
FVM 2D	−0.7065
FVM 3D	−0.7065
FEM 3D	−0.7069

Table 5.2: Maximum subsidence value for each method

Method	Subsidence maximum value [m]
FVM 2D	−0.6964
FVM 3D	−0.6964
FEM 3D	−0.6969

Table 5.3: Maximum subsidence value for each method

Tables 5.2 and 5.3 show the maximum values for the subsidence for each method for the cases presented in fig. 5.9b and 5.9c respectively.

The maximum subsidence is observed for the case in fig. 5.9b, as shown in table 5.2, since the medium, in the right half of the domain has 100 - vertical offset in [m]. The cases in fig. 5.7 and in fig. 5.9a have slightly lower subsidence, as shown also in table 5.1, since the vertical offset is the original one.

Finally, the least subsidence is predicted in the case in fig. 5.9c, since the right half of the domain has 100 + vertical offset in [m], which makes the medium stiffer than medium in the cases in fig. 5.7, 5.9a and 5.9b.

5.3.3. Stress calculation for plain strain subsidence test case

The stresses are calculated numerically with eq. 2.3 for all the above cases. Here the stresses are presented for the case that Young's modulus follows the distribution as depicted in fig. 5.8a and the subsidence is as shown in fig. 5.9a, where the reservoir stops in the middle of the domain in x direction and is located in 1000 m depth.

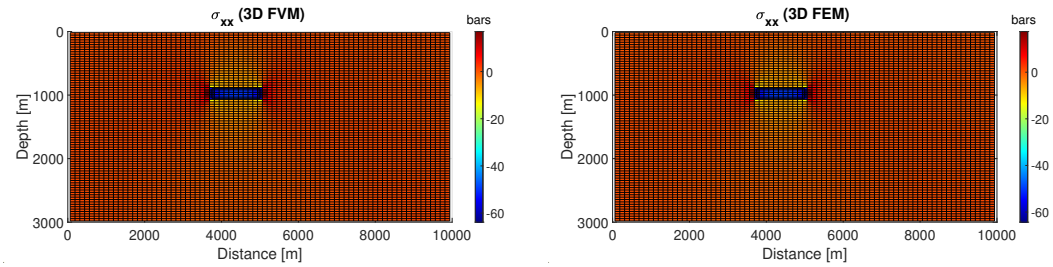

(a) 3D FVM numerical stress solution in horizontal direction (principal stress)

(b) 3D FEM numerical stress solution in horizontal direction (principal stress)

Figure 5.10: Plain strain subsidence test case: stresses calculated in fine scale with 3D FVM - 3D FEM with resolution : 80×80.

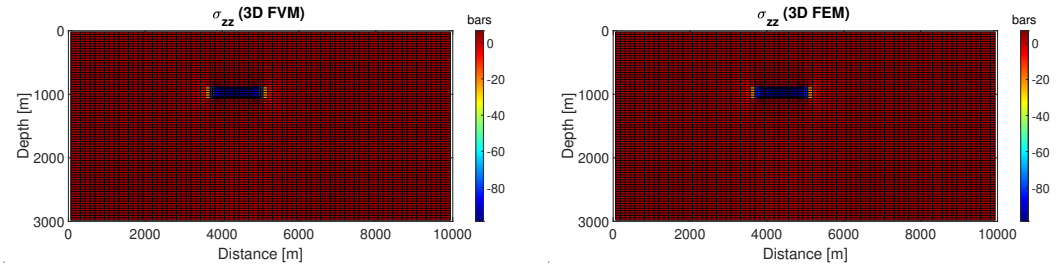

(a) 3D FVM numerical stress solution in vertical direction (principal stress)

(b) 3D FEM numerical stress solution in vertical direction (principal stress)

Figure 5.11: Plain strain subsidence test case: stresses calculated in fine scale with 3D FVM - 3D FEM with resolution : 80×80.

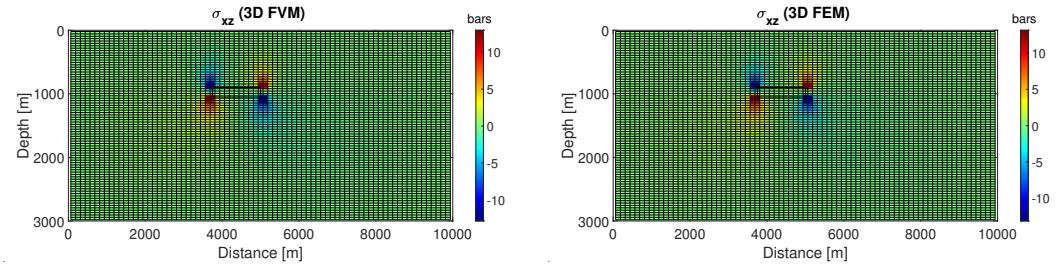

(a) 3D FVM numerical shear stress solution

(b) 3D FEM numerical shear stress solution

Figure 5.12: Plain strain subsidence test case: stresses calculated in fine scale with 3D FVM - 3D FEM with resolution : 80×80.

In fig. 5.10, 5.11 and 5.12 the results concern about the comparison between finite volume and finite element method in three dimensions. It is observed that the stress values in x and z direction do not exceed the initial pressure drop, which was 100 bars. The white spaces in fig. 5.10 - 5.12 exist because the stresses in the numerical approach are assigned in cell centers, contrary to the displacement, which are assigned in the cell vertices.

5.4. Vertical fault in an infinite reservoir test case

Consider a homogeneous porous and permeable inclusion Ω with boundary Γ undergoing an increase of pore pressure p inside a homogeneous infinite 3D domain with the same elastic properties as the inclusion. Flow to or from the outer domain is not possible, either because the outer domain is non-permeable or because there is an impermeable seal around the inclusion. An increase in pore pressure in the inclusion causes a reduction in effective stress in its matrix and consequently an elastic expansion of the inclusion [16]. The calculation of the computation of the displacements in and around the inclusion has been proposed by Eshelby [9].

After Biot [30] the three dimensional (3D) poroelasticity equations have been reproduced many times. Here it is considered an application of the theory in the form of 2D expressions for incremental displacements under plain strain conditions resulting from injection or production of fluids inside a reservoir. The inclusion Ω, which is formed from the fluid activity has the same elastic properties as the non-permeable infinite domain and they are uniform [16].

5.4.1. Reservoir geometry for vertical fault in an infinite reservoir test case

We deal with a reservoir with infinite boundaries and a vertical fault with the following geometry:

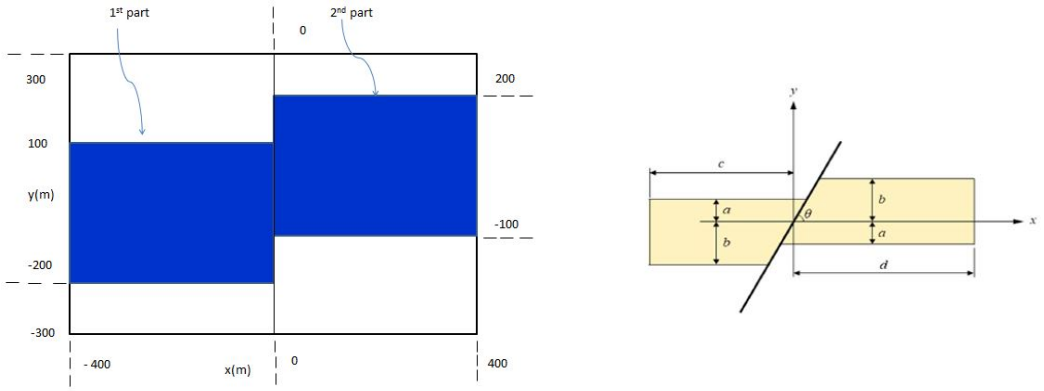

(a) Faulted reservoir (b) Reservoir with a displaced normal fault [16]

Figure 5.13: Reservoir geometry and dimensions.

From the fig. 5.13a and 5.13b we deduce the distances $\alpha = 100$ m, $b = 200$ m, while $c = d = inf$ and that $\theta = \frac{\pi}{2}$. The distance $b = 200$ m should not be confused with Biot's coefficient $b = 0.9$.

Property	Symbol	Property	Value
Poisson's ratio	v	0.15	[-]
Biot's coefficient	b	0.9	[-]
Lame's first parameter	λ	$2,78 \times 10^9$	[Pa]
Lame's second parameter	μ	$6,5 \times 10^9$	[Pa]
Incremental reservoir pressure	p	20×10^6	[Pa]

Table 5.4: Reservoir properties [16].

5.4.2. Pressure distribution in the boundaries of the reservoir for vertical fault in an infinite reservoir test case

It is assumed that there is uniform pressure distribution in the boundaries of the inclusion Ω and there is increase in the pore pressure, as a result of injection [16].

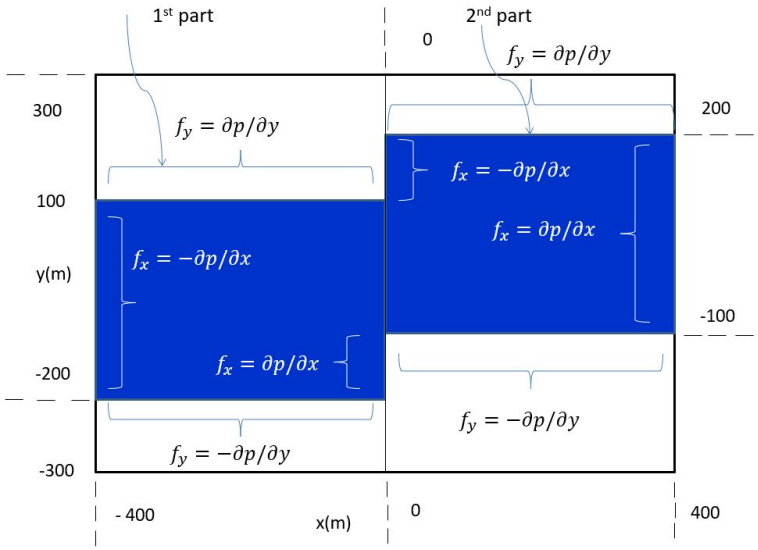

Figure 5.14: Distributed forces in the boundaries of the reservoir, due to the pressure increase.

The distributed pressure in the boundaries of the reservoir is added to the RHS and becomes part

of the force as suggested in eq. 3.1 and it is presented in fig. 5.14. For the simulation the reservoir is split in two boxes. When modelling the test case with 3D simulator, since the y direction is the reduced direction the force in y direction will be force in z direction $f_z = \pm\frac{\partial p}{\partial z}$ in fig. 5.14.

5.4.3. Analytical solutions for scaled displacements for vertical fault in an infinite reservoir test case

Linear elastic displacements, and stresses inside and outside a reservoir undergoing injection or production can be described with the "theory of inclusions" as introduced by Eshelby [9]. For that reason Green's functions $\tilde{g_{ij}}(x,y,z,\zeta,\xi,\psi)$, that give the displacement at point (x,y,z) in direction $i \in \{x,y,z\}$ as a result of a unit force at point (ζ,ξ,ψ) in direction $j \in \{x,y,z\}$. The x, y, z are Cartesian coordinates and the (ζ,ξ,ψ) are x, y, z coordinate values inside Ω.

The 2D plain strain version of the 3D Green's functions $\tilde{g_{ij}}(x,y,z,\zeta,\xi,\psi)$ can be obtained by integrating out the third (z) dimension, while taking account of the singularity at $(x,y,z) = (\zeta,\xi,\psi)$ [16].

The displacement is expressed as follows:

$$\vec{u_i}(x,y) = bp\int\limits_{\Omega_i^{\mathbf{u}}}\frac{\partial\vec{g_{ix}}}{\partial x} + \frac{\partial\vec{g_{iy}}}{\partial y}\delta\Omega = D\int\limits_{\Omega_i^{\mathbf{u}}}\vec{g}_i(x,y,\zeta,\xi)\delta\Omega, \tag{5.24}$$

where $\vec{g}_i(x,y,\zeta,\xi)$ are the Green's functions in x and y direction and b is the Biot's coefficient. The coefficient D is given by the formula:

$$D(\zeta,\xi) = \frac{(1-2v)bp}{2\pi(1-v)\mu}, \tag{5.25}$$

where v is the Poisson's ratio , μ is the shear modulus, b is the Biot's coefficient and p is the incremental pressure, which results from injection or production in the reservoir [16].

2D scaled analytical displacements relationships

For the case that we have an infinite reservoir with a vertical fault we have $c = d = \infty$, while $-c < x < d$, we find for the integral of g_x [16] .

$$\begin{aligned}\vec{G}_x(x,y) &= \int\limits_{-\infty}^{0}\int\limits_{-b}^{\alpha}\vec{g}_x(x,y,\zeta,\xi)\delta\xi\delta\zeta + \int\limits_{0}^{\infty}\int\limits_{-\alpha}^{b}\vec{g}_x(x,y,\zeta,\xi)\delta\xi\delta\zeta\\ &= \ln\left[x^2+(y-\alpha)^2\right]\times\frac{y-\alpha}{4} - \ln\left[x^2+(y-b)^2\right]\times\frac{y+b}{4}\\ &- \arctan 2\Big[\frac{(\alpha+b)x}{x^2+(y-\alpha)(y+b)}\Big]\times\frac{x}{2}\\ &+ \ln\left[x^2+(y+\alpha)^2\right]\times\frac{y+\alpha}{4} - \ln\left[x^2+(y-b)^2\right]\times\frac{y-b}{4}\\ &+ \arctan 2\Big[\frac{(\alpha+b)x}{x^2+(y-b)(y+\alpha)}\Big]\times\frac{x}{2}\end{aligned} \tag{5.26}$$

In a similar way the integral of g_y for an infinite reservoir is obtained as

$$\begin{aligned}\vec{G}_y(x,y) &= \ln\Big[\frac{x^2+(y-\alpha)^2}{x^2+(y-b)^2}\Big]\times\frac{x}{4}\\ &- \arctan 2\Big[\frac{(y-\alpha)}{x}\Big]\times\frac{y-\alpha}{2} + \arctan 2\Big[\frac{(y+b)}{x}\Big]\times\frac{y+b}{2}\\ &- \ln\Big[\frac{x^2+(y-b)^2}{x^2+(y+\alpha)^2}\Big]\times\frac{x}{4}\\ &+ \arctan 2\Big[\frac{(y+\alpha)}{-x}\Big]\times\frac{y+\alpha}{2} - \arctan 2\Big[\frac{(y-b)}{-x}\Big]\times\frac{y-b}{2}\end{aligned} \tag{5.27}$$

If the inclusion is Ω then the first part of the eq. 5.26 gives the Ω_{left} before the fault and the second part gives the Ω_{right} after the fault. The same holds for the eq. 5.27.

The parameters α and b are constants as shown in the fig. 5.13b, but their value (5.4) affects the scaled displacements in eq. 5.26, 5.27. Here again, the b distance should not be confused with Biot's coefficient.

A change in the sign of pressure affects the u_i in the 5.24, but not the G_i in the eq. 5.26 and 5.27. Also the positive value of pressure p, which is used in the definition of D in eq. 5.25 corresponds to injection in eq. 5.24 [16].

3D scaled analytical displacements relationships

In the three dimensional approach of the problem, the scaled displacement solutions are assumed as extensions of the eq. 5.26, 5.27. The third dimension will be part of the integration and equation 5.24 will take the form

$$\vec{u_i}(x,y,z) = bp \int\limits_{\Omega_i^{\mathbf{u}}} \frac{\partial \vec{g_{ix}}}{\partial x} + \frac{\partial \vec{g_{iy}}}{\partial y} + \frac{\partial \vec{g_{iz}}}{\partial z} \delta\Omega = D \int\limits_{\Omega_i^{\mathbf{u}}} \vec{g}_i(x,y,z,\zeta,\xi,\psi)\delta\Omega, \tag{5.28}$$

where $\vec{g}_i(x,y,z,\zeta,\xi,\psi)$ are the Green's functions in x, y and z direction, b is the Biot's coefficient and D is the scaling factor in order to converts the scaled displacements G_i into displacements u_i and is described in eq. 5.25. The integrals of the Green's functions are expressed as:

$$\begin{aligned}
\vec{G_x}(x,y,z) = &\int_{-\infty}^{0}\int_{-b}^{\alpha} \vec{g}_x(x,y,z,\zeta,\xi,\psi)\delta\psi\delta\xi\delta\zeta + \int_{0}^{\infty}\int_{-\alpha}^{b} \vec{g}_x(x,y,z,\zeta,\xi,\psi)\delta\psi\delta\xi\delta\zeta \\
&= \ln\left[x^2 + (z-\alpha)^2\right] \times \frac{z-\alpha}{4} - \ln\left[x^2 + (z-b)^2\right] \times \frac{z+b}{4} \\
&- \arctan 2\Big[\frac{(\alpha+b)x}{x^2 + (z-\alpha)(z+b)}\Big] \times \frac{x}{2} \\
&+ \ln\left[x^2 + (z+\alpha)^2\right] \times \frac{z+\alpha}{4} - \ln\left[x^2 + (z-b)^2\right] \times \frac{z-b}{4} \\
&+ \arctan 2\Big[\frac{(\alpha+b)x}{x^2 + (z-b)(z+\alpha)}\Big] \times \frac{x}{2}
\end{aligned} \tag{5.29}$$

As can be observed from eq. 5.29, the three dimensional analytical solution is the same as the two dimensional analytical solution for the scaled displacement in the x direction with the only difference that the Cartesian coordinates y from equation 5.26 are substituted with Cartesian coordinates z. In a similar way the integral of g_z for an infinite reservoir can be obtained as:

$$\begin{aligned}
\vec{G_z}(x,y,z) = &\ln\Big[\frac{x^2 + (z-\alpha)^2}{x^2 + (z-b)^2}\Big] \times \frac{x}{4} \\
&- \arctan 2\Big[\frac{(z-\alpha)}{x}\Big] \times \frac{z-\alpha}{2} + \arctan 2\Big[\frac{(z+b)}{x}\Big] \times \frac{z+b}{2} \\
&- \ln\Big[\frac{x^2 + (z-b)^2}{x^2 + (z+\alpha)^2}\Big] \times \frac{x}{4} \\
&+ \arctan 2\Big[\frac{(z+\alpha)}{-x}\Big] \times \frac{z+\alpha}{2} - \arctan 2\Big[\frac{(z-b)}{-x}\Big] \times \frac{z-b}{2}
\end{aligned} \tag{5.30}$$

In eq. 5.29, 5.30 the Green's functions depend only on x and z Cartesian coordinates, even if the equation is in 3 dimensions. This means that scaled displacements G_x and G_z have values only in x and z direction as result of the equations 5.29, 5.30. For the scaled displacement in y direction holds:

$$\vec{G_y}(x,y,z) = 0 \tag{5.31}$$

In the 3D FVM and in the 3D FEM the problem is reduced in y direction, so as to be simulated as 2D. As a result of that, the G_y analytical solution will be zero.

5.4.4. Analytical solutions for dimensionless stresses for vertical fault in an infinite reservoir test case

The analytical solutions for dimensionless stresses, which concern the geometry of the reservoir as presented in fig. 5.13a are given below [16]:

$$G_{xx}(x,y) = \arctan 2\Big[\frac{(\alpha+b)x}{x^2+(y-b)(y+\alpha)}\Big] - \arctan 2\Big[\frac{(\alpha+b)x}{x^2+(y-\alpha)(y+b)}\Big] \tag{5.32}$$

$$G_{yy}(x,y) = \arctan 2\Big[\frac{(y+\alpha)}{-x}\Big] - \arctan 2\Big[\frac{(y-b)}{-x}\Big] - \arctan 2\Big[\frac{(y-\alpha)}{x}\Big] + \arctan 2\Big[\frac{(y+b)}{x}\Big] \tag{5.33}$$

$$G_{xy}(x,y) = \frac{1}{2} \times \ln \frac{\big[x^2+(y-\alpha)^2\big]\big[x^2+(y+\alpha)^2\big]}{\big[x^2+(y-b)^2\big]\big[x^2+(y+b)^2\big]} \tag{5.34}$$

After the numerical calculation of displacement the stresses are calculated with the eq. 2.3. The dimensionless stresses are calculated from the following relationship:

$$G_{ij}(x,y) - 2\pi\delta_{\Omega} = \frac{\sigma_{ij}}{C}, \tag{5.35}$$

where the indexes i and j denote any direction of the stress, and C is a scaling parameter with magnitude $2.36 \times 10^6 N/m^2$ [16].

Relationship 5.35 allows the numerical evaluation of the dimensionless stresses G_{ij} and their comparison with the analytical ones, given in equations 5.32, 5.33 and 5.34.

5.4.5. Boundary conditions for vertical fault in an infinite reservoir test case

For two dimensions the governing equation that describes the boundary conditions is stated as:

$$\text{Prescribed boundary displacement:} \quad \vec{u_\Gamma} = \vec{u} \quad \text{on} \quad \Gamma^S \cup \Gamma^N \cup \Gamma^W \cup \Gamma^E \tag{5.36}$$

For three dimensions the governing equation that describes the boundary conditions is stated as:

$$\text{Prescribed boundary displacement:} \quad \vec{u_\Gamma} = \vec{u} \quad \text{on} \quad \Gamma^B \cup \Gamma^T \cup \Gamma^W \cup \Gamma^E \cup \Gamma^S \cup \Gamma^N \tag{5.37}$$

5.4.6. Numerical results for scaled displacements in vertical fault in an infinite reservoir test case

In this section the numerical results for the finite volume method in two and three directions and for the finite element method in three dimensions are plotted next to the analytical solutions that have been described in eq. 5.26, 5.27, 5.29, 5.30 and 5.31.

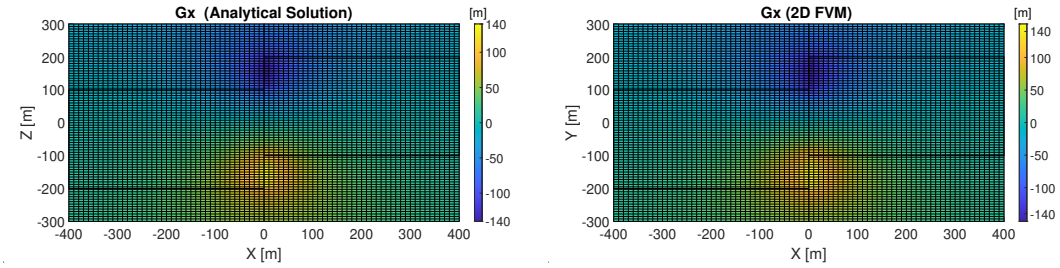

(a) Analytical solution of scaled displacement in x direction $\frac{u_x}{D}$ [m]

(b) Numerical solution of scaled displacement in x direction $\frac{u_x}{D}$ in 2D FVM [m]

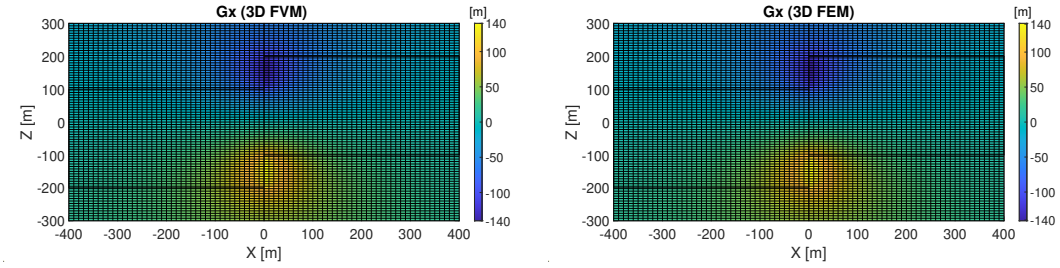

(c) Numerical solution of scaled displacement in x direction $\frac{u_x}{D}$ in 3D FVM [m]

(d) Numerical solution of scaled displacement in x direction $\frac{u_x}{D}$ in 3D FEM [m]

Figure 5.15: Comparison between analytical and numerical scaled displacements for FVM 2D, FVM 3D, FEM 3D with resolution : 80×80.

From the numerical results it is observed that scaled numerical solutions in x direction, presented in fig. 5.15b, 5.15c and 5.15d, agree with the analytical solution in x direction in fig. 5.15a. The horizontal displacements, shown in fig. 5.15 are concentrated in the areas where the reservoir rock juxtaposes the overburden and underburden [16].

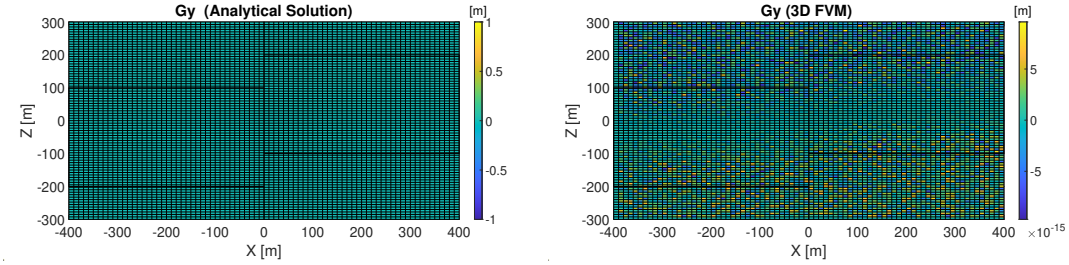

(a) Analytical solution of scaled displacement in y direction $\frac{u_y}{D}$ in 3D [m]

(b) Numerical solution of scaled displacement in y direction $\frac{u_y}{D}$ in 3D FVM [m]

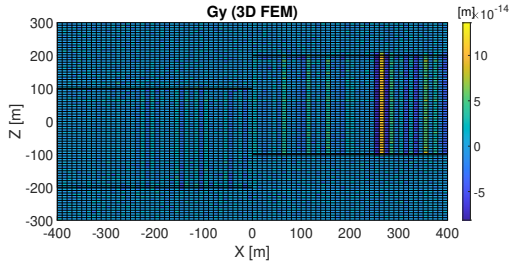

(c) Numerical solution of scaled displacement in y direction $\frac{u_y}{D}$ in 3D FEM [m]

Figure 5.16: Comparison between analytical and numerical scaled displacements for FVM 3D, FEM 3D with resolution : 80×80

The numerical solution in y direction (3D FVM - 3D FEM) in fig. 5.16b and 5.16c agree with the analytical solution in fig. 5.16a. This shows that the assumed analytical solution in y direction in eq. 5.31 results in a numerical solution, which is zero as well. The solutions G_y in fig. 5.16 concern only

the 3D FVM and the 3D FEM method.

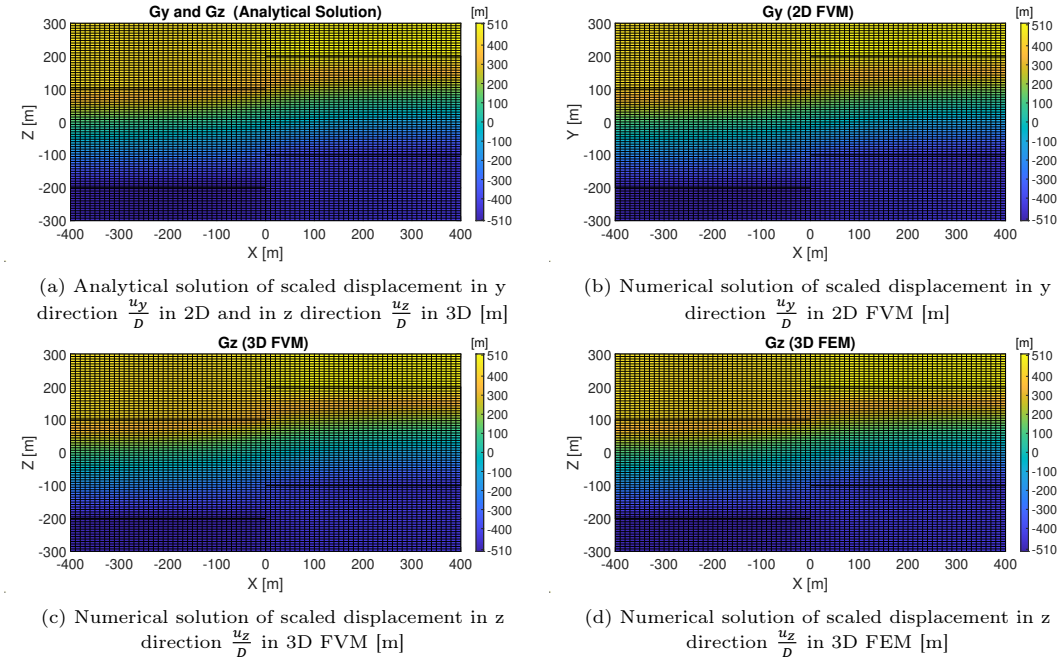

(a) Analytical solution of scaled displacement in y direction $\frac{u_y}{D}$ in 2D and in z direction $\frac{u_z}{D}$ in 3D [m]

(b) Numerical solution of scaled displacement in y direction $\frac{u_y}{D}$ in 2D FVM [m]

(c) Numerical solution of scaled displacement in z direction $\frac{u_z}{D}$ in 3D FVM [m]

(d) Numerical solution of scaled displacement in z direction $\frac{u_z}{D}$ in 3D FEM [m]

Figure 5.17: Comparison between analytical and numerical scaled displacements for FVM 2D, FVM 3D, FEM 3D with resolution : 80×80

The numerical solutions in y (2D FVM) and z direction (3D FVM - 3D FEM) presented in fig. 5.17b, 5.17c and 5.17d match as well with the analytical solution in fig. 5.17a. These vertical displacements, shown in fig. 5.17, are relatively smoothly following the throw of the fault [16].

5.4.7. Numerical results for dimensionless stresses in vertical fault in an infinite reservoir test case

In this section the numerical results for stresses for the finite volume in two and three dimensions as well as for the finite element method in three dimensions are presented next to the analytical solutions described in eq. 5.32, 5.33 and 5.34.

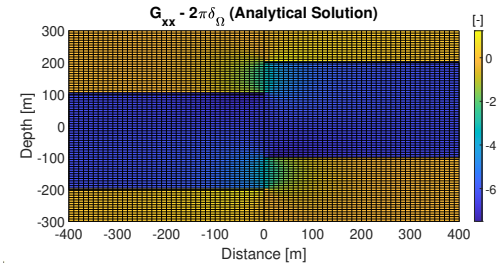

(a) Analytical solution of dimensionless horizontal stress $\frac{G_{xx}}{c}$ [-]

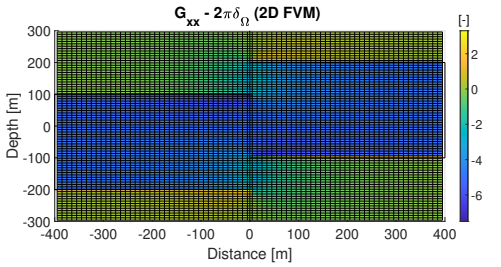

(b) Numerical solution of dimensionless horizontal stress $\frac{G_{xx}}{c}$ in 2D FVM [-]

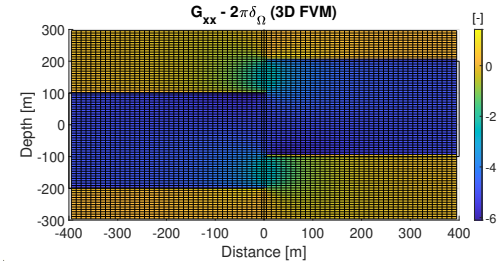

(c) Numerical solution of dimensionless horizontal stress $\frac{G_{xx}}{c}$ in 3D FVM [-]

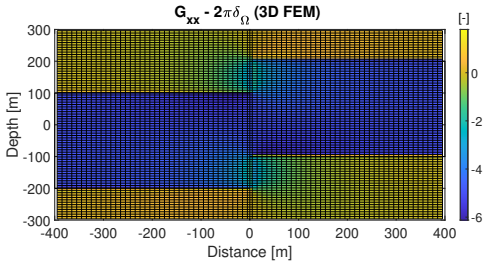

(d) Numerical solution of dimensionless horizontal stress $\frac{G_{xx}}{c}$ in 3D FEM [-]

Figure 5.18: Comparison between analytical and numerical dimensionless stresses for FVM 2D, FVM 3D, FEM 3D with resolution : 80×80

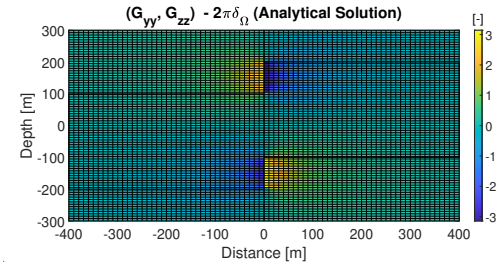

(a) Analytical solution of dimensionless vertical stress $\frac{G_{yy}}{c}$ in 2D and $\frac{G_{zz}}{c}$ in 3D [-]

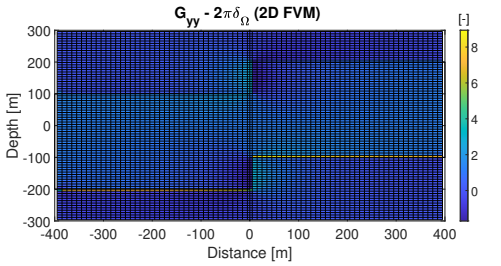

(b) Numerical solution of dimensionless vertical stress $\frac{G_{yy}}{c}$ in 2D FVM [-]

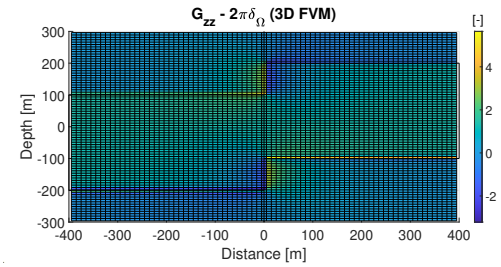

(c) Numerical solution of dimensionless vertical stress $\frac{G_{zz}}{c}$ in 3D FVM [-]

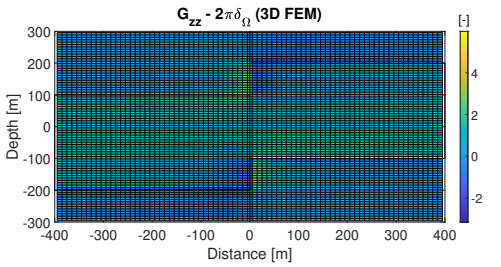

(d) Numerical solution of dimensionless vertical stress $\frac{G_{zz}}{c}$ in 3D FEM [-]

Figure 5.19: Comparison between analytical and numerical dimensionless stresses for FVM 2D, FVM 3D, FEM 3D with resolution : 80×80

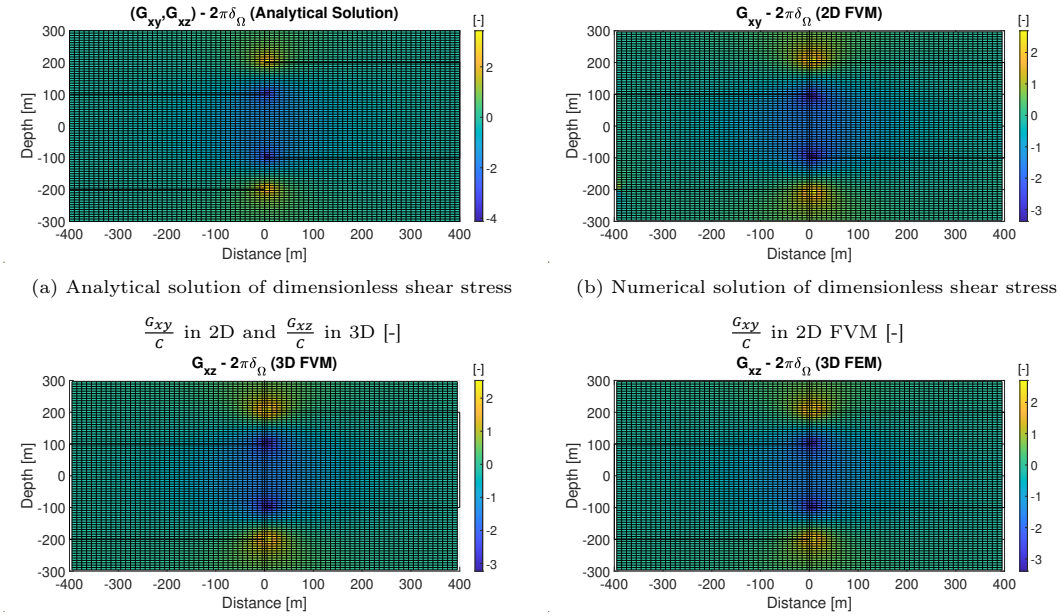

(a) Analytical solution of dimensionless shear stress $\frac{G_{xy}}{C}$ in 2D and $\frac{G_{xz}}{C}$ in 3D [-]

(b) Numerical solution of dimensionless shear stress $\frac{G_{xy}}{C}$ in 2D FVM [-]

(c) Numerical solution of dimensionless shear stress $\frac{G_{xz}}{C}$ in 3D FVM [-]

(d) Numerical solution of dimensionless shear stress $\frac{G_{xz}}{C}$ in 3D FEM [-]

Figure 5.20: Comparison between analytical and numerical dimensionless stresses for FVM 2D, FVM 3D, FEM 3D with resolution : 80×80

It is observed that fig. 5.18c, 5.19c and 5.20c of 3D FVM as well as the fig. 5.18d, 5.19d and 5.20d of the 3D FEM match to each other and to the analytical solutions in fig. 5.18a, 5.19a and 5.20a respectively. On the other hand fig. 5.18b, 5.19b and 5.20b of the 2D FVM show some differences, compared to the analytical solutions. The numerical calculation of the stresses, after the calculation of the displacements shows more obvious differences compared to the calculation of the numerical scaled displacements from the analytical scaled displacements.

The reason for this might be that we add another layer of approximation in our assumptions, as we calculate numerical dimensionless stresses, after the calculation of the scaled numerical displacements.

The biggest deviation from the analytical solutions is observed in the calculation of numerical vertical dimensionless stress G_{yy} in 2D and G_{zz} in 3D in fig. 5.19.

5.4.8. Error analysis in vertical fault in an infinite reservoir test case

In this section we refine the grid in order to observe the grid upon refinement. In order to check how accurate the solutions are in space, error analysis is conducted. Taylor's theorem [21] works accurately if the length of the domain is lower than the number of the elements, which are used to model the domain. For that cause we scale the dimensions of the domain making them 100 times lower. In eq. 5.26, 5.27, 5.29 and 5.30 it is clear that the scaled analytical solutions depend on the dimensions α and b. So when we scale the length and the width of the domain, α and b are also scaled and the displacement analytical solutions are re-scaled as well as the numerical ones. The re-scaled solutions are plotted below:

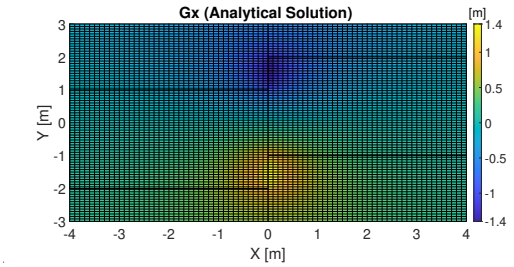

(a) Analytical solution of re-scaled displacement in x direction $\frac{u_x}{D}$ [m]

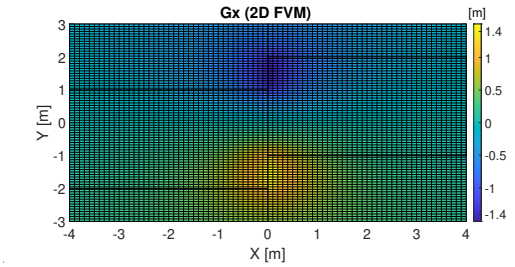

(b) Numerical solution of re-scaled displacement in x direction $\frac{u_x}{D}$ in 2D FVM [m]

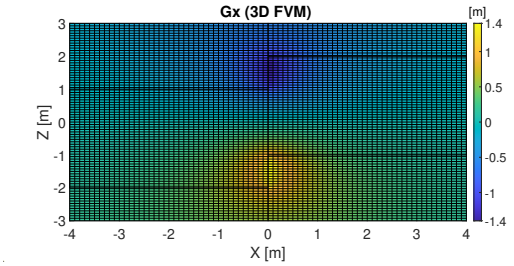

(c) Numerical solution of re-scaled displacement in x direction $\frac{u_x}{D}$ in 3D FVM [m]

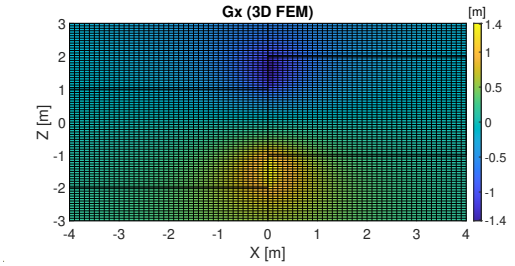

(d) Numerical solution of re-scaled displacement in x direction $\frac{u_x}{D}$ in 3D FEM [m]

Figure 5.21: Comparison between analytical and numerical re-scaled displacements for FVM 2D, FVM 3D, FEM 3D with resolution : 80×80

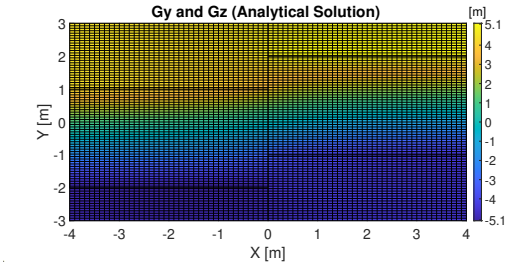

(a) Analytical solution of re-scaled displacement in y direction $\frac{u_y}{D}$ in 2D and in z direction $\frac{u_z}{D}$ in 3D [m]

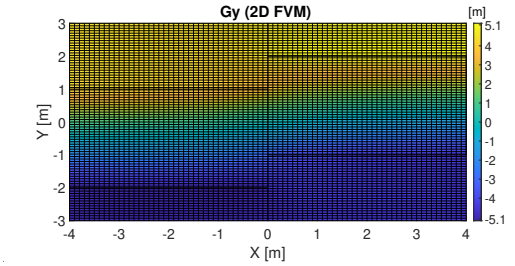

(b) Numerical solution of re-scaled displacement in y direction $\frac{u_y}{D}$ in 2D FVM [m]

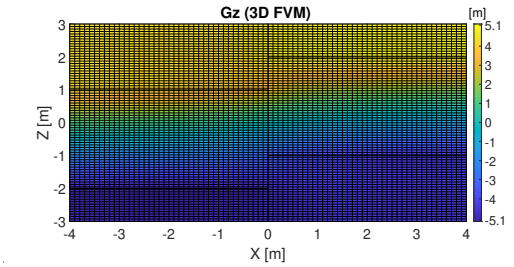

(c) Numerical solution of re-scaled displacement in z direction $\frac{u_z}{D}$ in 3D FVM [m]

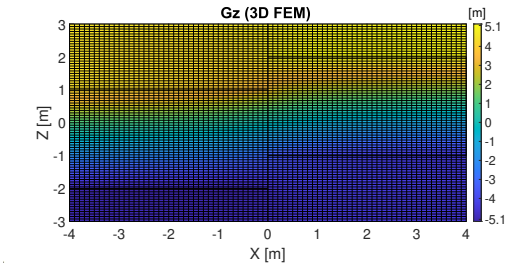

(d) Numerical solution of re-scaled displacement in z direction $\frac{u_z}{D}$ in 3D FEM [m]

Figure 5.22: Comparison between analytical and numerical re-scaled displacements for FVM 2D, FVM 3D, FEM 3D with resolution : 80×80

As it is observed from fig. 5.21 and 5.22, upon dividing the distances α and b by 100, the analytical and the numerical solutions are also divided by 100.

For the error analysis eq. 5.5 is used. For 2D FVM the error is calculated for grid resolutions $20 \times 20, 40 \times 40, 80 \times 80$ and 160×160 number of elements in x and y direction respectively. For 3D FVM and for 3D FEM the error is calculated for grid resolutions $20 \times 2 \times 20, 40 \times 2 \times 40, 80 \times 2 \times 80$ and $160 \times 2 \times 160$ number of elements in x y and z direction respectively.

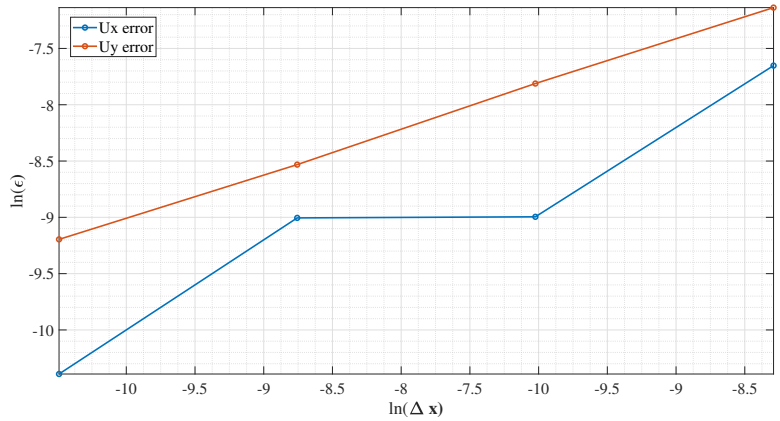

(a) FVM 2D Error analysis

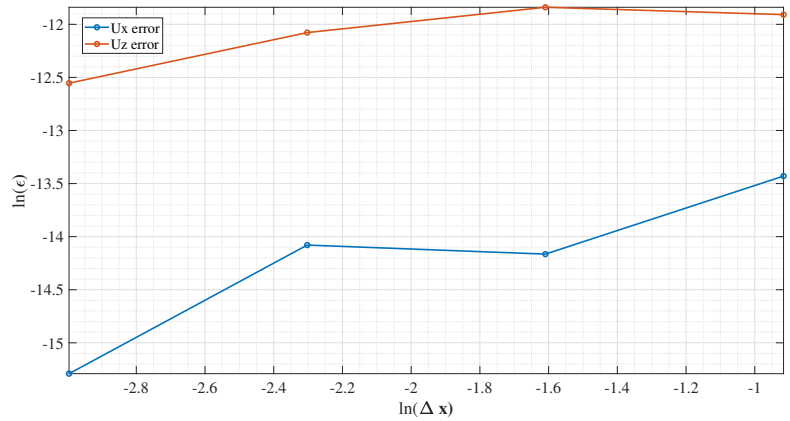

(b) FVM 3D Error analysis

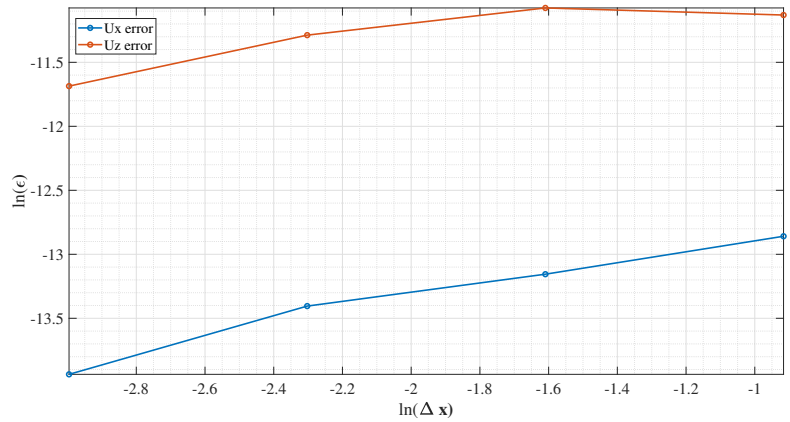

(c) FEM 3D Error analysis

Figure 5.23: Error plots of re-scaled displacement solutions in x and z direction for 3D FEM - 3D FVM and in x and y direction for 2D FVM

In fig. 5.23a the error analysis for the displacement solution in y direction is smoother than the one for the solution in the x direction. In fig. 5.23b and 5.23c the analysis for the horizontal and the vertical displacement solutions u_x and u_z respectively have oscillations.

The error analysis shows that the solutions are not second order accurate in space, probably due to the fact that the solutions are not smooth and continuous in order for the Taylor theorem to be valid.

6

Conclusions

A 3D FVM model is developed for computing deformation and stress for mechanics. The consistency check in the mechanical equilibrium test case has shown that the model is 2^{nd} order accurate in deformation calculation. Moreover, in uniaxial compression test case the deformation is estimated to be the same for 2D FVM, 3D FVM and 3D FEM models and the error analysis verifies those estimations. In the plain strain subsidence test case the subsidence is evaluated to be the same for in 2D FVM, 3D FVM and 3D FEM. Last but not least in the test or the vertical fault in an infinite reservoir assumptions have been made, so as to reproduce the scaled displacements in Jan Dirk Jansen's et al. paper [16]. The boundary conditions have been assumed to be Dirichlet in all the boundaries. The numerical scaled displacement solutions seem to be identical to the analytical but the error analysis shows that this is not the case and the numerical dimensionless stress calculation shows that there are deviations from the analytical ones solutions, especially in the 2D FVM. The scaled displacement solutions are not 2^{nd} order accurate in space, probably because the analytical solutions are not smooth functions in space. In conclusion, the 3D FVM simulator is created for modelling linear elasticity problems with and without pore pressure in the system. We hope that this thesis may inspire new researchers to extend this work in order implement it to non linear elastic problems and to study the geomechanical problems in coarser scales, improving in this way that model.

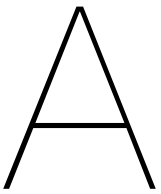

Finite volume in three dimensions

A.1. Flow chart

A simple flow chart of the 3D FVM code that has been developed in Matlab is provided below:

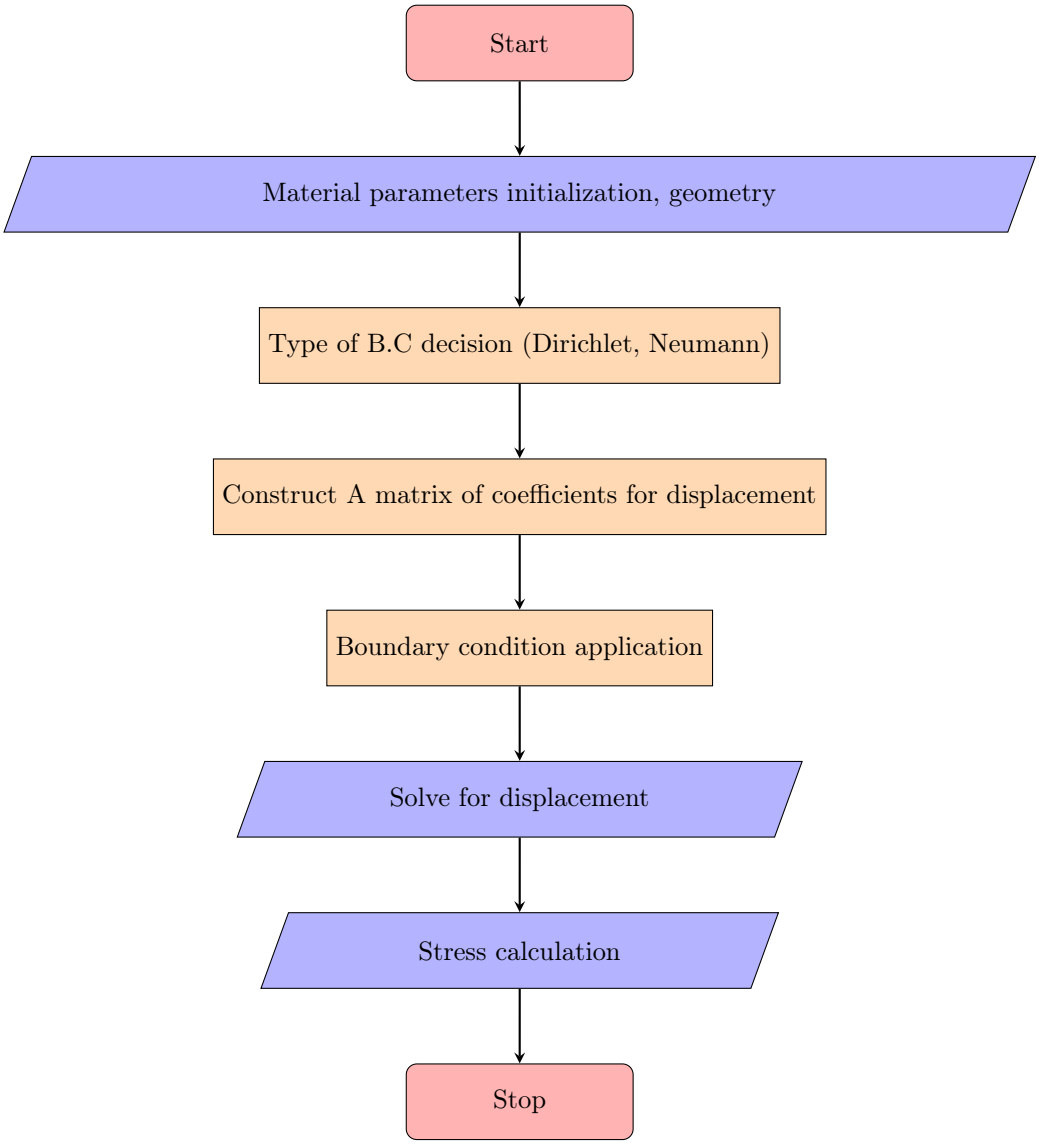

Figure A.1: Flow chart of 3D FVM simulator.

Fig. A.1 provides the general structure of the code. Examples about the construction of the A matrix and for the boundary conditions application in the code are provided below.

A.2. Code implementation

The code is solved for the displacement, so the A matrix consists of the integrated unknowns of the shape functions. The system is formulated as shown in eq. 3.50.The A_{xy} matrix for instance shows the contribution of the displacement in the y direction u_y in the x direction. For the integration inside the element control volume i, j, k, when it interacts with the stress control volume of $u_{i+1,j,k+1}$, which is presented in fig. 3.7 and described in eq. 3.40 - 3.48, we provide the code lines, which show the build of A matrices for the system A.1.

```
%=========================================
% add NWB corner (N - with '+', W - with "-", B -with "-") to
    --> SET stress CV (i+1,j,k+1)
%=========================================

%   (NWB corner of the CV; CV is to the SET from the IV)

```

```
7           ISET = Index3D_mine(Nx+1,Ny+1,Nz+1,i+1,j,k+1); % index of the
                neighbouring SET stress CV
8
9           % A_xx - contribution of Ux to Fx
10          A_xx(ISET,I_u1)   =  A_xx(ISET,I_u1) +G(Index_Lame)*ddY_x2z2
                (1)  - (L(Index_Lame)+2*G(Index_Lame))*ddX_y1z2(1)  -G(
                Index_Lame)*ddZ_x2y1(1);
11          A_xx(ISET,I_u2)   =  A_xx(ISET,I_u2) +G(Index_Lame)*ddY_x2z2
                (2)  - (L(Index_Lame)+2*G(Index_Lame))*ddX_y1z2(2)  -G(
                Index_Lame)*ddZ_x2y1(2);
12          A_xx(ISET,I_u3)   =  A_xx(ISET,I_u3) +G(Index_Lame)*ddY_x2z2
                (3)  - (L(Index_Lame)+2*G(Index_Lame))*ddX_y1z2(3)  -G(
                Index_Lame)*ddZ_x2y1(3);
13          A_xx(ISET,I_u4)   =  A_xx(ISET,I_u4) +G(Index_Lame)*ddY_x2z2
                (4)  - (L(Index_Lame)+2*G(Index_Lame))*ddX_y1z2(4)  -G(
                Index_Lame)*ddZ_x2y1(4);
14          A_xx(ISET,I_u5)   =  A_xx(ISET,I_u5) +G(Index_Lame)*ddY_x2z2
                (5)  - (L(Index_Lame)+2*G(Index_Lame))*ddX_y1z2(5)  -G(
                Index_Lame)*ddZ_x2y1(5);
15          A_xx(ISET,I_u6)   =  A_xx(ISET,I_u6) +G(Index_Lame)*ddY_x2z2
                (6)  - (L(Index_Lame)+2*G(Index_Lame))*ddX_y1z2(6)  -G(
                Index_Lame)*ddZ_x2y1(6);
16          A_xx(ISET,I_u7)   =  A_xx(ISET,I_u7) +G(Index_Lame)*ddY_x2z2
                (7)  - (L(Index_Lame)+2*G(Index_Lame))*ddX_y1z2(7)  -G(
                Index_Lame)*ddZ_x2y1(7);
17          A_xx(ISET,I_u8)   =  A_xx(ISET,I_u8) +G(Index_Lame)*ddY_x2z2
                (8)  - (L(Index_Lame)+2*G(Index_Lame))*ddX_y1z2(8)  -G(
                Index_Lame)*ddZ_x2y1(8);
18
19
20          % A_yy - contribution of Uy to Fy
21          A_yy(ISET,I_u1)   =  A_yy(ISET,I_u1) + (L(Index_Lame)+2*G(
                Index_Lame))*ddY_x2z2(1) -G(Index_Lame)*ddX_y1z2(1) -G(
                Index_Lame)*ddZ_x2y1(1);
22          A_yy(ISET,I_u2)   =  A_yy(ISET,I_u2) + (L(Index_Lame)+2*G(
                Index_Lame))*ddY_x2z2(2) -G(Index_Lame)*ddX_y1z2(2) -G(
                Index_Lame)*ddZ_x2y1(2);
23          A_yy(ISET,I_u3)   =  A_yy(ISET,I_u3) + (L(Index_Lame)+2*G(
                Index_Lame))*ddY_x2z2(3) -G(Index_Lame)*ddX_y1z2(3) -G(
                Index_Lame)*ddZ_x2y1(3);
24          A_yy(ISET,I_u4)   =  A_yy(ISET,I_u4) + (L(Index_Lame)+2*G(
                Index_Lame))*ddY_x2z2(4) -G(Index_Lame)*ddX_y1z2(4) -G(
                Index_Lame)*ddZ_x2y1(4);
25          A_yy(ISET,I_u5)   =  A_yy(ISET,I_u5) + (L(Index_Lame)+2*G(
                Index_Lame))*ddY_x2z2(5) -G(Index_Lame)*ddX_y1z2(5) -G(
                Index_Lame)*ddZ_x2y1(5);
26          A_yy(ISET,I_u6)   =  A_yy(ISET,I_u6) + (L(Index_Lame)+2*G(
                Index_Lame))*ddY_x2z2(6) -G(Index_Lame)*ddX_y1z2(6) -G(
                Index_Lame)*ddZ_x2y1(6);
27          A_yy(ISET,I_u7)   =  A_yy(ISET,I_u7) + (L(Index_Lame)+2*G(
                Index_Lame))*ddY_x2z2(7) -G(Index_Lame)*ddX_y1z2(7) -G(
                Index_Lame)*ddZ_x2y1(7);
28          A_yy(ISET,I_u8)   =  A_yy(ISET,I_u8) + (L(Index_Lame)+2*G(
                Index_Lame))*ddY_x2z2(8) -G(Index_Lame)*ddX_y1z2(8) -G(
                Index_Lame)*ddZ_x2y1(8);
29
```

```
30          % A_zz - contribution of Uz to Fz
31          A_zz(ISET,I_u1)   = A_zz(ISET,I_u1) - (L(Index_Lame)+2*G(
                Index_Lame))*ddZ_x2y1(1) -G(Index_Lame)*ddX_y1z2(1) +G(
                Index_Lame)*ddY_x2z2(1);
32          A_zz(ISET,I_u2)   = A_zz(ISET,I_u2) - (L(Index_Lame)+2*G(
                Index_Lame))*ddZ_x2y1(2) -G(Index_Lame)*ddX_y1z2(2) +G(
                Index_Lame)*ddY_x2z2(2);
33          A_zz(ISET,I_u3)   = A_zz(ISET,I_u3) - (L(Index_Lame)+2*G(
                Index_Lame))*ddZ_x2y1(3) -G(Index_Lame)*ddX_y1z2(3) +G(
                Index_Lame)*ddY_x2z2(3);
34          A_zz(ISET,I_u4)   = A_zz(ISET,I_u4) - (L(Index_Lame)+2*G(
                Index_Lame))*ddZ_x2y1(4) -G(Index_Lame)*ddX_y1z2(4) +G(
                Index_Lame)*ddY_x2z2(4);
35          A_zz(ISET,I_u5)   = A_zz(ISET,I_u5) - (L(Index_Lame)+2*G(
                Index_Lame))*ddZ_x2y1(5) -G(Index_Lame)*ddX_y1z2(5) +G(
                Index_Lame)*ddY_x2z2(5);
36          A_zz(ISET,I_u6)   = A_zz(ISET,I_u6) - (L(Index_Lame)+2*G(
                Index_Lame))*ddZ_x2y1(6) -G(Index_Lame)*ddX_y1z2(6) +G(
                Index_Lame)*ddY_x2z2(6);
37          A_zz(ISET,I_u7)   = A_zz(ISET,I_u7) - (L(Index_Lame)+2*G(
                Index_Lame))*ddZ_x2y1(7) -G(Index_Lame)*ddX_y1z2(7) +G(
                Index_Lame)*ddY_x2z2(7);
38          A_zz(ISET,I_u8)   = A_zz(ISET,I_u8) - (L(Index_Lame)+2*G(
                Index_Lame))*ddZ_x2y1(8) -G(Index_Lame)*ddX_y1z2(8) +G(
                Index_Lame)*ddY_x2z2(8);
39
40          % A_yx - contribution of Ux to Fy
41          A_yx(ISET,I_u1)  = A_yx(ISET,I_u1)  - G(Index_Lame)*ddY_y1z2
                (1) +L(Index_Lame)*ddX_x2z2(1);
42          A_yx(ISET,I_u2)  = A_yx(ISET,I_u2)  - G(Index_Lame)*ddY_y1z2
                (2) +L(Index_Lame)*ddX_x2z2(2);
43          A_yx(ISET,I_u3)  = A_yx(ISET,I_u3)  - G(Index_Lame)*ddY_y1z2
                (3) +L(Index_Lame)*ddX_x2z2(3);
44          A_yx(ISET,I_u4)  = A_yx(ISET,I_u4)  - G(Index_Lame)*ddY_y1z2
                (4) +L(Index_Lame)*ddX_x2z2(4);
45          A_yx(ISET,I_u5)  = A_yx(ISET,I_u5)  - G(Index_Lame)*ddY_y1z2
                (5) +L(Index_Lame)*ddX_x2z2(5);
46          A_yx(ISET,I_u6)  = A_yx(ISET,I_u6)  - G(Index_Lame)*ddY_y1z2
                (6) +L(Index_Lame)*ddX_x2z2(6);
47          A_yx(ISET,I_u7)  = A_yx(ISET,I_u7)  - G(Index_Lame)*ddY_y1z2
                (7) +L(Index_Lame)*ddX_x2z2(7);
48          A_yx(ISET,I_u8)  = A_yx(ISET,I_u8)  - G(Index_Lame)*ddY_y1z2
                (8) +L(Index_Lame)*ddX_x2z2(8);
49
50          % A_zx - contribution of Ux to Fz
51
52          A_zx(ISET,I_u1)   = A_zx(ISET,I_u1) - G(Index_Lame)*ddZ_y1z2
                (1) -L(Index_Lame)*ddX_x2y1(1);
53          A_zx(ISET,I_u2)   = A_zx(ISET,I_u2) - G(Index_Lame)*ddZ_y1z2
                (2) -L(Index_Lame)*ddX_x2y1(2);
54          A_zx(ISET,I_u3)   = A_zx(ISET,I_u3) - G(Index_Lame)*ddZ_y1z2
                (3) -L(Index_Lame)*ddX_x2y1(3);
55          A_zx(ISET,I_u4)   = A_zx(ISET,I_u4) - G(Index_Lame)*ddZ_y1z2
                (4) -L(Index_Lame)*ddX_x2y1(4);
56          A_zx(ISET,I_u5)   = A_zx(ISET,I_u5) - G(Index_Lame)*ddZ_y1z2
                (5) -L(Index_Lame)*ddX_x2y1(5);
```

```
57          A_zx(ISET,I_u6)   = A_zx(ISET,I_u6) - G(Index_Lame)*ddZ_y1z2
                (6) -L(Index_Lame)*ddX_x2y1(6);
58          A_zx(ISET,I_u7)   = A_zx(ISET,I_u7) - G(Index_Lame)*ddZ_y1z2
                (7) -L(Index_Lame)*ddX_x2y1(7);
59          A_zx(ISET,I_u8)   = A_zx(ISET,I_u8) - G(Index_Lame)*ddZ_y1z2
                (8) -L(Index_Lame)*ddX_x2y1(8);
60
61
62
63          % A_xy - contribution of Uy to Fx
64          A_xy(ISET,I_u1)   = A_xy(ISET,I_u1) -L(Index_Lame)*ddY_y1z2(1)
                + G(Index_Lame)*ddX_x2z2(1);
65          A_xy(ISET,I_u2)   = A_xy(ISET,I_u2) -L(Index_Lame)*ddY_y1z2(2)
                + G(Index_Lame)*ddX_x2z2(2);
66          A_xy(ISET,I_u3)   = A_xy(ISET,I_u3) -L(Index_Lame)*ddY_y1z2(3)
                + G(Index_Lame)*ddX_x2z2(3);
67          A_xy(ISET,I_u4)   = A_xy(ISET,I_u4) -L(Index_Lame)*ddY_y1z2(4)
                + G(Index_Lame)*ddX_x2z2(4);
68          A_xy(ISET,I_u5)   = A_xy(ISET,I_u5) -L(Index_Lame)*ddY_y1z2(5)
                + G(Index_Lame)*ddX_x2z2(5);
69          A_xy(ISET,I_u6)   = A_xy(ISET,I_u6) -L(Index_Lame)*ddY_y1z2(6)
                + G(Index_Lame)*ddX_x2z2(6);
70          A_xy(ISET,I_u7)   = A_xy(ISET,I_u7) -L(Index_Lame)*ddY_y1z2(7)
                + G(Index_Lame)*ddX_x2z2(7);
71          A_xy(ISET,I_u8)   = A_xy(ISET,I_u8) -L(Index_Lame)*ddY_y1z2(8)
                + G(Index_Lame)*ddX_x2z2(8);
72
73          % A_zy - contribution of Uy to Fz
74          A_zy (ISET,I_u1)   = A_zy (ISET,I_u1) -L(Index_Lame)*ddY_x2y1
                (1) + G(Index_Lame)*ddZ_x2z2(1);
75          A_zy (ISET,I_u2)   = A_zy (ISET,I_u2) -L(Index_Lame)*ddY_x2y1
                (2) + G(Index_Lame)*ddZ_x2z2(2);
76          A_zy (ISET,I_u3)   = A_zy (ISET,I_u3) -L(Index_Lame)*ddY_x2y1
                (3) + G(Index_Lame)*ddZ_x2z2(3);
77          A_zy (ISET,I_u4)   = A_zy (ISET,I_u4) -L(Index_Lame)*ddY_x2y1
                (4) + G(Index_Lame)*ddZ_x2z2(4);
78          A_zy (ISET,I_u5)   = A_zy (ISET,I_u5) -L(Index_Lame)*ddY_x2y1
                (5) + G(Index_Lame)*ddZ_x2z2(5);
79          A_zy (ISET,I_u6)   = A_zy (ISET,I_u6) -L(Index_Lame)*ddY_x2y1
                (6) + G(Index_Lame)*ddZ_x2z2(6);
80          A_zy (ISET,I_u7)   = A_zy (ISET,I_u7) -L(Index_Lame)*ddY_x2y1
                (7) + G(Index_Lame)*ddZ_x2z2(7);
81          A_zy (ISET,I_u8)   = A_zy (ISET,I_u8) -L(Index_Lame)*ddY_x2y1
                (8) + G(Index_Lame)*ddZ_x2z2(8);
82
83          % A_xz - contribution of Uz to Fx
84          A_xz (ISET,I_u1)   = A_xz (ISET,I_u1) -L(Index_Lame)*ddZ_y1z2
                (1) - G(Index_Lame)*ddX_x2y1(1);
85          A_xz (ISET,I_u2)   = A_xz (ISET,I_u2) -L(Index_Lame)*ddZ_y1z2
                (2) - G(Index_Lame)*ddX_x2y1(2);
86          A_xz (ISET,I_u3)   = A_xz (ISET,I_u3) -L(Index_Lame)*ddZ_y1z2
                (3) - G(Index_Lame)*ddX_x2y1(3);
87          A_xz (ISET,I_u4)   = A_xz (ISET,I_u4) -L(Index_Lame)*ddZ_y1z2
                (4) - G(Index_Lame)*ddX_x2y1(4);
88          A_xz (ISET,I_u5)   = A_xz (ISET,I_u5) -L(Index_Lame)*ddZ_y1z2
                (5) - G(Index_Lame)*ddX_x2y1(5);
```

```
89          A_xz (ISET,I_u6)   = A_xz (ISET,I_u6) -L(Index_Lame)*ddZ_y1z2
               (6) - G(Index_Lame)*ddX_x2y1(6);
90          A_xz (ISET,I_u7)   = A_xz (ISET,I_u7) -L(Index_Lame)*ddZ_y1z2
               (7) - G(Index_Lame)*ddX_x2y1(7);
91          A_xz (ISET,I_u8)   = A_xz (ISET,I_u8) -L(Index_Lame)*ddZ_y1z2
               (8) - G(Index_Lame)*ddX_x2y1(8);
92
93          % A_yz - contribution of Uz to Fy
94          A_yz (ISET,I_u1)   = A_yz (ISET,I_u1) +L(Index_Lame)*ddZ_x2z2
               (1)  - G(Index_Lame)*ddY_x2y1(1);
95          A_yz (ISET,I_u2)   = A_yz (ISET,I_u2) +L(Index_Lame)*ddZ_x2z2
               (2)  - G(Index_Lame)*ddY_x2y1(2);
96          A_yz (ISET,I_u3)   = A_yz (ISET,I_u3) +L(Index_Lame)*ddZ_x2z2
               (3)  - G(Index_Lame)*ddY_x2y1(3);
97          A_yz (ISET,I_u4)   = A_yz (ISET,I_u4) +L(Index_Lame)*ddZ_x2z2
               (4)  - G(Index_Lame)*ddY_x2y1(4);
98          A_yz (ISET,I_u5)   = A_yz (ISET,I_u5) +L(Index_Lame)*ddZ_x2z2
               (5)  - G(Index_Lame)*ddY_x2y1(5);
99          A_yz (ISET,I_u6)   = A_yz (ISET,I_u6) +L(Index_Lame)*ddZ_x2z2
               (6)  - G(Index_Lame)*ddY_x2y1(6);
100         A_yz (ISET,I_u7)   = A_yz (ISET,I_u7) +L(Index_Lame)*ddZ_x2z2
               (7)  - G(Index_Lame)*ddY_x2y1(7);
101         A_yz (ISET,I_u8)   = A_yz (ISET,I_u8) +L(Index_Lame)*ddZ_x2z2
               (8)  - G(Index_Lame)*ddY_x2y1(8);
```

A.3. Integrals calculation

The coefficients, which are derived from the integration of the derivatives, with respect to one direction x,y or z of the shape functions are the same when we have displacement for x y or z direction. This means that the double integral

$$\int_0^{\frac{dz}{2}}\int_0^{\frac{dx}{2}} \frac{\partial u_x}{\partial x}\,dx\,dz = \int_0^{\frac{dz}{2}}\int_0^{\frac{dx}{2}} \frac{\partial u_y}{\partial x}\,dx\,dz = \int_0^{\frac{dz}{2}}\int_0^{\frac{dx}{2}} \sum_{i=1}^{8} \vec{u_i}\frac{\partial N_i(x,y,z)}{\partial x}\,dx\,dz \tag{A.1}$$

In eq. A.1 the u_i can be displacement in x direction, so u_x or displacement in y direction, so u_y. The term $\frac{\partial N_i(x,y,z)}{\partial x}$ will not change because the shape functions are the same, so the coefficients or weights in other words will be the same.

A.3.1. Derivatives over x direction

The coefficients that multiply the displacement in each stress control volume depend on the stress control volume and of course on the formulas of the stresses themselves.The possible integrals of the shape function derivatives are given below:

$$D_{WB}^{x} = \int_{0}^{\frac{dz}{2}} \int_{0}^{\frac{dx}{2}} \frac{\partial u_{x,y}}{\partial x}\, dx\, dz = \frac{dx\, dz}{dx}[-\frac{3}{32}, \frac{3}{32}, \frac{3}{32}, -\frac{3}{32}, -\frac{1}{32}, \frac{1}{32}, \frac{1}{32}, -\frac{1}{32}][u_1, u_2, u_3, u_4, u_5, u_6, u_7, u_8]^{\mathrm{T}}$$

$$D_{WT}^{x} = \int_{\frac{dz}{2}}^{dz} \int_{0}^{\frac{dx}{2}} \frac{\partial u_{x,y}}{\partial x}\, dx\, dz = \frac{dx\, dz}{dx}[-\frac{1}{32}, \frac{1}{32}, \frac{1}{32}, -\frac{1}{32}, -\frac{3}{32}, \frac{3}{32}, \frac{3}{32}, -\frac{3}{32}][u_1, u_2, u_3, u_4, u_5, u_6, u_7, u_8]^{\mathrm{T}}$$

$$D_{ET}^{x} = \int_{\frac{dz}{2}}^{dz} \int_{\frac{dx}{2}}^{dx} \frac{\partial u_{x,y}}{\partial x}\, dx\, dz = \frac{dx\, dz}{dx}[-\frac{1}{32}, \frac{1}{32}, \frac{1}{32}, -\frac{1}{32}, -\frac{3}{32}, \frac{3}{32}, \frac{3}{32}, -\frac{3}{32}][u_1, u_2, u_3, u_4, u_5, u_6, u_7, u_8]^{\mathrm{T}}$$

$$D_{EB}^{x} = \int_{0}^{\frac{dz}{2}} \int_{\frac{dx}{2}}^{dx} \frac{\partial u_{x,y}}{\partial x}\, dx\, dz = \frac{dx\, dz}{dx}[-\frac{3}{32}, \frac{3}{32}, \frac{3}{32}, -\frac{3}{32}, -\frac{1}{32}, \frac{1}{32}, \frac{1}{32}, -\frac{1}{32}][u_1, u_2, u_3, u_4, u_5, u_6, u_7, u_8]^{\mathrm{T}}$$

$$D_{SB}^{x} = \int_{0}^{\frac{dz}{2}} \int_{0}^{\frac{dy}{2}} \frac{\partial u_{x,y,z}}{\partial x}\, dy\, dz = \frac{dy\, dz}{dx}[-\frac{9}{64}, \frac{9}{64}, \frac{3}{64}, -\frac{3}{64}, -\frac{3}{64}, \frac{3}{64}, \frac{1}{64}, -\frac{1}{64}][u_1, u_2, u_3, u_4, u_5, u_6, u_7, u_8]^{\mathrm{T}}$$

$$D_{ST}^{x} = \int_{\frac{dz}{2}}^{dz} \int_{0}^{\frac{dy}{2}} \frac{\partial u_{x,y,z}}{\partial x}\, dy\, dz = \frac{dy\, dz}{dx}[-\frac{3}{64}, \frac{3}{64}, \frac{1}{64}, -\frac{1}{64}, -\frac{9}{64}, \frac{9}{64}, \frac{3}{64}, -\frac{3}{64}][u_1, u_2, u_3, u_4, u_5, u_6, u_7, u_8]^{\mathrm{T}}$$

$$D_{NT}^{x} = \int_{\frac{dz}{2}}^{dz} \int_{\frac{dy}{2}}^{dy} \frac{\partial u_{x,y,z}}{\partial x}\, dy\, dz = \frac{dy\, dz}{dx}[-\frac{1}{64}, \frac{1}{64}, \frac{3}{64}, -\frac{3}{64}, -\frac{3}{64}, \frac{3}{64}, \frac{9}{64}, -\frac{9}{64}][u_1, u_2, u_3, u_4, u_5, u_6, u_7, u_8]^{\mathrm{T}}$$

$$D_{NB}^{x} = \int_{0}^{\frac{dz}{2}} \int_{\frac{dy}{2}}^{dy} \frac{\partial u_{x,y,z}}{\partial x}\, dy\, dz = \frac{dy\, dz}{dx}[-\frac{3}{64}, \frac{3}{64}, \frac{9}{64}, -\frac{9}{64}, -\frac{1}{64}, \frac{1}{64}, \frac{3}{64}, -\frac{3}{64}][u_1, u_2, u_3, u_4, u_5, u_6, u_7, u_8]^{\mathrm{T}}$$

$$D_{WS}^{x} = \int_{0}^{\frac{dy}{2}} \int_{0}^{\frac{dx}{2}} \frac{\partial u_{x,z}}{\partial x}\, dx\, dy = \frac{dx\, dy}{dx}[-\frac{3}{32}, \frac{3}{32}, \frac{1}{32}, -\frac{1}{32}, -\frac{3}{32}, \frac{3}{32}, \frac{1}{32}, -\frac{1}{32}][u_1, u_2, u_3, u_4, u_5, u_6, u_7, u_8]^{\mathrm{T}}$$

$$D_{WN}^{x} = \int_{\frac{dy}{2}}^{dy} \int_{0}^{\frac{dx}{2}} \frac{\partial u_{x,z}}{\partial x}\, dx\, dy = \frac{dx\, dy}{dx}[-\frac{1}{32}, \frac{1}{32}, \frac{3}{32}, -\frac{3}{32}, -\frac{1}{32}, \frac{1}{32}, \frac{3}{32}, -\frac{3}{32}][u_1, u_2, u_3, u_4, u_5, u_6, u_7, u_8]^{\mathrm{T}}$$

$$D_{EN}^{x} = \int_{\frac{dy}{2}}^{dy} \int_{\frac{dx}{2}}^{dx} \frac{\partial u_{x,z}}{\partial x}\, dx\, dy = \frac{dx\, dy}{dx}[-\frac{1}{32}, \frac{1}{32}, \frac{3}{32}, -\frac{3}{32}, -\frac{1}{32}, \frac{1}{32}, \frac{3}{32}, -\frac{3}{32}][u_1, u_2, u_3, u_4, u_5, u_6, u_7, u_8]^{\mathrm{T}}$$

$$D_{ES}^{x} = \int_{0}^{\frac{dy}{2}} \int_{\frac{dx}{2}}^{dx} \frac{\partial u_{x,z}}{\partial x}\, dx\, dy = \frac{dx\, dy}{dx}[-\frac{3}{32}, \frac{3}{32}, \frac{1}{32}, -\frac{1}{32}, -\frac{3}{32}, \frac{3}{32}, \frac{1}{32}, -\frac{1}{32}][u_1, u_2, u_3, u_4, u_5, u_6, u_7, u_8]^{\mathrm{T}}$$

A.3.2. Derivatives over y direction

$$D^y_{WB} = \int_0^{\frac{dz}{2}} \int_0^{\frac{dx}{2}} \frac{\partial u_{x,y,z}}{\partial y}\, dx\, dz = \frac{dx\, dz}{dy}[-\frac{9}{64}, -\frac{3}{64}, \frac{3}{64}, \frac{9}{64}, -\frac{3}{64}, -\frac{1}{64}, \frac{1}{64}, \frac{3}{64}][u_1, u_2, u_3, u_4, u_5, u_6, u_7, u_8]^\mathsf{T}$$

$$D^y_{WT} = \int_{\frac{dz}{2}}^{dz} \int_0^{\frac{dx}{2}} \frac{\partial u_{x,y,z}}{\partial y}\, dx\, dz = \frac{dx\, dz}{dy}[-\frac{3}{64}, -\frac{1}{64}, \frac{1}{64}, \frac{3}{64}, -\frac{9}{64}, -\frac{3}{64}, \frac{3}{64}, \frac{9}{64}][u_1, u_2, u_3, u_4, u_5, u_6, u_7, u_8]^\mathsf{T}$$

$$D^y_{ET} = \int_{\frac{dz}{2}}^{dz} \int_{\frac{dx}{2}}^{dx} \frac{\partial u_{x,y,z}}{\partial y}\, dx\, dz = \frac{dx\, dz}{dy}[-\frac{1}{64}, -\frac{3}{64}, \frac{3}{64}, \frac{1}{64}, -\frac{3}{64}, -\frac{9}{64}, \frac{9}{64}, \frac{3}{64}][u_1, u_2, u_3, u_4, u_5, u_6, u_7, u_8]^\mathsf{T}$$

$$D^y_{EB} = \int_0^{\frac{dz}{2}} \int_{\frac{dx}{2}}^{dx} \frac{\partial u_{x,y,z}}{\partial y}\, dx\, dz = \frac{dx\, dz}{dy}[-\frac{3}{64}, -\frac{9}{64}, \frac{9}{64}, \frac{3}{64}, -\frac{1}{64}, -\frac{3}{64}, \frac{3}{64}, \frac{1}{64}][u_1, u_2, u_3, u_4, u_5, u_6, u_7, u_8]^\mathsf{T}$$

$$D^y_{SB} = \int_0^{\frac{dz}{2}} \int_0^{\frac{dy}{2}} \frac{\partial u_{x,y}}{\partial y}\, dy\, dz = \frac{dy\, dz}{dy}[-\frac{3}{32}, -\frac{3}{32}, \frac{3}{32}, \frac{3}{32}, -\frac{1}{32}, -\frac{1}{32}, \frac{1}{32}, \frac{1}{32}][u_1, u_2, u_3, u_4, u_5, u_6, u_7, u_8]^\mathsf{T}$$

$$D^y_{ST} = \int_{\frac{dz}{2}}^{dz} \int_0^{\frac{dy}{2}} \frac{\partial u_{x,y}}{\partial y}\, dy\, dz = \frac{dy\, dz}{dy}[-\frac{1}{32}, -\frac{1}{32}, \frac{1}{32}, \frac{1}{32}, -\frac{3}{32}, -\frac{3}{32}, \frac{3}{32}, \frac{3}{32}][u_1, u_2, u_3, u_4, u_5, u_6, u_7, u_8]^\mathsf{T}$$

$$D^y_{NT} = \int_{\frac{dz}{2}}^{dz} \int_{\frac{dy}{2}}^{dy} \frac{\partial u_{x,y}}{\partial y}\, dy\, dz = \frac{dy\, dz}{dy}[-\frac{1}{32}, -\frac{1}{32}, \frac{1}{32}, \frac{1}{32}, -\frac{3}{32}, -\frac{3}{32}, \frac{3}{32}, \frac{3}{32}][u_1, u_2, u_3, u_4, u_5, u_6, u_7, u_8]^\mathsf{T}$$

$$D^y_{NB} = \int_0^{\frac{dz}{2}} \int_{\frac{dy}{2}}^{dy} \frac{\partial u_{x,y}}{\partial y}\, dy\, dz = \frac{dy\, dz}{dy}[-\frac{3}{32}, -\frac{3}{32}, \frac{3}{32}, \frac{3}{32}, -\frac{1}{32}, -\frac{1}{32}, \frac{1}{32}, \frac{1}{32}][u_1, u_2, u_3, u_4, u_5, u_6, u_7, u_8]^\mathsf{T}$$

$$D^y_{WS} = \int_0^{\frac{dy}{2}} \int_0^{\frac{dx}{2}} \frac{\partial u_{y,z}}{\partial y}\, dx\, dy = \frac{dx\, dy}{dy}[-\frac{3}{32}, -\frac{1}{32}, \frac{1}{32}, \frac{3}{32}, -\frac{3}{32}, -\frac{1}{32}, \frac{1}{32}, \frac{3}{32}][u_1, u_2, u_3, u_4, u_5, u_6, u_7, u_8]^\mathsf{T}$$

$$D^y_{WN} = \int_{\frac{dy}{2}}^{dy} \int_0^{\frac{dx}{2}} \frac{\partial u_{y,z}}{\partial y}\, dx\, dy = \frac{dx\, dy}{dy}[-\frac{3}{32}, -\frac{1}{32}, \frac{1}{32}, \frac{3}{32}, -\frac{3}{32}, -\frac{1}{32}, \frac{1}{32}, \frac{3}{32}][u_1, u_2, u_3, u_4, u_5, u_6, u_7, u_8]^\mathsf{T}$$

$$D^y_{EN} = \int_{\frac{dy}{2}}^{dy} \int_{\frac{dx}{2}}^{dx} \frac{\partial u_{y,z}}{\partial y}\, dx\, dy = \frac{dx\, dy}{dy}[-\frac{1}{32}, -\frac{3}{32}, \frac{3}{32}, \frac{1}{32}, -\frac{1}{32}, -\frac{3}{32}, \frac{3}{32}, \frac{1}{32}][u_1, u_2, u_3, u_4, u_5, u_6, u_7, u_8]^\mathsf{T}$$

$$D^y_{ES} = \int_0^{\frac{y}{2}} \int_{\frac{dx}{2}}^{dx} \frac{\partial u_{y,z}}{\partial y}\, dx\, dy = \frac{dx\, dy}{dy}[-\frac{1}{32}, -\frac{3}{32}, \frac{3}{32}, \frac{1}{32}, -\frac{1}{32}, -\frac{3}{32}, \frac{3}{32}, \frac{1}{32}][u_1, u_2, u_3, u_4, u_5, u_6, u_7, u_8]^\mathsf{T}$$

A.3.3. Derivatives over z direction

$$D^z_{WB} = \int_0^{\frac{dz}{2}} \int_0^{\frac{dx}{2}} \frac{\partial u_{y,z}}{\partial z}\, dx\, dz = \frac{dx\, dz}{dz}[-\frac{3}{32}, -\frac{1}{32}, -\frac{1}{32}, -\frac{3}{32}, \frac{3}{32}, \frac{1}{32}, \frac{1}{32}, \frac{3}{32}][u_1, u_2, u_3, u_4, u_5, u_6, u_7, u_8]^{\mathsf{T}}$$

$$D^z_{WT} = \int_{\frac{dz}{2}}^{dz} \int_0^{\frac{dx}{2}} \frac{\partial u_{y,z}}{\partial z}\, dx\, dz = \frac{dx\, dz}{dz}[-\frac{3}{32}, -\frac{1}{32}, -\frac{1}{32}, -\frac{3}{32}, \frac{3}{32}, \frac{1}{32}, \frac{1}{32}, \frac{3}{32}][u_1, u_2, u_3, u_4, u_5, u_6, u_7, u_8]^{\mathsf{T}}$$

$$D^z_{ET} = \int_{\frac{dz}{2}}^{dz} \int_{\frac{dx}{2}}^{dx} \frac{\partial u_{y,z}}{\partial z}\, dx\, dz = \frac{dx\, dz}{dz}[-\frac{1}{32}, -\frac{3}{32}, -\frac{3}{32}, -\frac{1}{32}, \frac{1}{32}, \frac{3}{32}, \frac{3}{32}, \frac{1}{32}][u_1, u_2, u_3, u_4, u_5, u_6, u_7, u_8]^{\mathsf{T}}$$

$$D^z_{EB} = \int_0^{\frac{dz}{2}} \int_{\frac{dx}{2}}^{dx} \frac{\partial u_{y,z}}{\partial z}\, dx\, dz = \frac{dx\, dz}{dz}[-\frac{1}{32}, -\frac{3}{32}, -\frac{3}{32}, -\frac{1}{32}, \frac{1}{32}, \frac{3}{32}, \frac{3}{32}, \frac{1}{32}][u_1, u_2, u_3, u_4, u_5, u_6, u_7, u_8]^{\mathsf{T}}$$

$$D^z_{SB} = \int_0^{\frac{dz}{2}} \int_0^{\frac{dy}{2}} \frac{\partial u_{x,z}}{\partial z}\, dy\, dz = \frac{dy\, dz}{dz}[-\frac{3}{32}, -\frac{3}{32}, -\frac{1}{32}, -\frac{1}{32}, \frac{3}{32}, \frac{3}{32}, \frac{1}{32}, \frac{1}{32}][u_1, u_2, u_3, u_4, u_5, u_6, u_7, u_8]^{\mathsf{T}}$$

$$D^z_{ST} = \int_{\frac{dz}{2}}^{dz} \int_0^{\frac{dy}{2}} \frac{\partial u_{x,z}}{\partial z}\, dy\, dz = \frac{dy\, dz}{dz}[-\frac{3}{32}, -\frac{3}{32}, -\frac{1}{32}, -\frac{1}{32}, \frac{3}{32}, \frac{3}{32}, \frac{1}{32}, \frac{1}{32}][u_1, u_2, u_3, u_4, u_5, u_6, u_7, u_8]^{\mathsf{T}}$$

$$D^z_{NT} = \int_{\frac{dz}{2}}^{dz} \int_{\frac{dy}{2}}^{dy} \frac{\partial u_{x,z}}{\partial z}\, dy\, dz = \frac{dy\, dz}{dz}[-\frac{1}{32}, -\frac{1}{32}, -\frac{3}{32}, -\frac{3}{32}, \frac{1}{32}, \frac{1}{32}, \frac{3}{32}, \frac{3}{32}][u_1, u_2, u_3, u_4, u_5, u_6, u_7, u_8]^{\mathsf{T}}$$

$$D^z_{NB} = \int_0^{\frac{dz}{2}} \int_{\frac{dy}{2}}^{dy} \frac{\partial u_{x,z}}{\partial z}\, dy\, dz = \frac{dy\, dz}{dz}[-\frac{1}{32}, -\frac{1}{32}, -\frac{3}{32}, -\frac{3}{32}, \frac{1}{32}, \frac{1}{32}, \frac{3}{32}, \frac{3}{32}][u_1, u_2, u_3, u_4, u_5, u_6, u_7, u_8]^{\mathsf{T}}$$

$$D^z_{WS} = \int_0^{\frac{dy}{2}} \int_0^{\frac{dx}{2}} \frac{\partial u_{x,y,z}}{\partial z}\, dx\, dy = \frac{dx\, dy}{dz}[-\frac{9}{64}, -\frac{3}{64}, -\frac{1}{64}, -\frac{3}{64}, \frac{9}{64}, \frac{3}{64}, \frac{1}{64}, \frac{3}{64}][u_1, u_2, u_3, u_4, u_5, u_6, u_7, u_8]^{\mathsf{T}}$$

$$D^z_{WN} = \int_{\frac{dy}{2}}^{dy} \int_0^{\frac{dx}{2}} \frac{\partial u_{x,y,z}}{\partial z}\, dx\, dy = \frac{dx\, dy}{dz}[-\frac{3}{64}, -\frac{1}{64}, -\frac{3}{64}, -\frac{9}{64}, \frac{3}{64}, \frac{1}{64}, \frac{3}{64}, \frac{9}{64}][u_1, u_2, u_3, u_4, u_5, u_6, u_7, u_8]^{\mathsf{T}}$$

$$D^z_{EN} = \int_{\frac{dy}{2}}^{dy} \int_{\frac{dx}{2}}^{dx} \frac{\partial u_{x,y,z}}{\partial z}\, dx\, dy = \frac{dx\, dy}{dz}[-\frac{1}{64}, -\frac{3}{64}, -\frac{9}{64}, -\frac{3}{64}, \frac{1}{64}, \frac{3}{64}, \frac{9}{64}, \frac{3}{64}][u_1, u_2, u_3, u_4, u_5, u_6, u_7, u_8]^{\mathsf{T}}$$

$$D^z_{ES} = \int_0^{\frac{y}{2}} \int_{\frac{dx}{2}}^{dx} \frac{\partial u_{x,y,z}}{\partial z}\, dx\, dy = \frac{dx\, dy}{dz}[-\frac{3}{64}, -\frac{9}{64}, -\frac{3}{64}, -\frac{1}{64}, \frac{3}{64}, \frac{9}{64}, \frac{3}{64}, \frac{1}{64}][u_1, u_2, u_3, u_4, u_5, u_6, u_7, u_8]^{\mathsf{T}}$$

A.4. Boundary conditions implementation

The boundary conditions are applied to all the nodes that exist in the boundaries or border of the depicted mesh in fig. 3.2. Below is provided the code implementation for the boundary condition in 3D FVM.

```
for i = 1:Nx+1
    for j = 1:Ny+1
        for k = 1:Nz+1
             l    = Index3D_mine(Nx+1,Ny+1,Nz+1,i,j,k);

            % Set all the values assigned to BC control volumes to 0
            % Set coefficient 1 for the known U

           if BC_flag(l) == 1
                A_xx(l,:)=0;
                A_xy(l,:)=0;
                A_xz(l,:)=0;
                A_xx(l,l)=1;
                % Force the RHS values to the known U : A*U_known =
                    U_known
                F(l)  = U_vect(l);
            end

             if BC_flag(l + (Nx+1)*(Ny+1)*(Nz+1)) == 1
                A_yy(l,:)=0;
                A_yx(l,:)=0;
                A_yz(l,:)=0;
                A_yy(l,l)=1;
                % Force the RHS values to the known U : A*U_known =
                    U_known
                F(l+(Nx+1)*(Ny+1)*(Nz+1))  = U_vect(l+(Nx+1)*(Ny+1)*(Nz+1)
                    );
            end

            if BC_flag(l+2*(Nx+1)*(Ny+1)*(Nz+1)) == 1
                A_zz(l,:)=0;
                A_zy(l,:)=0;
                A_zx(l,:)=0;
                A_zz(l,l)=1;
                % Force the RHS values to the known U : A*U_known =
                    U_known
                F(l+2*(Nx+1)*(Ny+1)*(Nz+1))  = U_vect(l+2*(Nx+1)*(Ny+1)*(
                    Nz+1));
            end

        end
    end
end
A = [A_xx A_xy A_xz; A_yx A_yy A_yz;A_zx A_zy A_zz];
```

As shown in the above code the points, which correspond to the boundaries, which are subjected to Dirichlet boundary conditions are given with the indexing: ”l” in the A matrices.The rows of the A matrices for these points become 0 and only the diagonal is one. In this way the desired displacement is assigned directly to the solution and this is the definition of the Dirichlet boundary condition. The ”marking” of the points, which correspond to the boundaries is achieved with the vector BC_flag, which reaches to the full length of the A matrix.

Bibliography

[1] C. A. Barton, M. D. Zoback, and D. Moos. Fluid flow along potentially active faults in crystalline rock. 23:683–686, (1995). doi: 10.1130/0091-7613(1995)023<0683:FFAPAF>2.3.CO;2.

[2] Brian Berkowitz. Characterizing flow and transport in fractured geological media: A review. *Advances in Water Resources*, 25:861–884, 2002. doi: 10.1016/S0309-1708(02)00042-8.

[3] N. Castelletto, H. Hajibeygi, and H. A. Tchelepi. Multiscale finite-element method for linear elastic geomechanics. *Journal of Computational Physics*, 331:337–356, 2017. doi: 10.1016/j.jcp.2016.11.044.

[4] C.Carstensen, D.Günther, J.Reininghaus, and J.Thiele. The arnold–winther mixed fem in linear elasticity. part i: Implementation and numerical verification. 197:3014–3023, (2008). doi: 10.1016/j.cma.2008.02.005.

[5] R.D. Cook. *Concepts and applications of finite element analysis*. John Wiley and Sons, 2002.

[6] M. Ferronato D. Baú, G. Gambolati, and P. Teatini. Basin-scale compressibility of the northern adriatic by the radioactivemarker technique. *Géotechnique*, 52(8):605–616, 2002. doi: 10.1680/geot.2002.52.8.605.

[7] R. Deb and P. Jenny. Finite volume–based modeling of flow induced shear failure along fracture manifolds. page 1922–1942, (2017). doi: 10.1002/nag.2707.

[8] Rajdeep Deb. Numerical modeling of fluid injection induced shear failure, tensile opening and flow-mechanics coupling. (2018). doi: 10.3929/ethz-b-000303929.

[9] J. D. Eshelby. The determination of the elastic field of an ellipsoidal inclusion, and related problems. 241:376–396, (1957). doi: 10.1098/rspa.1957.0133.

[10] R. Eymard, Gallouët, and R. Herbin. *Finite Volume Methods*, volume 7. Handbook of Numerical Analysis, (1997).

[11] Richard S. Falk. Finite element methods for linear elasticity. (2008).

[12] F.J.Gaspar, F.J.Lisbona, and P.N.Vabishchevich. Staggered grid discretizations for the quasi-static biot's consolidation problem. pages 888–898, (2006). doi: 10.1016/j.apnum.2005.07.002.

[13] Ed Fontes. Fem vs. fvm, (2018).

[14] Carl W. Hall. *Laws and Models*. Science, Engineering, and Technology, (1999). doi: ISBN9780849320187.

[15] Hughes and Thomas J. R. *Finite Element Method - Linear Static and Dynamic Finite Element Analysis*. Dover Publications.

[16] J. D. Jansen, P. Singhal, and F. C. Vossepoel. Insights from closed form expressions for injection and production induced stresses in displaced faults. *JGR Solid Earth*, 124:7193–7212, 2019. doi: 10.1029/2019JB017932.

[17] H. Jasak and H. G. Weller. Application of the finite volume method and unstructured meshes to linear elasticity. *International Journal for Numerical Methods in Engineering*, 2000. doi: 10.1002/(SICI)1097-0207(20000520)48:2<267::AID-NME884>3.0.CO;2-Q.

[18] J.Kim, C.Bailey, H.A.Tchelepi, and R.Juanes. Stability and convergence of sequential methods for coupled flow and geomechanics: Drained and undrained splits. pages 2094–2116, (2011). doi: 10.1016/j.cma.2011.02.011.

[19] K. Ramesh Kumar and H. Hajibeygi. Multi-scale nonlinear modeling of subsurface energy storage: Cyclic loading with inelastic creep deformation. (2020).

[20] Randall LeVeque. *Finite Volume Methods for Hyperbolic Problems*. Cambridge Texts in Applied Mathematics, (2002).

[21] 1850-1919 M. Spivak (1994). *Calculus (Third Edition)*. Houston, TX: Publish or Perish.

[22] E. L. Majer, Rahul Baria, Mitch Stark, Stephen Oates, Julian Bommer, Bill Smith, and Hiroshi Asanuma. Induced seismicity associated with enhanced geothermal systems. 36(3):185–222, (2007). doi: 10.1016/j.geothermics.2007.03.003.

[23] K. Olesen, B. Gervang, J. N. Reddy, and M. Gerritsma. A higher order equilibrium finite element method. 114:2094–2116, (2018). doi: 10.1002/nme.5785.

[24] G. Simpson. *Practical Finite Element Modeling in Earth Science Using Matlab*. Wiley-Blackwell, (2017). doi: 10.1002/9781119248644.

[25] Bjorn Sjodin. What's the difference between fem, fdm, and fvm?, (2016).

[26] William S. Slaughter. *The Linearized Theory of Elasticity*. Birkhäuser, (2002).

[27] I. Sokolova, M. G. Bastisya, and H. Hajibeygi. Multiscale finite volume method for finite-volume-based simulation of poroelasticity. *Journal of Computational Physics*, 379:309–324, 2019. doi: 10.1016/j.jcp.2018.11.039.

[28] E. Ucar, E. Keilegavlen, I. Berre, and J. M. Nordbotten. A finite-volume discretization for deformation of fractured media. page 993–1007, (2018). doi: 10.1016/j.apnum.2005.07.002.

[29] 1850-1919 Voigt, Woldemar. *Lehrbuch der kristallphysik (mit ausschluss der kristalloptik)*. Leipzig, Berlin, B.G. Teubner, (1910).

[30] H. F. Wang. *Theory of Linear Poroelasticity with Applications to Geomechanics and Hydrogeology.* Princeton: Princeton University Press., (2017). doi: 10.1515/9781400885688.

[31] P. Wenke and M. A. Wheel. A finite volume method for solid mechanics incorporating rotational degrees of freedom. *Computers and Structures*, 81:321–329, 2003. doi: 10.1016/S0045-7949(02)00439-X.

[32] Fanxiang Xu, Hadi Hajibeygi, and Lambertus J. Sluys. Multiscale extended finite element method for deformable fractured porous media. (2020).